Physics Theses & Dissertations   Physics

Summer 1989

Nuclear Fragmentation Energy and Momentum Transfer Distributions in Relativistic Heavy-Ion Collisions

Ferdous Khan
Old Dominion University

NUCLEAR FRAGMENTATION ENERGY AND MOMENTUM TRANSFER

DISTRIBUTIONS IN RELATIVISTIC HEAVY-ION COLLISIONS

by

Ferdous Khan
B.A. May 1981, Yale University
M.S. May 1984, University of Rhode Island

A Dissertation Submitted to the Faculty of
Old Dominion University in Partial Fulfillment of the
Requirements for the Degree of

DOCTOR OF PHILOSOPHY

APPLIED PHYSICS

OLD DOMINION UNIVERSITY
August, 1989

Approved by:

Dr. Govind S. Khandelwal

ABSTRACT

NUCLEAR FRAGMENTATION ENERGY AND MOMENTUM TRANSFER DISTRIBUTIONS IN RELATIVISTIC HEAVY-ION COLLISIONS

Ferdous Khan
Old Dominion University, 1989
Director: Dr. Govind S. Khandelwal

An optical model description of energy and momentum transfer in relativistic heavy-ion collisions, based upon composite particle multiple scattering theory, is presented. Transverse and longitudinal momentum transfers to the projectile are shown to arise from the real and absorptive part of the optical potential, respectively. Comparisons of fragment momentum distribution observables with experiments are made and trends outlined based on our knowledge of the underlying nucleon-nucleon interaction. Corrections to the above calculations are discussed. Finally, use of the model as a tool for estimating collision impact parameters is indicated.

DEDICATION

This dissertation is dedicated to my wife, Zeenat Khan, and daughter, Nora N. Khan for their love and understanding; to my parents for their inspiration and to Drs. G.S. Khandelwal, J.W. Wilson and L.W. Townsend for their trust and confidence in me.

ACKNOWLEDGMENTS

It is with the deepest respect and gratitude that I thank my advisor Professor Govind S. Khandelwal for his guidance throughout my graduate studies at the Old Dominion University. His contributions to my progress are too numerous to mention; his personal warmth and genuine interest in the student should be singled out. I thank Drs. J.W. Wilson and L.W. Townsend of NASA/Langley Research Center (HESB) for their guidance, trust and kindness. Without these outstanding individuals, my life would be far less enriched.

I want to thank Drs. J.W. Norbury and K.M. Maung for many discussions on nuclear scattering theory and friends F.A. Cucinotta, D.A. Olsgaard, and R.S. Sokrollah for their friendship. Finally, the constructive role that CEBAF has played on my education must be pointed out. In this regard, many thanks to Professor J.D. Walecka for sharing his knowledge, insights and vision of physics in general and nuclear physics in particular.

Without the assistance of Ms. Robin Dean and Mrs. Kathy Ganas on typing, this thesis would not be completed on schedule.

Thank you all!

TABLE OF CONTENTS

LIST OF TABLES

LIST OF FIGURES

CHAPTER I

INTRODUCTION

With the advent of relativistic heavy ion beams at Berkeley,
Saclay and Dubna, the experimental situation in high-energy nuclear
interactions has improved dramatically over the previous era of cosmic-
ray heavy-ion physics. Sophisticated experiments have challenged
theorists to come up with new theoretical tools and insights to under-
stand the new features apparent in relativistic heavy-ion collisions.
Traditional nuclear physics has been primarily about the nature of
nuclear matter at or near equilibrium. With heavy-ion beams, the
possibility of compressing nuclear matter to two or three times the
normal density and heating to temperatures ~ 100 MeV has opened up. It
is appropriate at this point then to review the salient features of
high energy heavy-ion collisions beginning with cosmic-ray heavy ion
physics.

Ever since the discovery of $Z > 2$ (where Z is the nuclear charge)
components in the primary cosmic radiation by Freier et al.[1,2], which
fulfilled a prediction by Alfven[3], the subject of high energy interac-
tions between nuclei has been of fundamental interest. The goal of
these pioneering studies focussed primarily on interaction mean free
paths and reaction cross-sections. The production of nuclear fragments
and determination of their isotopic composition was intensely studied
in order to infer from these data the conditions of their origin,
possible acceleration mechanisms and subsequent propagation. These

1

aspects of cosmic-ray heavy ion physics are thoroughly reviewed by Shapiro and Silberberg,[4] Waddington[5] and in the classic monograph by Powell.[6]

The qualitative classifications of the nuclear interactions in cosmic rays were performed first by Bradt and Peters.[7] The concepts of "Peripheral" (large impact parameter) and "Central" (small impact parameter) collisions were introduced by these authors. In a peripheral collision, part of the nucleus overlapping the target is sheared off while the remaining fragment proceeds at near the beam velocity. Both projectile and target fragmentation may be described as peripheral processes. In a central collision, both the nuclei are destroyed, involving high levels of excitation and the emission of large numbers of secondary fragments. Nucleons, light fragments and pions are copiously produced in central collisions.

Experimental studies of cosmic rays revealed many important features, in spite of low intensities and uncertainties in charge, mass and energy determinations. Bradt and Peters[7] analyzed the reaction cross sections using a semi-empirical "black sphere" expression

$$\sigma_{reac} = \pi \, r_o^2 \, (A_P^{1/3} + A_T^{1/3} - \delta)^2 \tag{1.1}$$

with A_P, A_T the mass numbers of beam and target, and δ an overlap parameter representing the diffuseness and partial transparency of nuclear surfaces. With fixed values of r_o and δ, reaction cross-sections could be reasonably predicted with equation (1.1). These cross-sections were assumed to be energy-independent for bombarding energies from .1 A GeV to 30 A GeV. The average number of fragments produced by the fragmentation of a certain projectile was also found to be nearly

energy-independent (to within ~20%). The Bradt-Peters "black sphere"

model was later refined and a "grey sphere" model was proposed[8] to

account for the reduction of geometric cross-section due to the trans-

parency of nuclear surfaces. Optical model calculations of reaction

cross-sections were also undertaken successfully by various authors[9,10]

and satisfactory agreement was found with experiment.

For cosmic rays, the reaction products studied were mainly mesons

and nucleons[11-15]. The experimental goal was to understand nucleus-

nucleus interaction as a superposition of independent nucleon-nucleon,

nucleon-nucleus or alpha-alpha collisions. Although successful in

achieving a broad understanding of such collisions, precise knowledge

of high energy interactions of nuclei could not be gained from these

studies due to low statistics and lack of control over experimental

conditions.

The first laboratory acceleration of relativistic heavy-ions was

accomplished in 1971 at the Princeton Particle Accelerator (PPA),

shortly followed by the Berkeley Bevatron[16]. Acceleration of alpha

particles began in Dubna 1970. Similar proposals were made at CERN for

heavy-ion experiments[17]. With the closing of PPA in 1972, Berkeley

BEVALAC became the only high energy heavy ion accelerator in the U.S.A.

Proposal for a Relativistic Heavy Ion Collider (RHIC) to be built at

Brookhaven National Laboratory in the 1990's is underway. Projects

that are also in progress are GANIL in France, Numatron in Japan,

Nuklotron in the U.S.S.R. and GSI in Darmstadt, West Germany.

The BEVALAC, proposed by Ghiorso[18], employs an 8.5 A MeV heavy ion

linear accelerator, the SUPERHILAC, to inject the ions into the

Bevatron which continues the acceleration of these ions to a maximum

energy of 2.6 A GeV. High intensity Uranium beams have recently been accelerated at the BEVALAC.

Experimental techniques at high energy heavy ion accelerators combine tools from both traditional low energy nuclear physics as well as high energy particle physics because of the wide range of charge, mass and energy. These techniques range from particle identification by ΔE-E and time of flight over 4π steradians for target fragmentation to high energy techniques such as magnetic spectrometers, measurements of dE/dx, rigidity, Time of Flight (TOF) for slow projectile particles. For relativistic particles Cerenkov radiation as well as the use of streamer chamber or other multiple track detectors are used. Detection by emulsions, plastics and AgCl monocrystals are also used because of their wide range of sensitivities, versatility and small demand for beam time. The availability of wide ranges of charge in heavy ion experiments pose difficulties for charge identification by dE/dx$\approx Z^2$ f(β) so that additional capabilities must be incorporated into the system. Excellent reviews of these aspects of detector development are the Heavy Ion Study Proceedings published by Lawrence Berkeley Laboratory (and GSI) every two years, where recent information on both experimental and theoretical aspects can be found.

In this work, we shall examine one aspect of relativistic heavy-ion collisions in detail. We shall formulate a theoretical framework to describe how momentum and energy are transferred to relativistic heavy ions. An optical model description of momentum and energy transfer based on the multiple scattering theory of nucleus-nucleus collisions will be presented.

Aside from the fundamental importance of the topic itself, the necessity for understanding these processes (energy-momentum transfer) arose due to the increasing sophistication of experiments. Single-particle inclusive experiments of the type Projectile + Target → Projectile Fragment[+ other products] form the basis of our knowledge on heavy ion projectile fragmentation. It was observed experimentally[19] in the fragmentation of ^{12}C and ^{16}O (2.1 A GeV) beams on targets ranging from H through Pb that the isotope production cross-sections were factorizable into

$$\sigma_{FBT} = \gamma_B^F \gamma_T \qquad (1.2)$$

where σ_{FBT} is the cross-section for producing the fragment; γ_B^F and γ_T are two terms that depend on the beam-fragment and target respectively. This suggests that the momentum of fragments in the projectile rest frame should also exhibit independence of target structure and beam energy. Indeed, in the rest frame of the projectile, the longitudinal momentum distributions of fragments show a statistical Gaussian dependence. Irrespective of projectile, beam energy ($\geq$ 1.05 A GeV) and target nucleus, the longitudinal momentum $P_{\parallel}$ distributions for all fragments from ^{12}C and ^{16}O projectiles are characterized by Gaussian shape with rms width $\sigma(P_{\parallel}) \simeq 50$ to 200 MeV/c. These longitudinal spectra are also downshifted by $<P_{\parallel}> \simeq -20$ to -130 MeV/c from the beam, showing that the mean velocities of these fragments are less than that of the beam. The rms widths $\sigma(P_{\parallel})$ and $\sigma(P_{\perp})$ of the longitudinal and transverse momentum spectra are found to be equal to within ~10%, consistent with isotropic production of fragments in a frame moving at

a velocity less than the beam velocity. The widths $\sigma(P_{\parallel})$ and $\sigma(P_{\perp})$, independent of target mass and beam energy, depend on the masses of the beam and the fragment. A parabolic shape reproduces the general trend of the data

$$\sigma(P_{\parallel}) = 2\sigma_o[x(1 - x)]^{1/2}; \quad x = \frac{A_F}{A_p} \qquad (1.3)$$

where A_p, A_F are the beam and fragment masses respectively, and σ_o is experimentally extracted from the data or predicted by theory.

The parabolic shape of the widths $\sigma(P_{\parallel})$ has been the subject of considerable attention of theorists[20-22] who explained this dependence using conservation of momentum. According to these theories, the Gaussian momentum distributions can be understood by treating the fragmenting nucleus as a Fermi gas and assuming (i) Momentum conservation, (ii) No correlation among nucleons in the parent nucleus, and (iii) Neglecting anti-symmetrization of the single particle states. Within these assumptions, one would predict (1.3) where σ_o is related to the Fermi momentum of the projectile (P_F) via

$$\sigma_o = \frac{P_F}{\sqrt{5}}$$

and also that $\qquad\qquad\qquad\qquad\qquad\qquad\qquad\qquad\qquad\qquad (1.4)$

$$\sigma(P_{\parallel}) \simeq \sigma(P_{\perp})$$

explaining the isotropic production of the fragments. These insights form the basis of much of the analyses of experimental data.

The simple Fermi gas picture of projectile fragmentation has been questioned by many authors. Nuclear structure and binding-energy

effects in determining the momentum widths has been pointed out[23].
Neglect of anti-symmetrization of single-particle states has been
questioned by Bertsch[24] who showed that the momentum widths would be
reduced from the free Fermi gas value due to correlations. Murphy[25]
has investigated the constraints of phase space on treating the projec-
tile as a Fermi gas which emits fragments that are also Fermi gases.
Recent experimental data[26] on the transverse momentum widths of Lantha-
num fragments also indicate the inadequacy of the simple Fermi gas
picture. Indeed, an alternate formulation[27] of projectile fragmenta-
tion abandons the Fermi gas picture and attempts to explain widths in
terms of neutron separation energies. It is clear that one needs to
bring in sophisticated theoretical insights to address structure and
binding energy effects, correlations, phase space constraints etc.

In this work, we attempt to address important but as yet unre-
solved questions, i.e. how are momentum and energy transferred to heavy
ions at high energies and how does energy-momentum transfer affect the
fragment momentum and energy spectra, fragmentation cross-sections and
their angular distributions.

To address the above questions, an optical model description of
momentum and energy transfer between relativistic heavy ion collisions
within the multiple scattering theory framework will be presented. The
inputs into our calculations will be the well-known nuclear ground
state densities and NN (nucleon-nucleon) two-body transition ampli-
tudes. The energy-dependence of the two-body amplitude will enable us
to address the above questions over the entire energy range from low to
intermediate and extremely high bombarding energies for any projectile-

<u>target</u> <u>combination</u>. New insights gained from this work, it is hoped, will unify a host of data on heavy ion (peripheral) fragmentation.

Previously, excitation energy calculations have been undertaken by Hufner[28] et al. within the Glauber theory framework. Fricke[29] has calculated the excitation energy of "anomalons" detected in heavy ion experiments using an impulsive excitation picture. Phenomenological[30] and semi-empirical estimates of the excitation energy in heavy ion collisions also exist (these are not based on two-body interaction parameters).

The new feature of this work is the introduction of a complex momentum transfer vector which results from the use of a complex two-body transition amplitude that satisfies unitarity and is used to analyze experiments. The real (imaginary) part of the two-body inter-action, folded with the appropriate densities for nucleon-nucleus or nucleus-nucleus scattering gives rise to the real (imaginary) part of the optical potential. The imaginary part accounts for inelastic scatterings as well as true absorption, and as will be shown, gives rise to longitudinal momentum transfer. The reaction cross-section in Glauber theory, for example, is obtained from the imaginary part of the phase shift computed from the imaginary part of the optical potential. The real part of the complex momentum transfer vector represents trans-verse momentum transfer due to elastic scattering at high energy. In a fragmentation experiment, the projectile (or target) fragments are detected. It has been found that these fragments emerge with less than the beam velocity i.e. the longitudinal momentum spectra of these fragments are "downshifted" by -20 Mev/c to -130 Mev/c depending on the fragment. This "momentum downshift" is naturally explained in this

work as due to longitudinal momentum transfer to the projectile by the target. This arises due to inelastic scatterings that occur as the projectile traverses the target. The transverse momentum transfer due to elastic scatterings, is separately obtained from the real part of the interaction. Calculation of momentum transfer allows us to calculate the means and widths of transverse (and longitudinal) momentum spectra for fragments for any projectile-target combination, using as inputs nuclear ground state densities, NN transition amplitude utilizing the currently available theories of projectile fragmentation.

Since the two-body interaction that is used is energy dependent, the validity of these insights can be tested at extremely relativistic energies ($\geq$ 10 A Gev) as well as at lower ($\leq$ 1 A GeV) bombarding energies, assuming the validity of the underlying model at these two extremes. Silicon beams have now been accelerated to energies ≈14.5 A GeV (at Brookhaven), Oxygen and Sulphur beams to 60 A Gev and 200 A GeV at CERN. The momentum spectra of fragments look remarkably similar to those at 2.1 A GeV. Lower ($\leq$ 1 A GeV) energy data on these same fragments is harder to come by; the paucity of available data prevents a systematic study of the reaction mechanism and its evolution as a function of bombarding energy. With the methods described herein, one can now perform a theoretical calculation within this model. Such calculations have been included in this work for possible future comparisons.

Another often studied question in nucleon-nucleus as well as nucleus-nucleus collisions is the validity of the constant velocity assumption that is frequently made. Within this model,we have a

computationally tractable scheme for addressing this question. Longitudinal momentum transfer to the beam nucleus inherently challenges the notion of constant velocity. The magnitude of the momentum transfer is responsible for change in velocity. We have developed a scheme that takes into account corrections to the constant velocity assumption used in our formalism. Another correction we address is the possible Coulomb effects as the electromagnetic fields generated at these energies are substantial enough to require such an analysis.

We have also derived a theory of energy transfer (based on multiple scattering theory) along the lines of our theory of momentum transfer. Experiments are seldom able to measure the excitation energy of fragments; it is rather inferred or extracted from observed cross-sections (using models such as the "Ablation-Abrasion" model). Our calculation of excitation energy for projectiles and projectile fragments introduces a comprehensive framework for performing these energy transfer calculations using NN interaction parameters as inputs. No comparisons could be made with experimental data because of the absence of the latter. However, sophisticated experiments in the future may change this situation.

The remainder of this work is organized as follows: In Chapter II, the multiple scattering theory of nucleus-nucleus collisions is reviewed and the optical model discussed within this context. In Chapter III, the formulation of momentum and energy transfer in nucleus-nucleus collisions is made within the multiple scattering theory framework. Chapter IV contains numerical results on momentum transfer (longitudinal and transverse), momentum downshifts and momentum widths, preceded by discussions on the theoretical understanding

and experimental facts on these topics. Corrections are discussed in

Chapter V. The first is the "deceleration correction" arising from

the transfer modification of the constant velocity assumption at high,

intermediate and low bombarding energies. The second is the more

familiar Coulomb correction. We conclude by discussing the major new

insights gained in this work as well as indicating possible directions

for future research.

CHAPTER II

MULTIPLE SCATTERING THEORY OF NUCLEUS-NUCLEUS COLLISIONS

Multiple scattering theory provides a reliable and fundamentally correct description of hadron-nucleus as well as nucleus-nucleus collisions at intermediate (~ 100 A MeV to 500 A MeV) and high (>500 A MeV) incident energies.[31-39] In these theories, the complex many-body problem of A_p projectile nucleons interacting with A_T target constituents is formulated in terms of two-body interactions. The success of these theories is well documented and is reviewed quite frequently in the literature.

Our goal in this chapter is to review multiple scattering theory in order to formulate the problem of momentum transfer and excitation-energy deposition in nucleus-nucleus collisions. We shall review the main results of the multiple scattering theory of nucleus-nucleus collisions. Following Wilson,[39,40] a set of coupled equations relating all entrance channels to all exit channels will be derived. An optical potential V_{opt} will be extracted under certain approximations.

II.a Review of Multiple Scattering Theory

We shall review multiple scattering theory of nucleus-nucleus collisions to find an expression for the multiple scattering series. Collision of a composite projectile (mass number A_p) with a composite target (mass number A_T) will be considered. The formulation of this problem and its solution can be found in references 39-42. The

12

Hamiltonian for the combined system of $N = (A_p + A_T)$ nucleons can be written as

$$H = \sum_{j=1}^{A_p} T_j + \sum_{i<j} V_{ij} + \sum_{\alpha=1}^{A_T} T_\alpha + \sum_{\alpha<\beta} V_{\alpha\beta} + \sum_{\alpha j} V_{\alpha j} \qquad (2.1)$$

where Roman indices refer to the projectile constituents and Greek indices to targets. The first two terms in (2.1) are, respectively, the kinetic energy and potential energy operators for the projectile and are written as

$$H_p = \sum_{j=1}^{A_p} T_j + \sum_{i<j} V_{ij} \qquad (2.2)$$

Similarly, the third and fourth terms are the target kinetic and potential energy operators. The last term is the interaction term between αth and jth constituents of the target and projectile. One can decouple the center of mass motion of the projectile as

$$H_p = \frac{\vec{P}_p^2}{2M_n A_p} + h_p \qquad \text{with} \qquad \vec{P}_p = \sum_{j=1}^{A_p} \vec{P}_j \qquad (2.3)$$

where h_p is the internal Hamiltonian of the projectile which depends neither on $\vec{P}_p$ nor on its canonically conjugate position variable. Similar results obtain for the target

$$H_T = \frac{\vec{P}_T^2}{2M_n A_T} + h_T \qquad ; \qquad \vec{P}_T = \sum_{\alpha=1}^{A_T} \vec{P}_\alpha \qquad (2.4)$$

where h_T is the internal Hamiltonian of the target. Then the full Hamiltonian can be written as

$$H = \frac{\vec{P}^2}{2M_n (A_p+A_T)} + \frac{(A_p+A_T)}{2M_n A_p A_T} \vec{k}^2 + h_p + h_T + V_I \qquad ; \hbar = 1 \qquad (2.5)$$

where the overall center of mass momentum operator is

$$\vec{P} = \vec{P}_p + \vec{P}_T$$

and the projectile momentum compared to the overall center of mass is

$$\vec{k} = \vec{P}_p - \frac{A_p \vec{P}_p}{(A_p + A_T)} - \frac{A_T \vec{P}}{(A_p + A_T)} - \vec{P}_T \qquad (2.7)$$

and the interaction is the sum of two body interactions

$$V_I = \sum_{\alpha=1}^{A_T} \sum_{j=1}^{A_p} V_{\alpha j} \qquad (2.8)$$

The first term in (2.5) is the N-body center of mass motion energy, decoupled from the other terms. The second is the kinetic energy of relative motion of the projectile and the target. The projectile relative position variable appears only in the interaction term term V_I. The projectile and target internal Hamiltonians h_p and h_T are coupled to the relative motion through the interaction V_I. As the separation between the projectile and target becomes larger, V_I tends to zero. We assume that well defined states are prepared in the entering state and observed in the final state. We define these (in operator notation) to be eigenstates of the free projectile-target Hamiltonian

$$(H_p + H_T) \ \phi = E\phi \qquad (2.9)$$

The full wave function satisfies the Schrodinger equation

$$H\psi = E\psi \qquad (2.10)$$

where ψ consists of a superposition of a free state plus a scattered state

$$\psi = \phi + \psi_{scat} \qquad (2.11)$$

with $\qquad \psi_{scat} = GT \ \phi$

where the Green's function is defined as

$$(E - H_p - H_T)^{-1}G = 1 \qquad (2.12)$$

and the transition operator is defined as

$$T = V + VGT \tag{2.13}$$

and the wave operator Ω as

$$\psi = \Omega\phi \tag{2.14}$$

The wave operator satisfies the Lippman-Schwinger equation

$$\Omega = 1 + GV\Omega \tag{2.15}$$

so that the transition operator is formally given by

$$T = V\Omega \tag{2.16}$$

The goal is to find a series for T. For nucleus-nucleus collisions this series was derived by Wilson.[40] For a single projectile, this series reduces to the familiar Watson[31] series. Using the Eikonal approximation, Glauber[33] theory is recovered from Wilson's.

Wilson[39,40] observed that the transition operator for the scattering of α constituent from the jth constituent can be written as

$$t_{\alpha j} = v_{\alpha j} + v_{\alpha j} \, G \, t_{\alpha j} \tag{2.17}$$

which satisfies a Lippman-Schwinger type equation. The wave operator which transforms the entering free state up to the collision of α and j constituents can be written as

$$w_{\alpha j} = 1 + \sum_{(\beta k) \neq (\alpha j)} G \, t_{\beta k} \, w_{\beta k} \tag{2.18}$$

The interpretation of the above equation is as follows. The propagation to the time just before α and j constituents collide is the sum of an operator which brings the initial free state plus the scattered part from the scattering of all other β and k constituents. The full wave operator then consists of the wave operator which

transforms the system to the α-j collision plus the contribution due to scattering of the αth and jth constituents i.e.

$$\Omega = w_{\alpha j} + G\, t_{\alpha j}\, w_{\alpha j} \tag{2.19}$$

which can be written as

$$\Omega = 1 + \sum_{\alpha j} G\, t_{\alpha j}\, w_{\alpha j} \tag{2.20}$$

Wilson then proves that the series given by equations (2.17)-(2.20) constitutes an exact representation of the scattering process defined by these equations. Consider the product

$$V_{\alpha j}\Omega = v_{\alpha j}\, w_{\alpha j} + v_{\alpha j}\, G\, t_{\alpha j}\, w_{\alpha j}$$

$$= (v_{\alpha j} + v_{\alpha j}\, G\, t_{\alpha j})\, w_{\alpha j}$$

$$= t_{\alpha j}\, w_{\alpha j} \tag{2.21}$$

Summing over α and j one obtains

$$T = \sum_{\alpha j} V_{\alpha j}\,\Omega = \sum_{\alpha j} t_{\alpha j}\, w_{\alpha j} \tag{2.22}$$

This completes the proof.[39]

The Green's function G are true N-body operators. One neglects binding effects at high energy and replaces G by free N-body operators G_0 which satisfy

$$(E - \sum_j T_j - \sum_\alpha T_\alpha)\, G_0 = 1 \tag{2.23}$$

Watson's form of the impulse approximation consists of writing $t_{\alpha j}$ as

$$t_{\alpha j} = v_{\alpha j} + v_{\alpha j}\, G_0\, t_{\alpha j} \tag{2.24}$$

so that the above operator acts as a two-body transition amplitude. By iteration of the above the multiple scattering series obtains

$$T = \sum_\alpha \sum_j t_{\alpha j} + \sum_{(\beta k)\neq(\alpha j)} t_{\beta k}\, G\, t_{\alpha j} + \ldots \tag{2.25}$$

which constitutes a formal solution to the exact scattering problem. The replacement $G \rightarrow G_o$ renders the $t_{\alpha j}$ essentially two-body operators and the series for T above, equation (2.25) becomes a series of two-body operators.

The above series reduces to the Watson[31] series when the projectile is a single particle, as previously mentioned. Next we shall derive an optical potential operator whose Born series is equivalent to the multiple scattering series expansion (2.25). Such an operator is V_{opt}, defined from

$$T_{opt} = V_{opt} + V_{opt} \ G \ T_{opt} \qquad (2.26)$$

as

$$V_{opt} = \sum_{\alpha} \sum_{j} t_{\alpha j} \qquad (2.27)$$

From which we obtain

$$T = T_{opt} - \sum_{\alpha j} t_{\alpha j} \ G \ t_{\alpha j} - \cdots \qquad (2.28)$$

Retaining the first term in (2.26), the optical model is obtained with

$$T_{opt} - T \simeq V_{opt} \ G \ V_{opt} / (A_p \cdot A_T) \qquad (2.29)$$

since $t_{\alpha j} \simeq \dfrac{V_{opt}}{(A_p A_T)}$ where A_p, A_T are the mass numbers of the projectile and the target, respectively.

The approximate Lippman-Schwinger equation for the effective potential operator is given by

$$\Omega' = 1 + G \ V_{opt} \ \Omega' \qquad (2.30)$$

where the first order correction to the model is $0 \ (\dfrac{1}{A_p A_T})$.

II.b Coupled Channel Equations

Using the multiple scattering theory of nucleus-nucleus collisions following Reference 39-42, a set of coupled equations will be derived. An equivalent Schrodinger equation will be extracted from the formalism developed so far. We shall focus on the Green's function

$$G = \sum_{k,m,\mu} \frac{|g_{p,m}g_{T,\mu}\phi_k> <g_{p,m}g_{T,\mu}\phi_k|}{E - E^P_m - E^T_\mu - \varepsilon_k + i\eta} \qquad (2.31)$$

where E^P_m, E^T_μ refer to the projectile and target internal states and

$$\varepsilon_k = \frac{(A_p+A_T)\vec{k}^2}{2M_n A_p A_T} = \frac{\vec{k}^2}{2\mu_{red}} \qquad (2.32)$$

with the Green's function G from (2.31) inserted into (2.11) and projecting onto configuration space yields

$$\psi'(\vec{x},\vec{\xi}_p,\vec{\xi}_T) = g_{p,o}(\vec{\xi}_p)\, g_{T,o}(\vec{\xi}_T)\, \phi_k(\vec{x})$$

$$- \frac{2M_n A_p A_T}{(A_p+A_T)} \sum_{m,\mu} \int d^3\vec{y}\, d^3\vec{\xi}_p\, d^3\vec{\xi}_T\, \frac{\exp(ik_{m\mu}|\vec{x}-\vec{y}|)}{4\pi\,|\vec{x}-\vec{y}|}$$

$$\times\ g_{p,m}(\vec{\xi}_p)g_{T,u}(\vec{\xi}_T)g^*_{p,m}(\vec{\xi}_p')g^*_{T,u}(\vec{\xi}_T')$$

$$\times\ V_{opt}(\vec{y},\vec{\xi}_p',\vec{\xi}_T')\ \psi'(\vec{y},\vec{\xi}_p',\vec{\xi}_T') \qquad (2.33)$$

where

$$\phi_k(\vec{x}) = \frac{1}{(2\pi)^{3/2}}\, e^{i\vec{k}\cdot\vec{x}} \qquad (2.34a)$$

$$\vec{\xi}_p = (\vec{r}_1, \vec{r}_2, \ldots \vec{r}_{A_p})$$

(2.34b)

$$\vec{\xi}_T = (\vec{s}_1, \vec{s}_2, \ldots \vec{s}_{A_T})$$

(2.34c)

and

$$k_{m\mu}^2 = \vec{k}^2 + \frac{2M_n A_p A_T}{(A_p + A_T)} \; [(E_{p,o} - E_m^p) + (E_{T,o} - E_m^T)]$$

(2.35)

and $g_{p,m}(\vec{\xi}_p)$ and $g_{T,\mu}(\vec{\xi}_T)$ are the projectile and target internal many-body wavefunctions. Now, following Foldy and Walecka[43], we assume that the energy transfer is small compared to the incident kinetic energy

$$k_{m\mu} \propto k$$

(2.36)

Using the closure approximation, (2.39) can be written as

$$\psi'(\vec{x}, \vec{\xi}_p, \vec{\xi}_T) = g_{p,o}(\vec{\xi}_p) \; g_{T,o}(\vec{\xi}_T) \; \phi_k(\vec{x}) - \frac{1}{4\pi} \int d^3\vec{y} \; \frac{\exp(ik|\vec{x}-\vec{y}|)}{|\vec{x}-\vec{y}|}$$

$$\times \; \frac{2M_n A_p A_T}{(A_p + A_T)} \; V_{opt}(\vec{y}, \vec{\xi}_p, \vec{\xi}_T) \; \psi'(\vec{y}, \vec{\xi}_p, \vec{\xi}_T) \ldots$$

(2.37)

The equivalent Schrodinger equation follows from the above equation

$$(\vec{\nabla}_x^2 + \vec{k}^2) \; \psi'(\vec{x}, \vec{\xi}_p, \vec{\xi}_T) = \frac{2M_n A_p A_T}{(A_p + A_T)} \; V_{opt}(\vec{x}, \vec{\xi}_p, \vec{\xi}_T) \; \psi'(\vec{x}, \vec{\xi}_p, \vec{\xi}_T)$$

(2.38)

We express the fact that the projectile and target internal wave functions are not eigenstates of the optical potential operator and the initial states are mixed into various modes of final excited states as follows

$$\psi'(\vec{x}, \vec{\xi}_p, \vec{\xi}_T) = \sum_{m,\mu} \psi_{m\mu}(\vec{x}) \; g_{p,m}(\vec{\xi}_p) \; g_{T,\mu}(\vec{\xi}_T)$$

(2.39)

The coupled equations then can be written as[42]

$$(\vec{\nabla}_x^2 + \vec{k}^2)\ \psi_{m\mu}(\vec{x}) = \frac{2M_n A_p A_T}{(A_p + A_T)}\ \sum_{m'\mu'}\ V_{m\mu,m'\mu'}(\vec{x})\psi_{m'\mu'}(\vec{x}) \qquad (2.40)$$

which is the desired equation. Here

$$V_{m\mu,m'\mu'}(\vec{x}) = (g_{p,m}\ g_{T,\mu}|V_{opt}|g_{p,m'}g_{T,\mu'}) \qquad (2.41)$$

The coupled equations (2.40) for composite particle scattering relate all the entrance channels of the system labelled by projectile quantum number m and target quantum number μ to all the exit channels. In (2.40), A_p and A_T are the mass numbers of the projectile and target, subscripts m and μ label the eigenstates of the projectile and target; M_n is the constituent nucleon mass, $\vec{k}$ is the projectile momentum relative to the center of mass, $\vec{x}$ is the projectile position vector relative to the target and

$$V_{opt}(\vec{x},\ \vec{\xi}_p,\ \vec{\xi}_T) = \Sigma_{\alpha j}\ t_{\alpha j}\ (\vec{x}_\alpha,\ \vec{x}_j) \qquad (2.42)$$

The internal coordinates $\vec{\xi}_p$ and $\vec{\xi}_T$ have been defined in (2.34) and the transition amplitude $t_{\alpha j}$ have been introduced in (2.17).

Next we shall write the coupled equations (2.40) in matrix form. Introducing the wave vector

$$\overline{\psi}(\vec{x}) = \begin{bmatrix} \psi_{00}(\vec{x}) \\ \psi_{01}(\vec{x}) \\ \psi_{10}(\vec{x}) \\ \psi_{11}(\vec{x}) \\ \vdots \end{bmatrix} \qquad (2.43)$$

and the potential matrix

$$\bar{U}(\vec{x}) = \frac{2M_n A_p A_T}{(A_p + A_T)} \begin{bmatrix} V_{00,00}(\vec{x}) & V_{00,01}(\vec{x}) & V_{00,10}(\vec{x}) & \cdots \\ V_{01,00}(\vec{x}) & V_{01,01}(\vec{x}) & V_{01,10}(\vec{x}) & \cdots \\ V_{10,00}(\vec{x}) & V_{10,01}(\vec{x}) & V_{10,10}(\vec{x}) & \cdots \\ V_{11,00}(\vec{x}) & V_{11,01}(\vec{x}) & V_{11,10}(\vec{x}) & \cdots \\ \vdots & \vdots & \vdots \end{bmatrix}$$

$$(2.44)$$

The coupled equations (2.40) can be written in matrix form as

$$\left[\vec{\nabla}_x^2 + \vec{k}^2 \right] \vec{\psi}(\vec{x}) = \bar{U}(\vec{x})\, \vec{\psi}(\vec{x}) \tag{2.45}$$

Using the definition of the potential as given by equation (2.42), (2.41) can also be written as

$$V_{m\mu,m'\mu'}(\vec{x}) = \sum_{\alpha j} \langle g_{p,m}(\vec{\xi}_p)\, g_{T,\mu}(\vec{\xi}_T)\, |t_{\alpha j}(\vec{x}_\alpha, \vec{x}_j)|\, g_{p,m'}(\vec{\xi}_p)\, g_{T,\mu'}(\vec{\xi}_T) \rangle$$

$$= \sum_{\alpha j} \int \rho_{T,\mu\mu'}(\vec{r}_\alpha)\, t_{\alpha j}(\vec{x}_\alpha, \vec{x}_j)\, \rho_{p,mm'}(\vec{r}_j)\, d^3\vec{r}_j\, d^3\vec{r}_\alpha \tag{2.46}$$

where

$$\rho_{p,mm'}(\vec{r}_j) = \int g_{p,m}^*(\vec{\xi}_p)\, \delta^3(\vec{r}_j - \vec{\xi}_{p,j})\, g_{p,m'}(\vec{\xi}_p)\, d^3\vec{\xi}_p \tag{2.47}$$

and

$$\rho_{T,\mu\mu'}(\vec{r}_\alpha) = \int g_{T,\mu}^*(\vec{\xi}_T)\, \delta^3(\vec{r}_\alpha - \vec{\xi}_{T,\alpha})\, g_{T,\mu'}(\vec{\xi}_T) d^3\vec{\xi}_T \tag{2.48}$$

This completes our review of multiple scattering theory. We shall now discuss the formulation of problems of momentum transfer and excitation energy deposition in nucleus-nucleus collisions, guided by

the multiple scattering approach. Before we proceed, however, a brief review of the optical model is in order, since we shall use the optical potential in our work.

II.c The Optical Model

The optical model is defined as the approximation of (2.40) for the elastic scattered part as[39,40]

$$(\vec{\nabla}_x^2 + \vec{k}^2) \, \psi \, (\vec{x}) = \frac{2M_n A_p A_T}{(A_p + A_T)} \, W(\vec{x}) \, \psi(\vec{x}) \tag{2.49}$$

where

$$\psi(\vec{x}) \simeq \psi_{00} \, (\vec{x}) \tag{2.50}$$

and

$$W(\vec{x}) = \langle g_{T,0} \, g_{P,0} | V_{opt} | g_{T,0} \, g_{P,0} \rangle \tag{2.51}$$

with coupling to various excited internal states neglected. This is correct at small momentum transfer or near forward scattering. The corresponding approximate wave function is called the coherent scattered wave and it dominates the forward scattered component. To evaluate the optical potential we calculate the Fourier transform of a single term of (2.51)

$$\langle g_{T,0} \, g_{P,0} | t_{\beta\ell}(K,\vec{q}) | g_{T,0} \, g_{P,0} \rangle = F_{T,0}(\vec{q}) \, F_{P,0}(\vec{q}) t_{\beta\ell} \, (K,\vec{q}) \tag{2.52}$$

where this term will be recognized as the single scattering term of the multiple scattering series; $\vec{q}$ is the momentum transfer and $F_{P,0}(\vec{q})$ and $F_{T,0}(\vec{q})$ are the Fourier transforms of the single particle density of the projectile and target, respectively. The nucleon-nucleon interaction will be assumed to be constituent averaged as follows[40]

$$\tilde{t} = (A_p A_T)^{-1} [N_p N_T \, t_{nn} + Z_p Z_T \, t_{pp} + (Z_p N_T + N_p Z_T) \, t_{np}] \qquad (2.53)$$

where N_p, N_T are the neutron numbers and Z_p, Z_T are the proton numbers the projectile and target, respectively. The optical potential is obtained by evaluating (2.42) (summing over constituents) as[40]

$$W(\vec{x}) = A_p A_T \int d^3\vec{\xi} \, \rho_T \, (\vec{\xi}) \int d^3\vec{\xi'} \, \rho_p \, (\vec{x} + \vec{\xi} + \vec{\xi'}) \, \tilde{t} \, (k, \, \vec{\xi'}) \qquad (2.54)$$

where ρ_p, ρ_T are the projectile and target single-particle densities

$\tilde{t}(k,\vec{y})$ is the energy and space dependent two-body transition amplitude. We have arrived at the expression for the optical potential used to analyze heavy-ion scattering cross sections. The input parameters are the nuclear ground state densities and the two-body transition amplitudes which will be discussed in Chapter IV.

CHAPTER III

MOMENTUM AND ENERGY TRANSFER IN HEAVY-ION COLLISIONS

In this chapter we shall address the problem of momentum and energy transfer in nucleus-nucleus collisions in the framework of multiple scattering theory. In the last chapter, we reviewed the multiple scattering series, derived the coupled channel equations and discussed the optical model. We shall use these tools in the formulation of the problems of momentum and energy transfer in nucleus-nucleus collisions. Starting with the reduced Schrodinger equation for the combined system, an approximate expression for the wave operator will be derived. Momentum transfer to the projectile as well as its excitation energy due to collision will then be evaluated.

III.a Momentum Transfer

Our starting point will be the formulation of the problem of A_p projectile constituents colliding with A_T target constituents as in equation (2.1). Following equations (2.1)-(2.4), the combined Hamiltonian has been written in (2.5) as

$$H = \frac{\vec{P}^2}{2M_n(A_p+A_T)} + \frac{(A_p+A_T)}{2M_n A_p A_T}\vec{k}^2 + h_p + h_T + V_I \qquad (2.5)$$

The N-body center of mass motion energy, the first term in (2.5) has been decoupled from the other terms. The second term is the relative motion kinetic energy, with $\vec{k}$ as in equation (2.7). The third and fourth terms, h_p and h_T are the internal Hamiltonians of the projectile and target with

24

---

and $\quad h_p \ g_{p,m} \ (\vec{\xi}_p) = \epsilon_{p,m} \ g_{p,m}(\vec{\xi}_p)$ (3.1a)

$h_T \ g_{T,\mu}(\vec{\xi}_T) = \epsilon_{T,\mu} \ g_{T,\mu}(\vec{\xi}_T)$ (3.1b)

where $g_{p,m}(\vec{\xi}p)$, $g_{T,\mu}(\vec{\xi}_T)$ are the internal many-body wave functions of the projectile and the target respectively; $\epsilon_{p,m}$ and $\epsilon_{T,\mu}$ are the corresponding eigenvalues. The eigenstates are orthonormal and complete

$\sum_m \ g_{p,m}(\vec{\xi}_p) \ g_{p,m}^*\ (\vec{\xi}_p') = \delta(\vec{\xi}_p - \vec{\xi}_p')$ (3.2a)

$\sum_\mu \ g_{T,\mu}(\vec{\xi}_T) \ g_{T,\mu}^*\ (\vec{\xi}_T') = \delta(\vec{\xi}_T - \vec{\xi}_T')$ (3.2b)

In the overall center of mass frame

$\vec{P}_p = \sum_j \vec{P}_j = \vec{k}$ (3.3a)

$\vec{P}_T = \sum_\alpha \vec{P}_\alpha = -\vec{k}$ (3.3b)

and $\quad \vec{P}_p + \vec{P}_T = 0$ (3.3c)

Then, the Hamiltonian is

$H = \dfrac{1}{2\mu_{red}} \ \vec{k}^2 + h_p + h_T + V_I \ ; \quad \mu_{red} = \dfrac{m_n \ A_p A_T}{(A_p + A_T)} = \text{reduced mass}$ (3.4)

The Schrodinger equation (in coordinate space) can now be written as

$\left[- \dfrac{1}{2\mu} \ \vec{\nabla}_x^2 + h_p + h_T + V_I \right] \psi \ (\vec{x}, \ \vec{\xi}_p, \ \vec{\xi}_T) = E \ \psi \ (\vec{x}, \ \vec{\xi}_p, \ \vec{\xi}_T)$ (3.5)

We seek solutions of the form[42]

$$\psi \ (\vec{x}, \ \vec{\xi}_p, \ \vec{\xi}_T) = \left[\phi \ (\vec{x}, \vec{\xi}_p, \vec{\xi}_T) \right] \ g_{p,m}(\vec{\xi}_p) \ g_{T,\mu}(\vec{\xi}_T) \ \frac{e^{i\vec{k}\cdot\vec{x}}}{(2\pi)^{3/2}} \qquad (3.6)$$

where the bracketed term $\left[\phi \ (\vec{x}, \vec{\xi}_p, \vec{\xi}_T) \right]$ is the desired wave operator.

Assuming that the source of the beam is along the direction -z, we expect

$$\lim_{z \to -\infty} \left[\phi \ (\vec{x}, \vec{\xi}_p, \vec{\xi}_T) \right] = 1 \qquad (3.7)$$

and

$$\lim_{z \to -\infty} \left[\psi(\vec{x}, \ \vec{\xi}_p, \ \vec{\xi}_T) \right] = g_{p,m}(\vec{\xi}_p) \ g_{T,\mu} \ (\vec{\xi}_T) \ \frac{e^{i\vec{k}\cdot\vec{x}}}{(2\pi)^{3/2}} \qquad (3.8)$$

Inserting (3.6) into (3.5) yields

$$\left[- \frac{1}{2\mu_{red}} \vec{\nabla}_x^2 - \frac{1}{2\mu_{red}} i\vec{k}\cdot\vec{\nabla}_x + \frac{1}{2\mu_{red}} \vec{k}^2 + \varepsilon_{po} + K_p + \varepsilon_{To} + K_T + V_I \right]$$

$$\phi \ (\vec{x}, \ \vec{\xi}_p, \ \vec{\xi}_T) = E \ \phi \ (\vec{x}, \vec{\xi}_p, \vec{\xi}_T) \qquad (3.9)$$

where (3.1a), (3.1b) have been used. K_p and K_T refer to internal motion (Fermi motion) of the projectile and target respectively. We now note that

$$E = \frac{1}{2\mu} \vec{k}^2 + \varepsilon_{p,o} + \varepsilon_{T,o} \qquad (3.10)$$

Solving for the wave operator [$\phi \ (\vec{x}, \vec{\xi}_p, \vec{\xi}_T)$] in (3.9) is in general difficult. Considerable simplifications occur at high energy when [$\phi \ (\vec{x}, \vec{\xi}_p, \vec{\xi}_T)$] is assumed to be slowly varying. Then, the second derivate in (3.9) can be dropped.[43] Internal Fermi motion K_p and K_T

can also be neglected. Using (3.10) and the above assumptions, the approximate wave operator [ϕ $(\vec{x}, \vec{\xi_p}, \vec{\xi_T})$] can be written as

$$\phi\ (\vec{x},\ \vec{\xi_p}\ ,\ \vec{\xi_T})\ =\ \exp\left[-\ i\ \frac{\mu}{k}\ \int_{-\infty}^{z} V_I\ (\vec{x'},\ \vec{\xi_p},\ \vec{\xi_T})\ dz'\right] \tag{3.11}$$

$$=\ \exp\left[-\ \frac{i}{v}\ \int_{-\infty}^{z}\ V_I\ (\vec{x'},\ \vec{\xi_p},\ \vec{\xi_T})\ dz'\right] \tag{3.12}$$

where

$$\vec{k}\ =\ \mu\vec{v}\qquad ;\qquad \vec{v}\ =\ \text{relative velocity} \tag{3.13}$$

Now (3.6) reads

$$\psi\ (\vec{x},\ \vec{\xi_p},\ \vec{\xi_T})\ =\ \frac{1}{(2\pi)^{3/2}}\ \exp\left[-\ \frac{i}{v}\ \int_{-\infty}^{z}\ V_I\ (\vec{x'},\ \vec{\xi_p},\ \vec{\xi_T})\ dz'\right]$$

$$x\ g_{p,m}(\vec{\xi_p})\ g_{T,\mu}(\vec{\xi_T})\ e^{i\vec{k}\cdot\vec{x}} \tag{3.14}$$

Using (3.14), we shall next evaluate the total momentum of the projectile. Total momentum can be defined as the expectation value of the sums of single nucleon momentum operators of the projectile between (3.14), i.e.

$$\vec{P}_{total}=\ <\psi\ (\vec{x},\ \vec{\xi_p},\ \vec{\xi_T})\ \left[-i\sum_{j=1}^{A_p}\vec{\nabla}_{\xi_{p,j}}\right]\ \psi\ (\vec{x},\ \vec{\xi_p},\ \vec{\xi_T})>$$

$$=\ <\ g_{p,m}\ (\vec{\xi_p})\ g_{T,\mu}(\vec{\xi_T})\ |\exp\ (-i\vec{k}\cdot\vec{x})\ \exp\left(+i/v\ \int_{\infty}^{z}\ V_I(\vec{x'},\ \vec{\xi_p},\ \vec{\xi_T})dz'\right)$$

$$\left[-\ i\sum_{j=1}^{A_p}\vec{\nabla}_{\xi_{p,j}}\right]\ \exp\left(-i/v\ \int_{\infty}^{z}\ V_I(\vec{x'},\ \vec{\xi_p},\ \vec{\xi_T})dz'\right)$$

$$\exp\ (i\vec{k}\cdot\vec{x})\ |\ g_{p,m'}(\vec{\xi_p})\ g_{T,\mu'}(\vec{\xi_T})> \tag{3.15}$$

Equation (3.15) is our expression of interest. Note that the single nucleon momentum operators act with respect to the internal coordinates of the projectile. Note also that we write the interaction term $V_I(\vec{x}, \vec{\xi}_p, \vec{\xi}_T)$ as the sum of two-body interactions between the αth and jth constituent. Since the projectile and target internal eigenstates $g_{p,m}$ and $g_{T,u}$ are not eigenstates of the wave operator, the above is still a coupled channel problem.

We shall now make a series of approximations in order to solve (3.15). Note that the wave operator in (3.[?]) was obtained from equation (3.9) by integration. This assumes that the interaction V_I commutes with itself along different points of a straight line trajectory. If they do not commute, however, then a power series[44] solution is appropriate as

$$\phi(\vec{x}, \vec{\xi}_p, \vec{\xi}_T) - 1 - \left(\frac{i}{v}\right) \int_{-\infty}^{z} V_I(\vec{x}', \vec{\xi}_p, \vec{\xi}_T) dz' + \left(-\frac{i}{v}\right)^2 \int_{-\infty}^{z} dz' \int_{-\infty}^{z'} dz''$$

$$V_I(\vec{x}', \vec{\xi}_p, \vec{\xi}_T) \times V_I(\vec{x}'', \vec{\xi}_p, \vec{\xi}_T) + \ldots \qquad (3.16)$$

$$- \exp\left[-\frac{i}{v} \int_{-\infty}^{z} V_I(\vec{x}', \vec{\xi}_p, \vec{\xi}_T) dz'\right]_{+} \qquad (3.17)$$

where bracket [ ]$_+$ implies an ordering in analogy with time ordering, i.e., the argument with earlier z in V_I occurs to the left of the V_I with argument with later z. However, if the interactions V_I at different points along a straightline trajectory commute, then (3.12) becomes[44]

$$\phi \ (\vec{x}, \ \vec{\xi}_p, \ \vec{\xi}_T) = \exp \left[-\frac{i}{v} \ \int_\infty^\infty V_I(\vec{x'}, \ \vec{\xi}_p, \ \vec{\xi}_T) dz' \right] \qquad (3.18)$$

We will assume that the interactions along a straightline trajectory commute and replace the wave operator (3.17) by (3.18). A plausibility argument will be given to justify the above.

When the collision time is short compared to the period of orbital motion of the constituent nucleons, then the interactions V_I at two successive positions along a trajectory commute, i.e.[45,46]

$$\left[V_I(\vec{x'}, \ \vec{\xi}_p, \ \vec{\xi}_T) \ , \ V_I(\vec{x''}, \ \vec{\xi}_p, \ \vec{\xi}_T) \right] = 0 \qquad (3.19)$$

Ordering in (3.17) becomes inconsequential, and the upper limit in all the integrals can be replaced by infinity to yield (3.18). Using (3.18), we can rewrite (3.15) as

$$\vec{P}_{total} = \langle g_{p,m} \ (\vec{\xi}_p) \ g_{T,\mu}(\vec{\xi}_T) | \exp(-i\vec{k}\cdot\vec{x})$$

$$\exp \left(+i/v \ \int_\infty^\infty V_I(\vec{x'}, \ \vec{\xi}_p, \ \vec{\xi}_T) dz' \right) \left[-i \sum_{j=1}^{A_p} \vec{\nabla}_{\vec{\xi}_{p,j}} \right]$$

$$\exp \left(-i/v \ \int_\infty^\infty V_I(\vec{x'}, \ \vec{\xi}_p, \ \vec{\xi}_T) dz' \right) \exp (i\vec{k}\cdot\vec{x}) | \ g_{p,m'}(\vec{\xi}_p) \ g_{T,\mu'}(\vec{\xi}_T) \rangle$$
$$(3.20)$$

In the light of equations (2.43), (2.44) and (2.45) it may be instructive to look at the following decomposition of the potential matrix[42]

$$\overline{V} = \overline{V}_{diag} + \overline{V}_{off-diag} = \overline{V}_d + \overline{V}_{o.d.} \qquad (3.21)$$

where diagonal and off-diagonal elements have been indicated explic-
itly. It has been shown that for forward scattering at high
energies, the diagonal elements in $\bar{V}$ dominate over the off-diagonal
elements[40]

$$\bar{V}_{diag} \gg \bar{V}_{off\text{-}diag} \tag{3.22}$$

Then (3.20) can be written as

$$\vec{P}_{total} = \langle g_{p,m} (\vec{\xi}_p) \, g_{T,\mu}(\vec{\xi}_T) | \exp(-i\vec{k}\cdot\vec{x}) \quad \exp\left(i/v \int_{-\infty}^{\infty} (\bar{V}_d + \bar{V}_{o.d}) \, dz' \right)$$

$$\left[-i \sum_{j=1}^{A_p} \vec{\nabla}_{\xi_{p,j}} \right] \exp\left(-i/v \int_{-\infty}^{\infty} (\bar{V}_d + \bar{V}_{o.d}) dz' \right) \exp(+i\vec{k}\cdot\vec{x}) | g_{p,m'}(\vec{\xi}_p) \, g_{T,\mu}(\vec{\xi}) \rangle$$

$$= \langle g_{p,m}(\vec{\xi}_p) g_{T,\mu}(\vec{\xi}_T) | \exp\left(i/v \int_{-\infty}^{\infty} \bar{V}_d(\vec{x}', \vec{\xi}_p, \vec{\xi}_T) \, dz' \right)(1 + \frac{i}{v} \int_{-\infty}^{\infty} \bar{V}_{o.d} dz' + \dots)$$

$$\left[-i \sum_{j=1}^{A_p} \vec{\nabla}_{\xi_{p,j}} \right] \exp\left(-i/v \int_{-\infty}^{\infty} \bar{V}_d(\vec{x}', \vec{\xi}_p, \vec{\xi}_T) dz' \right)(1 - \frac{i}{v} \int_{-\infty}^{\infty} \bar{V}_{o.d} \, dz' + \dots)$$

$$x \mid g_{p,m'}(\vec{\xi}_p) \, g_{T,\mu'}(\vec{\xi}_T) \rangle \tag{3.23}$$

$$= \langle g_{p,m} (\vec{\xi}_p) \, g_{T,\mu}(\vec{\xi}_T) | \exp\left(i/v \int_{-\infty}^{\infty} \bar{V}_d(\vec{x}', \vec{\xi}_p, \vec{\xi}_T) dz' \right) \left[-i \sum_{j=1}^{A_p} \vec{\nabla}_{\xi_{p,j}} \right]$$

$$\exp\left(-i/v \int_{-\infty}^{\infty} V_d(\vec{x}', \vec{\xi}_p, \vec{\xi}_T) dz' \right) \mid g_{p,m}(\vec{\xi}_p) \, g_{T,\mu}(\vec{\xi}_T) \rangle \tag{3.24}$$

+ other terms.............

It is now obvious that the other terms in the series will involve
the off-diagonal elements which are smaller (by (3.22)). The first
term in the series involves only diagonal elements. In the spirit of

the coherent approximation[42], we shall retain only the first term in (3.24).

Now, applying the identity[45]

$$e^{iA} B e^{-iA} = B + i [A, B] + \frac{i^2}{2} [A, [A, B]] + \ldots \tag{3.25}$$

leads to

$$\vec{P}_{total} = \left\langle g_{p,m} (\vec{\xi}_p) g_{T,\mu}(\vec{\xi}_T) \left| -i \sum_{j=1}^{A_p} \vec{\nabla}_{\xi_{p,j}} \right| g_{p,m} (\vec{\xi}_p) g_{T,\mu} (\vec{\xi}_T) \right\rangle$$

$$- \left\langle g_{p,m} (\vec{\xi}_p) g_{T,\mu}(\vec{\xi}_T) \left| \sum_{j=1}^{A_p} \vec{\nabla}_{\xi_{p,j}} \int_{-\infty}^{\infty} V_d(\vec{x'}, \vec{\xi}_p, \vec{\xi}_T) \frac{dz'}{v} \right|$$

$$g_{p,m} (\vec{\xi}_p) g_{T,\mu}(\vec{\xi}_T) \right\rangle \tag{3.26}$$

Notice that the first term can be thought of as the momentum of the projectile before the collision. It may be taken to the left-hand side of (3.26) and momentum transfer defined as

$$\vec{P}_{total} - \vec{P}_{before} = \vec{P}_{transfer}$$

$$= - \left\langle g_{p,m} (\vec{\xi}_p) g_{T,\mu}(\vec{\xi}_T) \left| \sum_{j=1}^{A_p} \vec{\nabla}_{\xi_{p,j}} \int_{-\infty}^{\infty} V_d(\vec{x'}, \vec{\xi}_p, \vec{\xi}_T) \frac{dz'}{v} \right|$$

$$g_{p,m} (\vec{\xi}_p) g_{T,\mu}(\vec{\xi}_T) \right\rangle \tag{3.27}$$

$$= - \left\langle g_{p,o}(\vec{\xi}_p) g_{T,o}(\vec{\xi}_T) \left| \sum_{j=1}^{A_p} \vec{\nabla}_{\xi_{p,j}} \int_{-\infty}^{\infty} V_{opt}(\vec{x'}, \vec{\xi}_p, \vec{\xi}_T) \frac{dz'}{v} \right|$$

$$g_{p,o} (\vec{\xi}_p) g_{T,o}(\vec{\xi}_T) \right\rangle \tag{3.28}$$

where in the spirit of the optical model discussed in the last chapter,

$\psi_{m\mu} \simeq \psi_{oo}$ has been used in going from (3.27) to (3.28).

Having identified through equation (2.27) the optical potential

$$V_{opt} = \sum_{\alpha=1}^{A_T} \sum_{j=1}^{A_p} t_{\alpha j} \qquad (3.29)$$

we can substitute the above in equation (3.28) and obtain

$$\vec{P}_{transfer} = - <g_{p,o} (\vec{\xi}_p)\, g_{T,o}(\vec{\xi}_T) \left| \sum_{j=1}^{A_p} \vec{\nabla}_{\xi_{p,j}} \int_{-\infty}^{\infty} \sum_{\alpha=1}^{A_T} \sum_{j=1}^{A_p} \right.$$

$$\left. t_{\alpha j}\, (\vec{x}', \vec{\xi}_p, \vec{\xi}_T)\, \frac{dz'}{v} \right| g_{p,o} (\vec{\xi}_p)\, g_{T,o}(\vec{\xi}_T) > \qquad (3.30)$$

Equation (3.30) above is the desired expression for momentum transfer in the relativistic heavy ion collisions. Using the multiple scattering theory formulation of nucleus nucleus collisions of Wilson,[39,40] we have seen that the optical potential can be calculated in terms of transition amplitudes rather than two-body potentials. We obtained above an expression for momentum transfer in relativistic heavy ion collisions using these experimentally well determined transition amplitudes. Equation (3.30) has been explicitly evaluated in the Appendix, with the result expressed as $\vec{P}_{tran}^{\alpha j}$ and $\vec{P}_{tran} = \sum_{\alpha j} \vec{P}_{tran}^{\alpha j}$ where $\vec{P}_{tran}^{\alpha j}$ is the momentum transfer in the collision between αth and jth constituents. Explicitly, these are given by

$$\vec{P}_{tran}^{\alpha j} = -\int d^3\vec{\xi}_p\, \rho_j(\vec{\xi}_p) \int d^3\vec{\xi}_T\, \rho_\alpha(\vec{\xi}_T) \left[\vec{\nabla}_{\xi_p} \int_{-\infty}^{\infty} t_{\alpha j}\, (\vec{x} + \vec{\xi}_p - \vec{\xi}_T)\, \frac{dz'}{v} \right]$$

$$(3.31)$$

where α and j refer to the αth and jth constituents of the target and projectile, respectively; $\rho_\alpha(\vec{\xi}_T)$ and $\rho_j(\vec{\xi}_p)$ are their single particle densities, and the gradient is with respect to projectile coordinates only. The total momentum transfer is

$$\vec{P}_{tran} = - \sum_\alpha \sum_j \vec{P}^{\alpha j}_{tran}$$

$$= - (A_p A_T) \int d^3\vec{\xi}_p \rho_p(\vec{\xi}_p) \int d^3\vec{\xi}_T \rho_T(\vec{\xi}_T) \left[\vec{\nabla}_{\xi_p} \int_{-\infty}^{\infty} \tilde{t} \ (\vec{x}', \ \vec{\xi}_{p'}, \vec{\xi}_T) \ \frac{dz'}{v} \right]$$

$$(3.32)$$

where $\rho \ (\vec{\xi}_p)$ and $\rho \ (\vec{\xi}_T)$ are the nuclear densities of the projectile and target with mass numbers A_p and A_T, respectively, and the two-body transition amplitude $t_{\alpha j}$ has been averaged over constituent type as

$$\tilde{t} = (A_p A_T)^{-1} \left[Z_p Z_T \ t_{pp} + N_p N_T \ t_{nn} + (N_p Z_T + N_T Z_p) \ t_{np} \right] \qquad (3.33)$$

with Z_p, Z_T the projectile and target charge numbers; N_p, N_T the neutron numbers and A_p, A_T the mass numbers, respectively. (The notation for the transition amplitudes is t_{pp} for proton-proton, t_{nn} for neutron-neutron, and t_{np} for neutron-proton.)

A unique feature of this work is the use of the two-body transition amplitude (in (3.32)) which is complex. The constituent averaged two-body transition amplitude is obtained from the first order t-matrix used in previous studies of nucleus-nucleus collisions as

$$\tilde{t}\ (e,\ \vec{x})\ =\ -\ \sqrt{e/m}\ \ \sigma(e)\ \boxed{\alpha(e)\ +\ i}\ \boxed{2\pi B(e)}^{-3/2}\ \exp(-\ \frac{\vec{x}^2}{2B(e)}) \tag{3.34}$$

where e is the two-nucleon kinetic energy in their center of mass frame; $\sigma(e)$ is the nucleon-nucleon total cross section; $\alpha(e)$ is the ratio of the real to the imaginary part of the forward scattering amplitude, and B(e) is the nucleon-nucleon slope parameter. Values for these parameters, taken from various compilations, are listed in references 39-42.

The resulting momentum transfer, equation (3.32), where the transition amplitude (3.34) appears is also complex. The real part of the momentum transfer, which comes from the real part of the complex optical potential, is the contribution arising from elastic scattering. It is purely transverse. The imaginary component, which comes from the absorptive part of the complex optical potential, is the longitudinal momentum transfer. To show this, we symbolically rewrite equation (3.32) as

$$\vec{P}_{transfer}\ =\ (Q_R\ +\ i\ Q_I)\ \hat{b} \tag{3.35}$$

where $i = \sqrt{-1}$ and $\hat{b}$ is the unit vector transverse to the beam direction. If $\hat{z}$ denotes the beam direction (with $-\hat{z}$ the source) then we know that

$$i\hat{b}\ =\ -\ \hat{z} \tag{3.36}$$

since $i = \sqrt{-1}$ is an operator which rotates a unit vector counter clockwise through $\pi/2$ radians.[47] Therefore (3.35) becomes

$$\vec{P}_{transfer} = Q_R \, \hat{b} - Q_I \, \hat{z} \tag{3.37}$$

which can be relabelled as

$$\vec{P}_{transfer} = Q_\perp \, \hat{b} - Q_\| \, \hat{z} \tag{3.38}$$

The transverse ($Q_\perp$) and longitudinal ($Q_\|$) components can be immediately written as

$$Q_\perp = - A_p A_T \int d^3\vec{\xi}_p \, \rho_p(\vec{\xi}_p) \int d^3\vec{\xi}_T \, \rho_T(\vec{\xi}_T) \left[\vec{\nabla}_{\xi_p} \int_{-\infty}^{\infty} Re \, \tilde{t} \, (\vec{x}' + \vec{\xi}_p - \vec{\xi}_T) \, \frac{dz'}{v} \right]$$

$$\tag{3.39}$$

and

$$Q_\| = - A_p A_T \int d^3\vec{\xi}_p \, \rho_p(\vec{\xi}_p) \int d^3\vec{\xi}_T \, \rho_T(\vec{\xi}_T) \left[\vec{\nabla}_{\xi_p} \int_{-\infty}^{\infty} Im \, \tilde{t} \, (\vec{x}' + \vec{\xi}_p - \vec{\xi}_T) \, \frac{dz'}{v} \right]$$

$$\tag{3.40}$$

The above has a close analogy in optics where complex refractive index is used to account for absorption. The resulting attenuation of the incident wave is then along the direction of incidence. Similarly, momentum loss due to inelastic scatterings and absorption as the projectile traverses through the target is in the longitudinal direction, while the elastic scattering gives rise to transverse momentum transfer (specially true at high energy where forward scattering dominates).

IIIb. Energy Transfer

Having developed the formalism for momentum transfer, we shall also find an expression for energy transfer (excitation energy) to the projectile. Again, our basis will be the multiple scattering theory framework discussed previously. We will assume in light of the discus-

sion in Appendix B that the sudden approximation is valid, i.e., colli-
sion time t_{coll} is short compared with the period of orbital motion of
nucleons in the nucleus. This is best evaluated by taking the expecta-
tion value of the sum of nucleon energy operators (the internal
Hamiltonian of the projectile H_p) with approximate wave functions given
by (3.14).

$$E = \langle \psi \, (\vec{x}, \vec{\xi}_p, \vec{\xi}_T) \left| -\frac{1}{2m_n} \sum_{j=1}^{A_p} \vec{\nabla}_{\xi_{p,j}}^2 + \sum_{i<j} V_{ij} \right| \psi \, (\vec{x}, \vec{\xi}_p, \vec{\xi}_T) \rangle \qquad (3.41)$$

Expanding the above yields

$$E = \langle g_{p,m}(\vec{\xi}_p) \, g_{T,\mu}(\vec{\xi}_T) \left| \exp \, (-i\vec{k}\cdot\vec{x}) \, \exp \left(i/v \int_{-\infty}^{\infty} V_I(\vec{x}', \, \vec{\xi}_p, \, \vec{\xi}_T) dz' \right) \right.$$

$$\left[-\frac{1}{2m_n} \sum_{j=1}^{A_p} \vec{\nabla}_{\xi_{p,j}}^2 + \sum_{i<j} V_{ij} \right] \exp \left(-i/v \int_{-\infty}^{\infty} V_I \, (\vec{x}', \, \vec{\xi}_p, \, \vec{\xi}_T) dz' \right)$$

$$\exp \, (i\vec{k}\cdot\vec{x}) \left| g_{p,m'}(\vec{\xi}_p) \, g_{T,\mu'}(\vec{\xi}_T) \rangle \right.$$

$$= \langle g_{p,m}(\vec{\xi}_p) \, g_{T,\mu}(\vec{\xi}_T) \left| \exp \left(i/v \int_{-\infty}^{\infty} (V_d + V_{o.d}) dz' \right) \right[-\frac{1}{2m_n} \sum_{j=1}^{A_p} \vec{\nabla}_{\xi_{p,j}}^2$$

$$+ \sum_{i<j} V_{ij} \right] \exp \left(-i/v \int_{-\infty}^{\infty} (V_d + V_{o.d}) dz' \right) \left| g_{p,m'}(\vec{\xi}_p) \, g_{T,\mu}(\vec{\xi}_T) \rangle \right.$$

$$\cong \langle g_{p,o}(\vec{\xi}_p) \, g_{T,o}(\vec{\xi}_T) \left| \exp \left(i/v \int_{-\infty}^{\infty} V_{opt} \, (\vec{x}', \, \vec{\xi}_p, \, \vec{\xi}_T) dz' \right) \times \right.$$

$$\left[-\frac{1}{2m_n} \sum_{j=1}^{A_p} \vec{\nabla}^2_{\xi_{p,j}} + \sum_{i<j} V_{ij} \right] \exp\left(-i/v \int_{-\infty}^{\infty} V_{opt} \; (\vec{x}', \; \vec{\xi}_p, \; \vec{\xi}_T) dz' \right)$$

$$\times \Bigg| \; <g_{p,o} \; (\vec{\xi}_p) \; g_{T,o}(\vec{\xi}_T)> \qquad\qquad (3.42)$$

The explicit derivation of the above expressions is detailed in Appendix A. The final result for energy transfer is

$$E^* = E - E_o + 0 \; (\frac{1}{A_p})$$

$$\cong \frac{1}{2m_n} \; <g_{p,o} \; (\vec{\xi}_p) \; g_{T,o}(\vec{\xi}_T) \Bigg| \; \sum_{j=1}^{A_p} \left(\vec{\nabla}_{\xi_{p,j}} \int_{-\infty}^{\infty} V_{opt} \; (\vec{x}', \; \vec{\xi}_p, \; \vec{\xi}_T) \; \frac{dz'}{v} \right)^2$$

with

$$\Bigg| \; g_{p,o} \; (\vec{\xi}_p) \; g_{T,o}(\vec{\xi}_T) > \; + 0 \; (\frac{1}{A_p}) \qquad (3.43)$$

$$E_o = <g_{p,o} \; (\vec{\xi}_p) \; g_{T,o}(\vec{\xi}_T) \Bigg| - \frac{1}{2m_n} \sum_{j=1}^{A_p} \vec{\nabla}^2_{\xi_{p,j}} + \sum_{i<j} V_{ij} \Bigg| g_{p,o}(\vec{\xi}_p) \; g_{T,o}(\vec{\xi}_T)>$$

$$(3.44)$$

Evaluation of the above equation for E^* yields an expression for energy transfer as

$$E^* = \frac{1}{2m_n} A_p A_T \int d^3\vec{\xi}_p \; \rho_p(\vec{\xi}_p) \int d^3\vec{\xi}_T \; \rho_T(\vec{\xi}_T) \left[\vec{\nabla}_{\xi_p} \int_{-\infty}^{\infty} \tilde{t} \; (\vec{x}', \; \vec{\xi}_p, \; \vec{\xi}_T) \; \frac{dz'}{v} \right]^2$$

$$(3.45)$$

where the definition of V_{opt}, equation (3.29) has been used, and we neglect terms $0(1/A_p)$. All the symbols above have been defined in our previous derivation in section IIIa.

CHAPTER IV

NUMERICAL RESULTS ON MOMENTUM AND ENERGY TRANSFER DISTRIBUTIONS

In this chapter, we address specifically the momentum and energy transfer distributions in nuclear fragmentation reactions. Having studied in Chapter II the multiple scattering theory of nucleus nucleus collisions and in Chapter III the formulation of the problem of energy and momentum transfer in heavy ion collisions based on the multiple scattering theory, we shall discuss a variety of topics in heavy ion reactions with these insights. First, we briefly review the experimental situation as it pertains to our topics of interest. We next discuss the currently available theories of heavy ion fragmentation reactions. We present calculations on the momentum and energy transfer distributions in relativistic heavy ion collisions and indicate how to incorporate our results in the existing theoretical framework. Our primary focus will be on the momentum spectra of fragments, including the effects of momentum transfer on the spectra. Input parameters are briefly discussed next. Numerical results on momentum "downshifts" and widths are presented for a variety of projectile-target combinations and compared with experiment.

IV.a The Experimental and Theoretical Background

Most of our information on fragmentation reactions comes from single particle inclusive reactions of the type[48-51]

$$\text{Beam} + \text{Target} \rightarrow \text{Fragment} + \text{Other Products} \qquad (4.1)$$

Two concepts stand out in describing the projectile (or target) fragmentation data. They are called "limiting fragmentation" and "factorization," respectively. "Limiting fragmentation" implies that distribution of fragments approaches a limiting form as the bombarding energy is increased. "Factorization" means that the cross section for production of a particular fragment (written as σ_{FBT}) is a product of a factor γ_T which depends on the target and γ_B^F which depends on the beam and fragment, i.e.

$$\sigma_{FBT} = \gamma_T \, \gamma_B^F \qquad (4.2)$$

Further analysis[52] suggests that another prescription, called "weak factorization" could better describe the data

$$\sigma_{FBT} = \gamma_B^F \, \gamma_B^T \qquad (4.3)$$

where γ_B^T depends both on the beam and the target.

Experimental measurements[19] of widths and means of longitudinal and transverse momentum spectra of fragments of ^{12}C and ^{16}O on targets ranging from H through Pb revealed the following features. In the projectile rest frame, the longitudinal momentum distributions for all fragments from ^{12}C and ^{16}O (with the exception of protons) show, irrespective of beam energy and target, the following characteristics:

(a) Gaussian shape, with root mean square widths $\sigma(P_{\parallel}) \simeq 50$ to 200 MeV/c and downshifts $<P_{\parallel}> = -20$ to -130 MeV/c. Thus the mean velocities of the fragments are less than that of the beam.

(b) Rms widths $\sigma(P_{\parallel})$ and $\sigma(P_{\perp})$ are equal to an accuracy of 10%, consistent with isotropic production of fragments.

(c) $\sigma(P_{\parallel})$ and $\langle P_{\parallel}\rangle$ are independent of target mass and beam energy but depend on the beam and fragment.

The general trend of the widths $\sigma(P_{\parallel})$ is reproduced by a parabolic dependence on the fragment mass where

$$\sigma(P_{\parallel}) = 2\sigma_0 \ [x(1-x)]^{1/2} \quad ; \quad x = \frac{A_F}{A_p} = \frac{\text{Fragment mass number}}{\text{Projectile mass number}} \quad (4.4)$$

where σ_0 is a constant.

The parabolic dependence has been explained by a variety of theoretical approaches[20-22] including the conservation of momentum. Feshbach and Huang[20] and later Goldhaber[22] pointed out that the Gaussian momentum distributions could be understood by treating the fragmenting nucleus as a Fermi gas and assuming (a) momentum conservation (b) no correlation among nucleons and (c) neglect of antisymmetrization of the single particle distributions. Based on this model, the parabolic dependence of the widths $\sigma(P_{\parallel})$ on fragment mass A_F could be reproduced (as in equation (4.4)), as well as the isotropy $\sigma(P_{\parallel}) \simeq \sigma(P_{\perp})$ could be understood. More importantly, Goldhaber[22] also pointed out that the widths and means of momentum distributions could be modified according to

$$\sigma_x'^2 = \sigma_x^2 + \frac{F^2}{A^2} \, Q_x^2 \qquad (4.5a)$$

$$P_x' = P_x + \frac{F}{A} \, Q_x \qquad (4.5b)$$

where σ_x^2 is the unmodified Gaussian width, $\sigma_x'^2$ is the modified width, Q_x is the momentum transfer in any direction x; F and A are the frag-

ment and parent mass numbers respectively and unmodified widths are

related to Fermi momentum P_F of the parent as

$$\sigma_x^2 = \frac{F(A-F)}{A} \sigma_o^2 \tag{4.6a}$$

$$' \quad = \frac{F(A-F)}{A} \frac{P_F^2}{5} \tag{4.6b}$$

The longitudinal momentum downshift is given by (4.5b) as

$$\Delta P_{\|} = P_{\|}' - P_{\|} = -\frac{F}{A} Q_{\|} \tag{4.7}$$

where $Q_{\|}$ is the magnitude of the longitudinal momentum transfer

obtained from equation (3.40). Recalling that $Q_{\|}$ is a function of

impact parameter, an appropriate method for choosing it for each frag-

ment is necessary. Before that however, we shall present input parame-

ters required in our calculation. (Note the comprehensive list of

references 53-88 on the experimental and theoretical overview of the

subject).

IV.c. Input Parameters

Having derived expressions for momentum and energy transfer, we

shall use them to calculate quantities of interest.

The NN transition amplitude in coordinate space has been intro-

duced in equation (3.34) and the notation explained.

Values of $\sigma(e)$, $\alpha(e)$ and $B(e)$ are discussed in references 62 and

86, including an estimate of experimental uncertainty. Average values

are given by

$$\sigma(e) = \frac{1}{(A_p + A_T)} \ [(Z_p + Z_T) \ \sigma_{pp}(e) + (N_p + N_T)\sigma_{np}(e)] \tag{4.8a}$$

$$\alpha(e) = \frac{[(Z_p + Z_T) \ \sigma_{pp}(e) \ \alpha_{pp}(e) + (N_p + N_T) \ \sigma_{np}(e) \ \alpha_{np}(e)]}{(A_p + A_T) \ [\sigma_{pp}(e) + \sigma_{np}(e)]} \tag{4.8b}$$

Some representative values are listed in Table 1. In addition, the "non-diffractive" slope parameters B(e) from these references will be replaced by "diffractive" slope parameters

$$B(e) = \left[10 + .5 \ \ln \ (S'/S_0) \right] (GeV/c)^{-2} \tag{4.9}$$

with $S_0 \simeq 1 \ (GeV/c)^{-2}$ and S' = square of the NN center of mass energy. This is because diffractive slope parameters are appropriate for scattering near forward directions. The single particle densities are related to the nuclear wave function by

$$\rho_{A_p} (\vec{r}) = \frac{1}{A_p} \sum_{\alpha=1}^{A_p} \ <g_0(\vec{\xi}_p) \ | \ \delta \ (\vec{r} - \vec{r}_\alpha) \ | \ g_0(\vec{\xi}_p)> \tag{4.10a}$$

$$\rho_{A_T} (\vec{s}) = \frac{1}{A_T} \sum_{j=1}^{A_T} \ <g_0(\vec{\xi}_T) \ | \ \delta \ (\vec{s} - \vec{s}_j) \ | \ g_0(\vec{\xi}_T)> \tag{4.10b}$$

for the projectile and target, respectively. The above are understood as

$$\rho_{A_p} (\vec{r}) = \frac{1}{A_p} \left[N_p \ \rho_n(\vec{r}) + Z_p \ \rho_p(\vec{r}) \right] \tag{4.11a}$$

$$\rho_{A_T} (\vec{s}) = \frac{1}{A_T} \left[N_T \ \rho_n(\vec{s}) + Z_T \ \rho_p(\vec{s}) \right] \tag{4.11b}$$

where Z_p, N_p are the projectile proton and neutron numbers and Z_T, N_T are the target proton and neutron numbers, respectively. We assume for

Table 1. Values of NN input parame::ters $\sigma(e)$ for NN — np and NN—pp for various incident energies. Data from compilations in references 62,86.

E_{inc} (A GeV)	$\sigma_{np}(e)$ (mb)	σ_{pp} (e) (mb)
.025	378.255	130.31
.050	140.38	41.00
.075	98.35	39.63
.100	71.73	27.23
.125	59.15	23.83
.150	52.09	24.13
.175	46.59	23.79
.200	42.80	23.09
.225	40.09	22.45
.250	37.94	22.21
.275	36.29	22.37
.300	35.15	22.78
.400	34.03	25.19
.500	34.82	32.46
.600	36.03	39.28
.700	36.98	43.02
.800	37.84	45.51
.900	38.76	47.01
1.000	39.68	47.65
2.000	42.96	45.18
3.000	43.19	42.50

light nuclei $\rho_n (\vec{r}) \simeq \rho_p (\vec{r})$ since Coulomb repulsion by protons plays only a small role in light nuclei. Proton densities are taken from compilation of charge radii from electron scattering experiments. The effect of finite proton radius is taken into account by extracting the matter densities according to reference 62. The nuclear charge density is taken as

$$\rho_{c,A}(\vec{r}) - \int \rho_p (\vec{r'}) \, \rho_A (\vec{r} + \vec{r'}) \, d^3 \vec{r'} \tag{4.12}$$

where $\rho p(\vec{r'})$ is the proton charge density.

In this work, the densities of nuclei for $A \geq 20$ was taken to be of the Woods-Saxon type

$$\rho(r) - \rho_o \left[1 + \exp\left(\frac{r - R}{a}\right) \right]^{-1} \tag{4.13}$$

with R the half density radius and a related to the skin thickness as $t - 4.4a$. For $A < 20$, Harmonic-well densities were used. The parameters are listed in Table 2.

IV.c. Numerical Results

A. Momentum Downshifts

Experimental data on momentum downshifts are available[19] for the fragmentation of ^{16}O and ^{12}C on targets ranging from H through Pb. In Figures 1-18, momentum transfers to $^{16}O(2.1$ A GeV), $^{12}C(2.1$ A GeV) and ^{12}C (1.05 A GeV) projectiles are plotted as a function of impact parameter b (fm). Momentum transfer is in units of MeV/c. Longitudinal and transverse momentum transfers are shown separately.

Table 2:   Nuclear charge distribution parameters
from electron scattering data
(HW — Harmonic-well; WS — Woods-Saxon)

Nucleus	Distribution	γ (HW) or t, fm (WS)	a, fm (HW) or R, fm (WS)
^{9}Be	HW	.611	1.791
^{12}C	HW	1.247	1.649
^{16}O	HW	1.544	1.833
^{27}Al	WS	2.501	3.05
^{64}Cu	WS	2.504	4.20
^{108}Ag	WS	2.354	5.139
^{139}La	WS	2.354	5.71
^{208}Pb	WS	2.416	6.624

Harmonic-well: $\rho_c(r) = \rho_0 \left(1 + \gamma \left(\dfrac{r}{a}\right)^2\right) \exp\left(\dfrac{-r^2}{a^2}\right)$.

Woods-Saxon: $\rho_c(r) = \rho_0 \left[1 + \exp\left(\dfrac{r-R}{a}\right)\right]^{-1}$
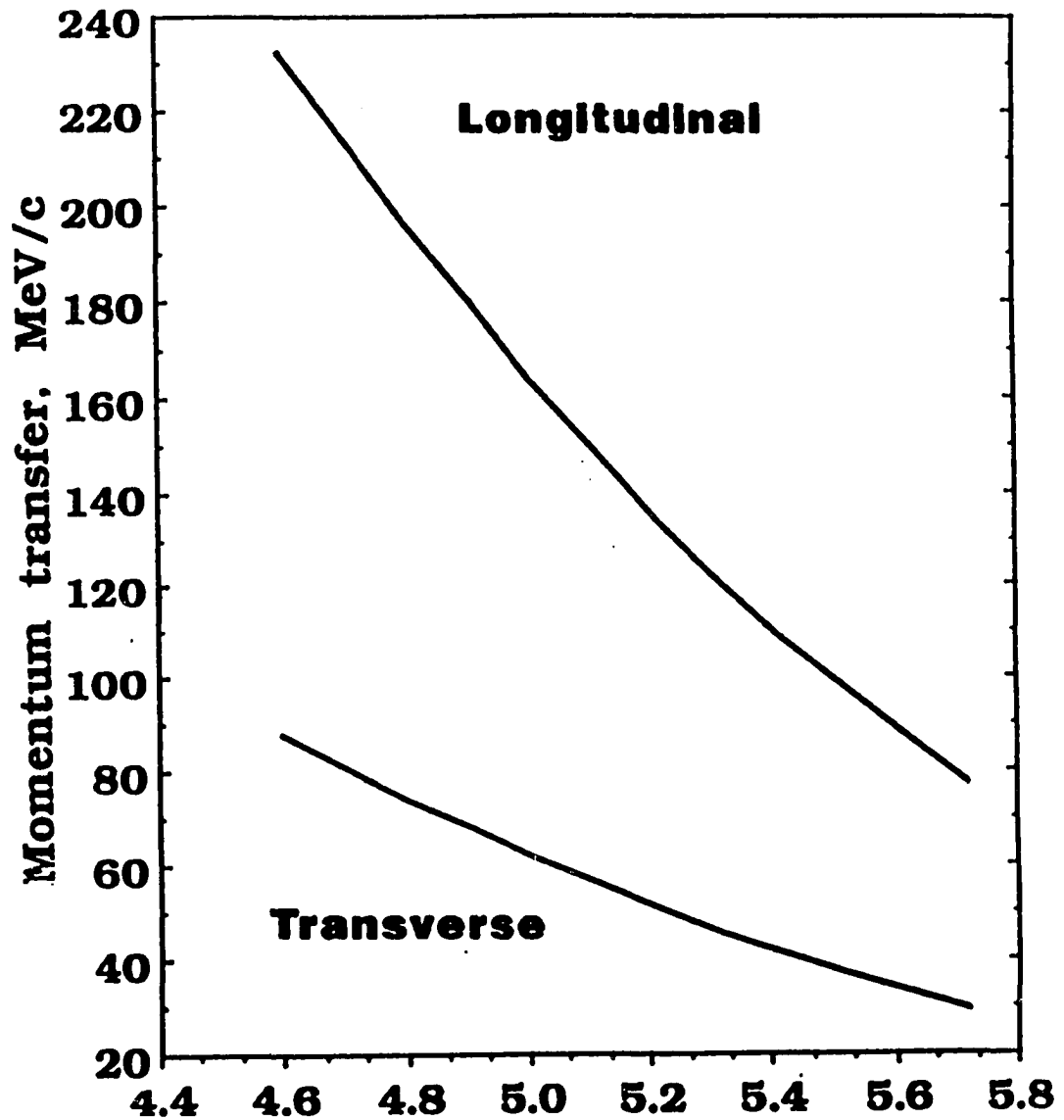
Figure I: Momentum transfer (MeV/c) to ^{16}O projectile by the ^9Be target as a function of impact parameter (fm) in the reaction ^{16}O (2.1 AGeV) + ^9Be → Projectile Fragment + X, where X is unidentified. Harmonic-well densities were used for both the projectile and the target.

Momentum transfer (MeV/c) to ^{16}O projectile by the ^{12}C target as a function of impact parameter (fm) in the reaction ^{16}O (2.1 AGeV) + ^{12}C → Projectile Fragment + X, where X is unidentified. Harmonic-well densities were used for both the projectile and the target.

Figure 3: Momentum transfer (MeV/c) to ^{16}O projectile by the Al target as a function of impact parameter (fm) in the reaction ^{16}O (2.1 AGeV) + Al → Projectile Fragment + X, where X is unidentified. Harmonic-well density was used for the projectile and Woods-Saxon density for the target.

Figure 4: Momentum transfer (MeV/c) to ^{16}O projectile by the Cu target as a function of impact parameter (fm) in the reaction ^{16}O (2.1 AGeV) + Cu → Projectile Fragment + X, where X is unidentified. Harmonic-well density was used for the projectile and Woods-Saxon density for the target.

Fig. 5 Momentum transfer (MeV/c) to ^{16}O projectile by the Ag target as a function of Impact parameter (fm) In the reaction ^{16}O (2.1 AGeV) + Ag → Projectile Fragment + X, where X Is unidentified. Harmonic-well density was used for the projectile and Woods-Saxon density for the target.

Figure 6: Momentum transfer (MeV/c) to ^{16}O projectile by the Pb target as a function of impact parameter (fm) in the reaction ^{16}O (2.1 AGeV) + Pb → Projectile Fragment + X, where X is unidentified. Harmonic-well density was used for the projectile and Woods-Saxon density for the target.
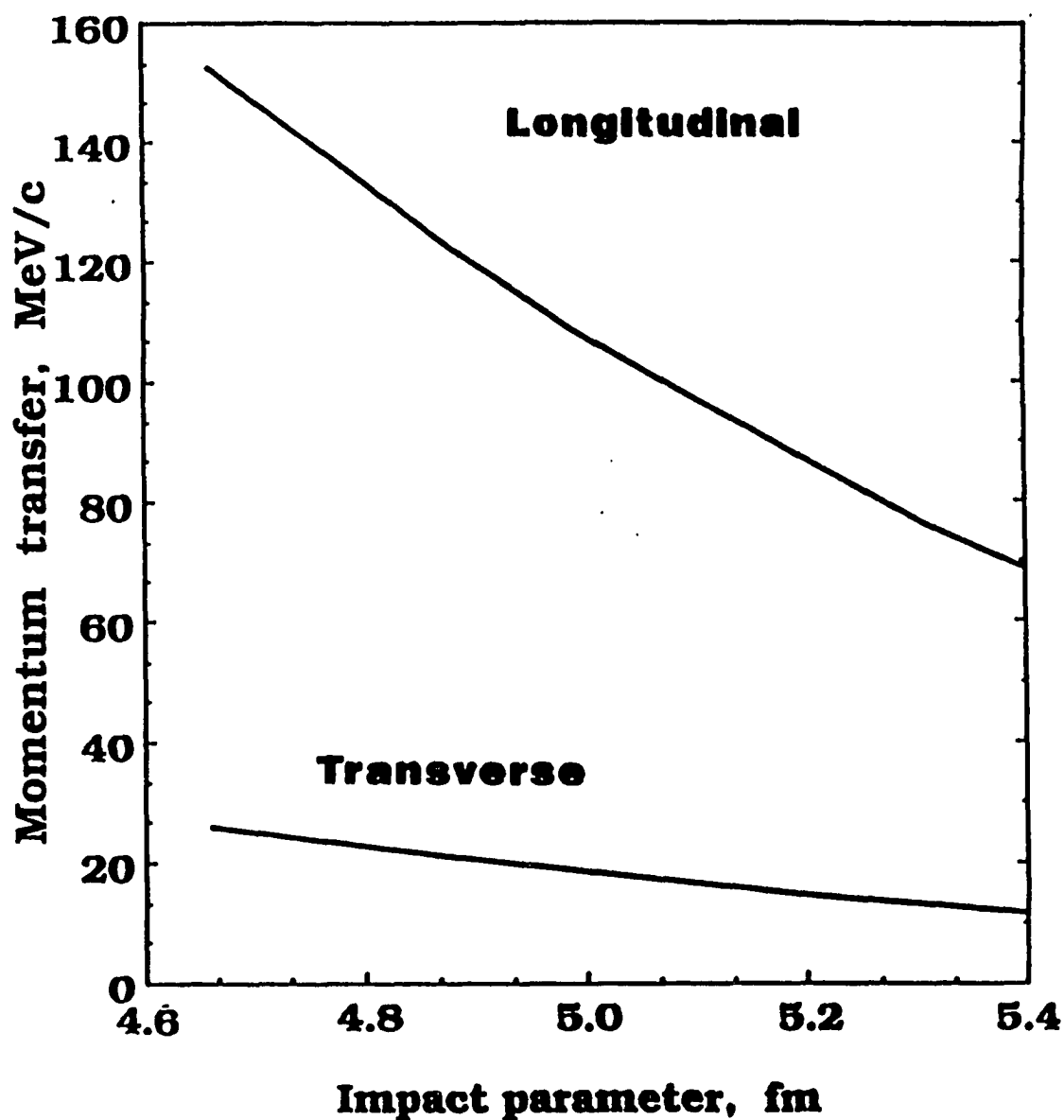
Figure 7: Momentum transfer (MeV/c) to ^{12}C projectile by the Be target as a function of impact parameter (fm) in the reaction ^{12}C (1.05 AGeV) + ^9Be → Projectile Fragment + X, where X is unidentified. Harmonic-well densities were used for both the projectile and the target.
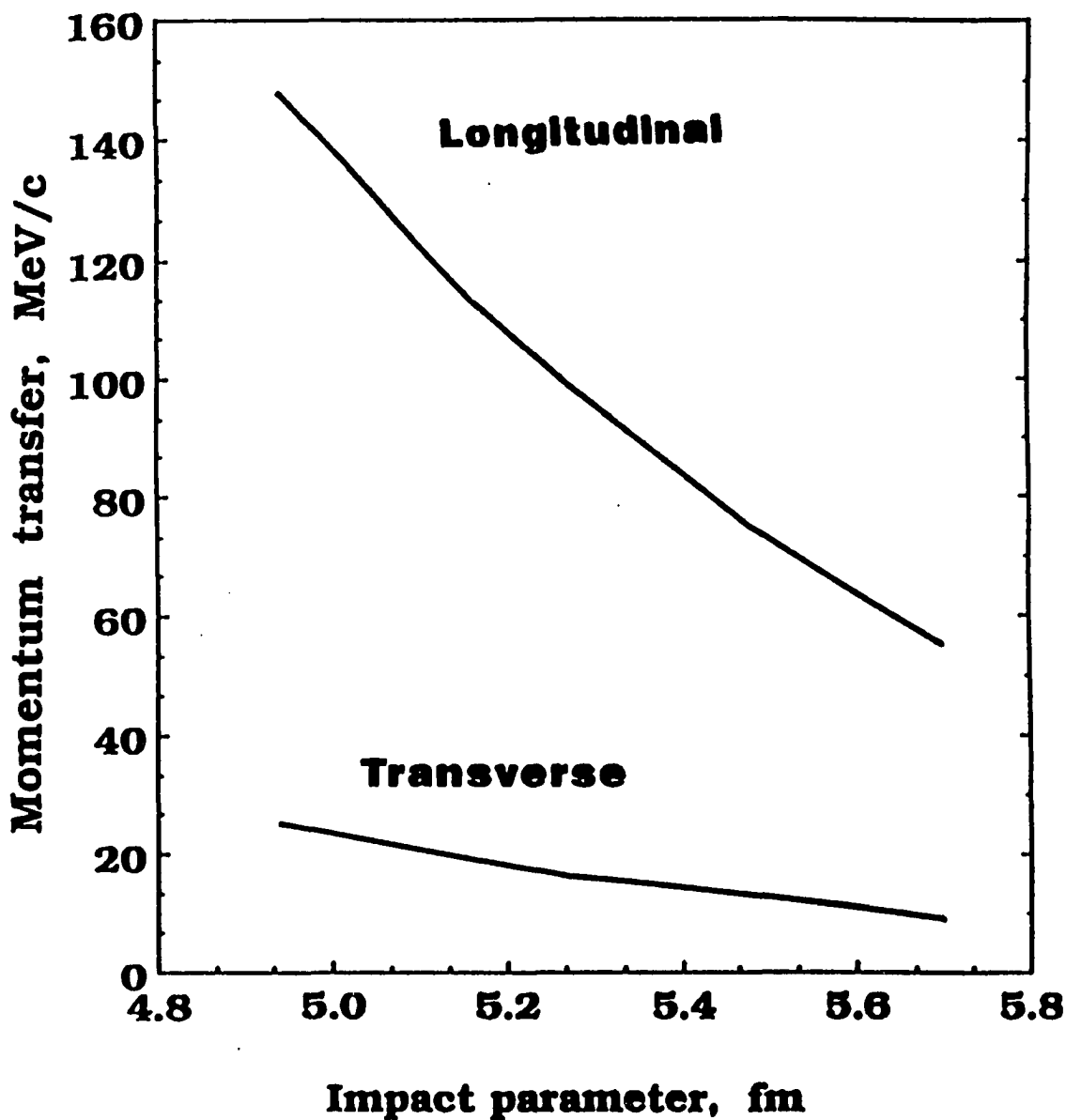
Figure 8:   Momentum transfer (MeV/c) to ^{12}C projectile by the ^{12}C target as a function of impact parameter (fm) in the reaction ^{12}C (1.05 AGeV) + $^{12}C \rightarrow$ Projectile Fragment + X, where X is unidentified. Harmonic-well densities were used for both the projectile and the target.

Figure 10: Momentum transfer (MeV/c) to ^{12}C projectile by the Cu target as a function of impact parameter (fm) in the reaction ^{12}C (1.05 AGeV) + Cu → Projectile Fragment + X, where X is unidentified. Harmonic-well density was used for the projectile, and Woods-Saxon was used for the target.
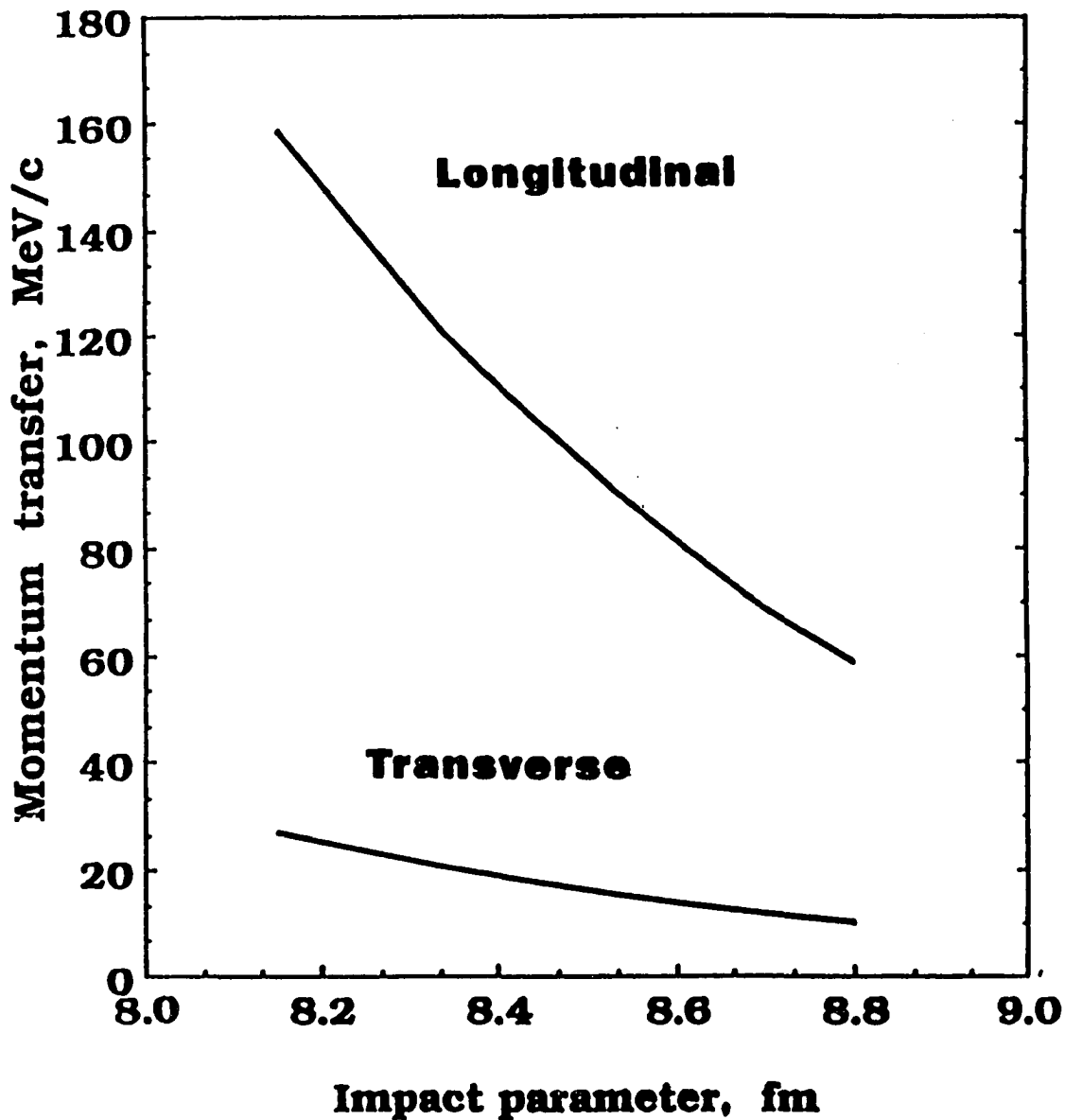
Figure 11: Momentum transfer (MeV/c) to ^{12}C projectile by the Ag target as a function of impact parameter (fm) in the reaction ^{12}C (1.05 AGeV) + Ag → Projectile Fragment + X, where X is unidentified. Harmonic-well density was used for the projectile, and Woods-Saxon was used for the target.
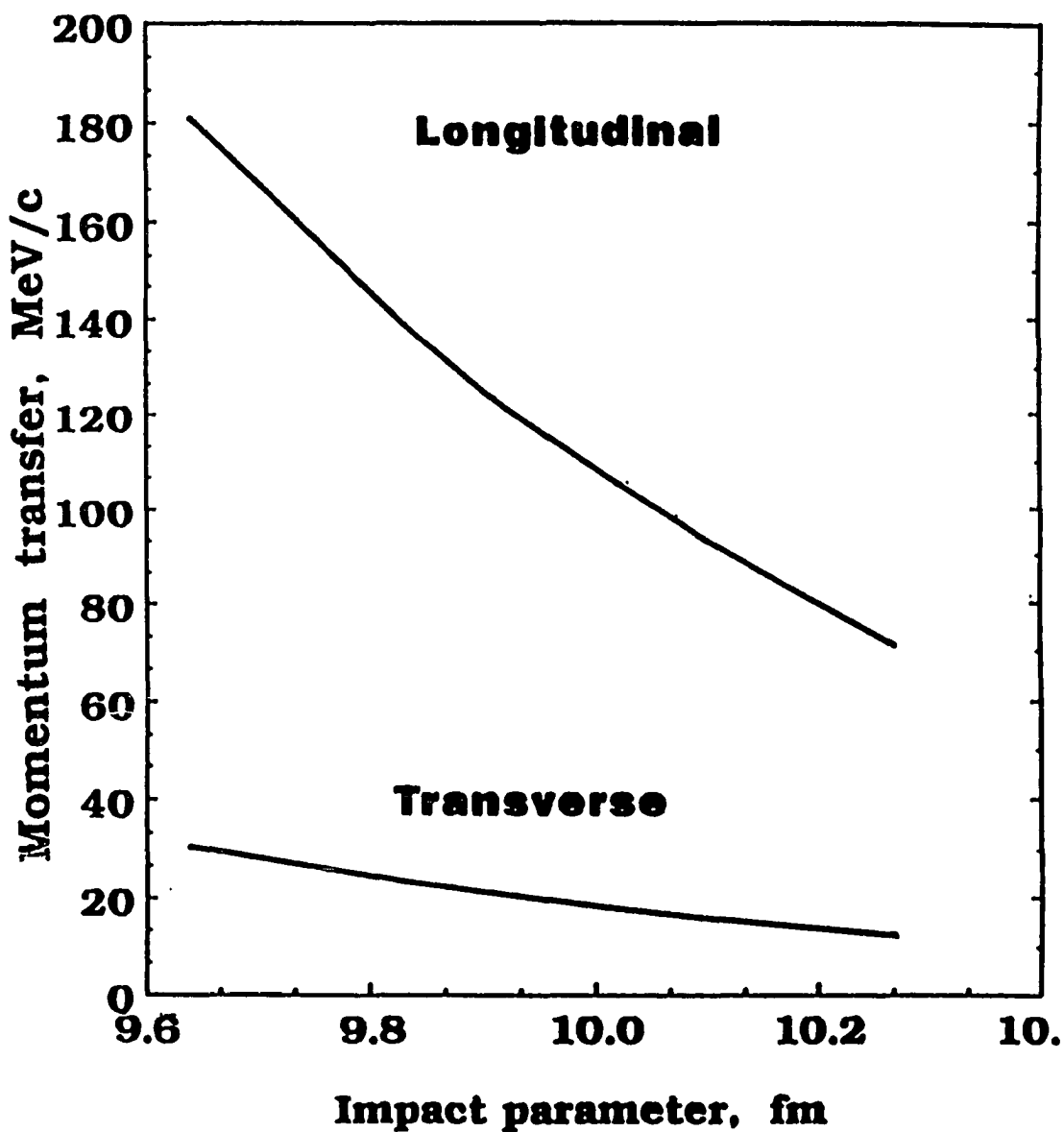
Fig. 12 Momentum transfer (MeV/c) to ^{12}C projectile by the Pb target as a function of impact parameter (fm) in the reaction ^{12}C (1.05 AGeV) + Pb → Projectile Fragment + X, where X is unidentified. Harmonic-well density was used for the projectile, and Woods-Saxon was used for the target.
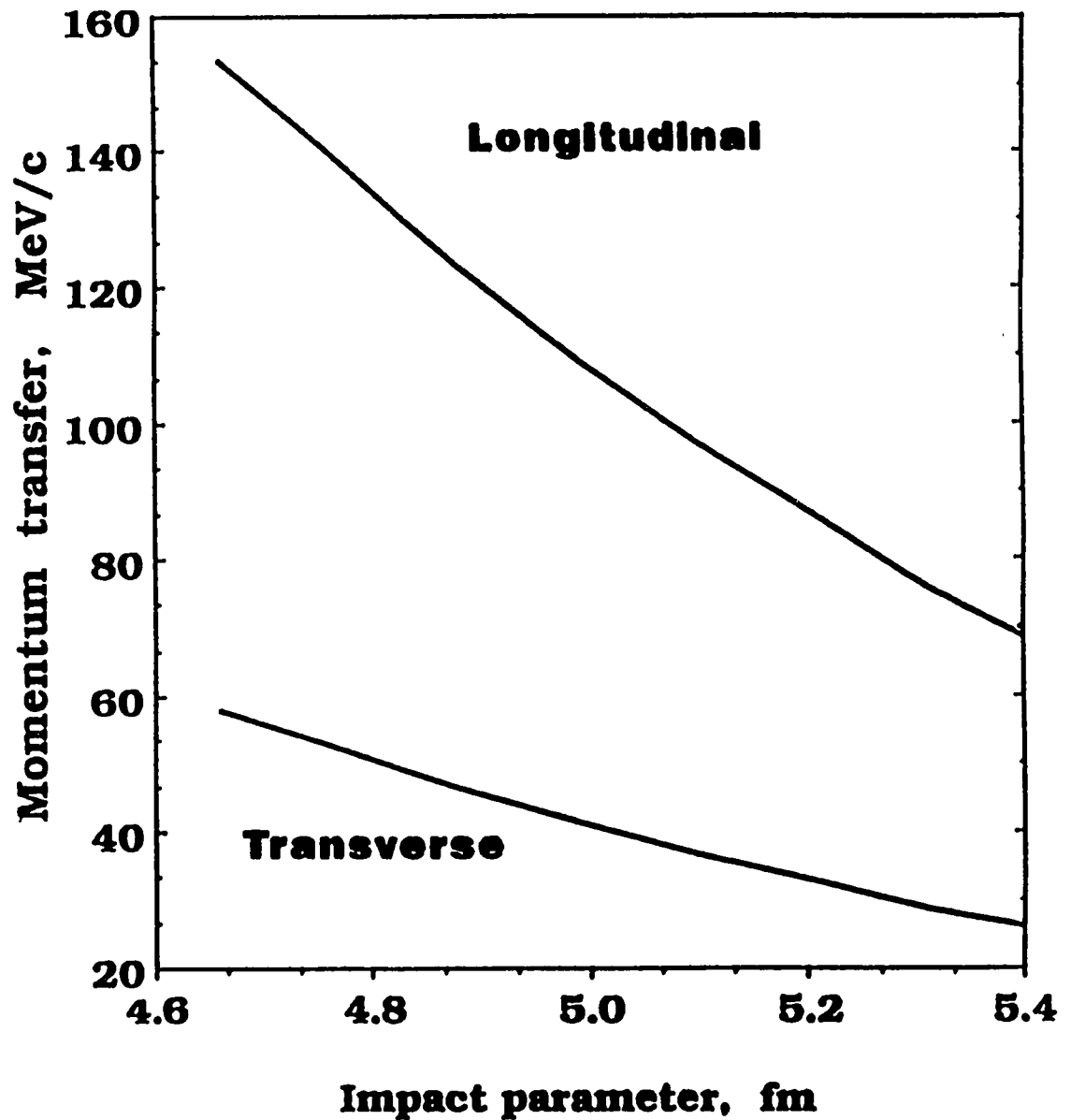
Figure 13: Momentum transfer (MeV/c) to ^{12}C projectile by the Be target as a
function of impact parameter (fm) in the reaction ^{12}C (2.1 AGeV) + ^{9}Be
→ Projectile Fragment + X, where X is unidentified. Harmonic-well
densities were used for both the projectile and the target.
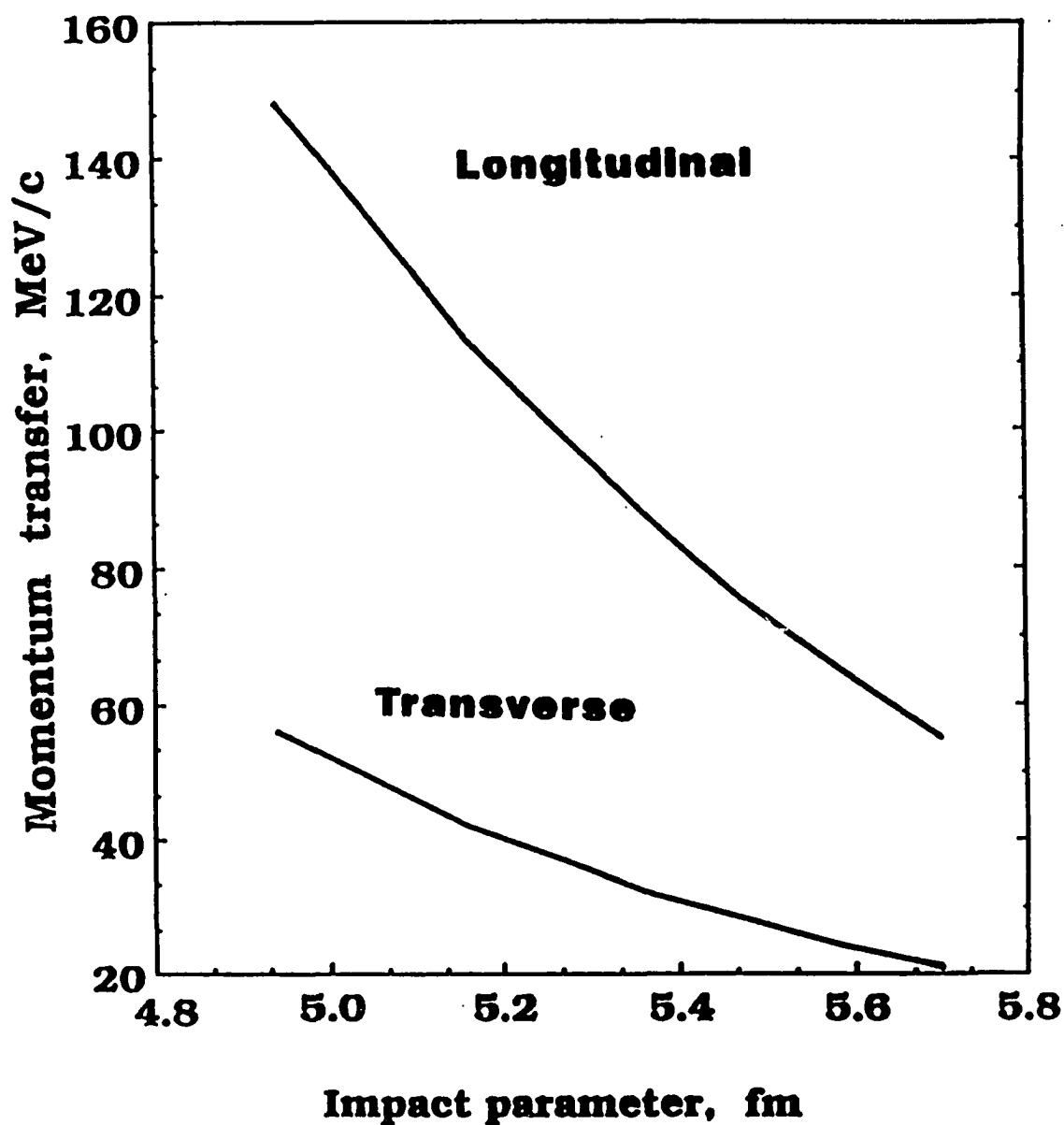
Figure 14: Momentum transfer (MeV/c) to ^{12}C projectile by the ^{12}C target as a function of impact parameter (fm) in the reaction ^{12}C (2.1 AGeV) + ^{12}C→ Projectile Fragment + X, where X is unidentified. Harmonic-well densities were used for both the projectile and the target.
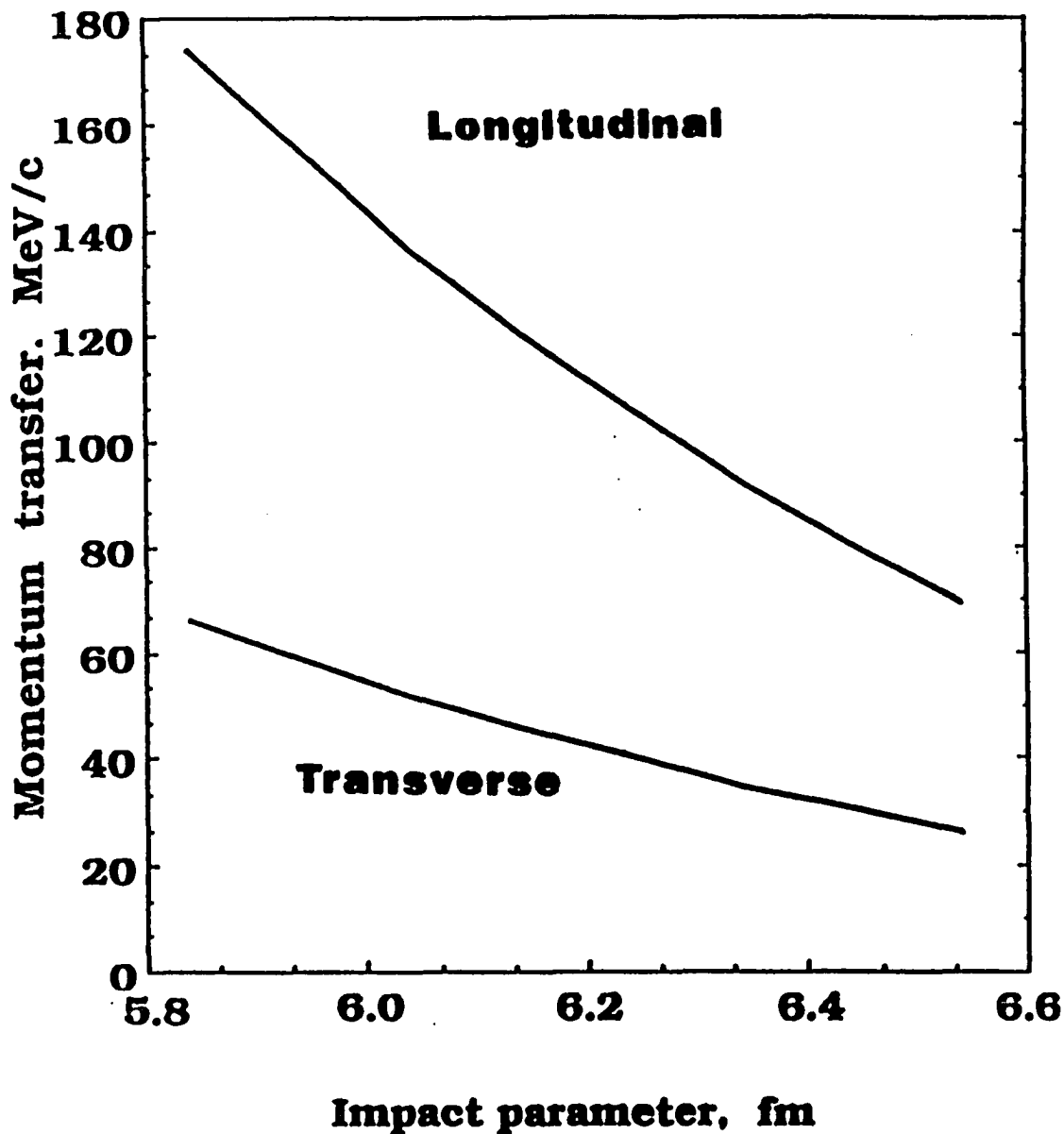
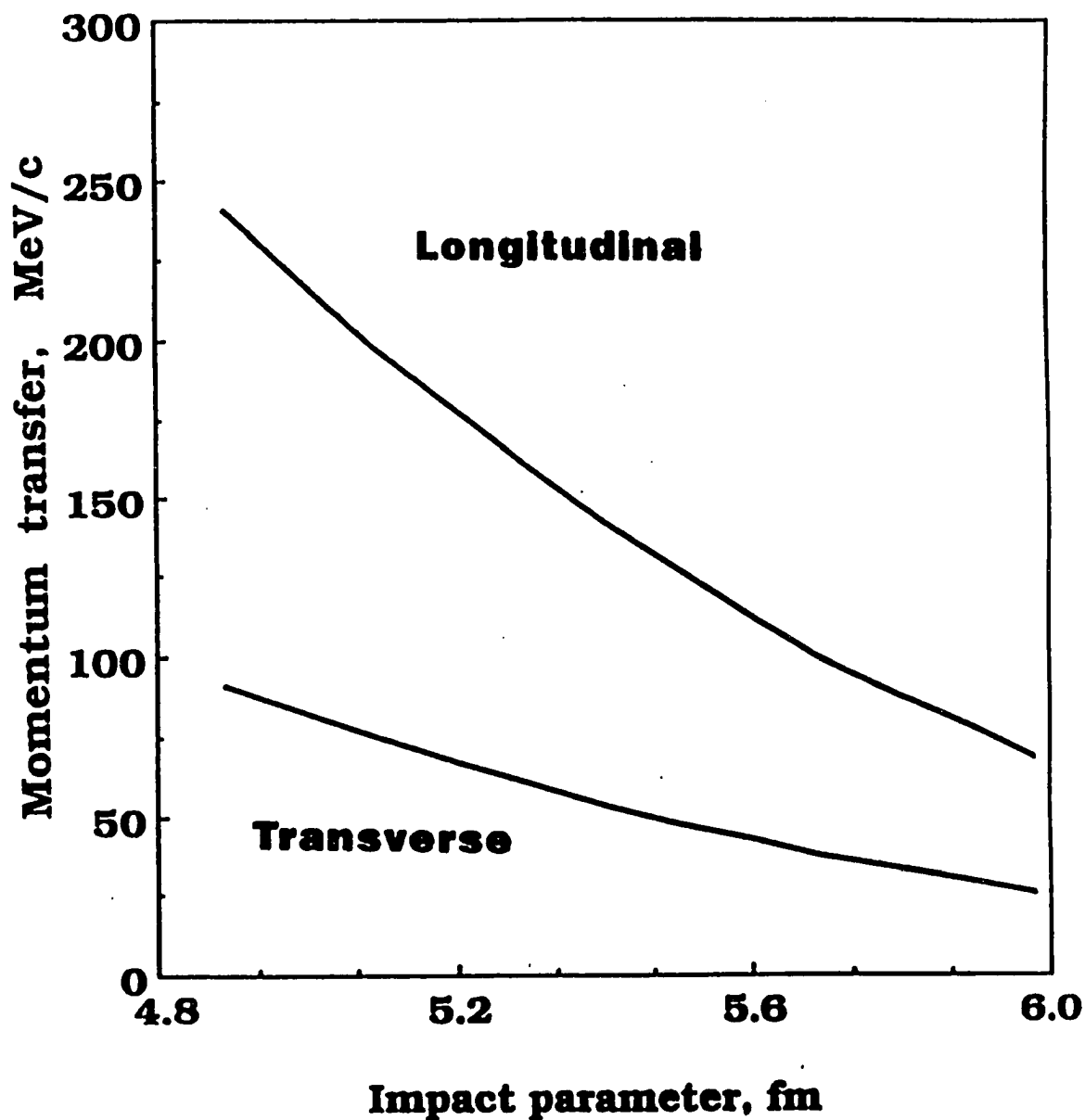Fig. 15 Momentum transfer (MeV/c) to ^{12}C projectile by the ^{27}Al target as a function of impact parameter (fm) in the reaction ^{12}C (2.1 AGeV) + ^{27}Al → Projectile Fragment + X, where X is unidentified. Harmonic-well density was used for the projectile, and Woods-Saxon was used for the target.
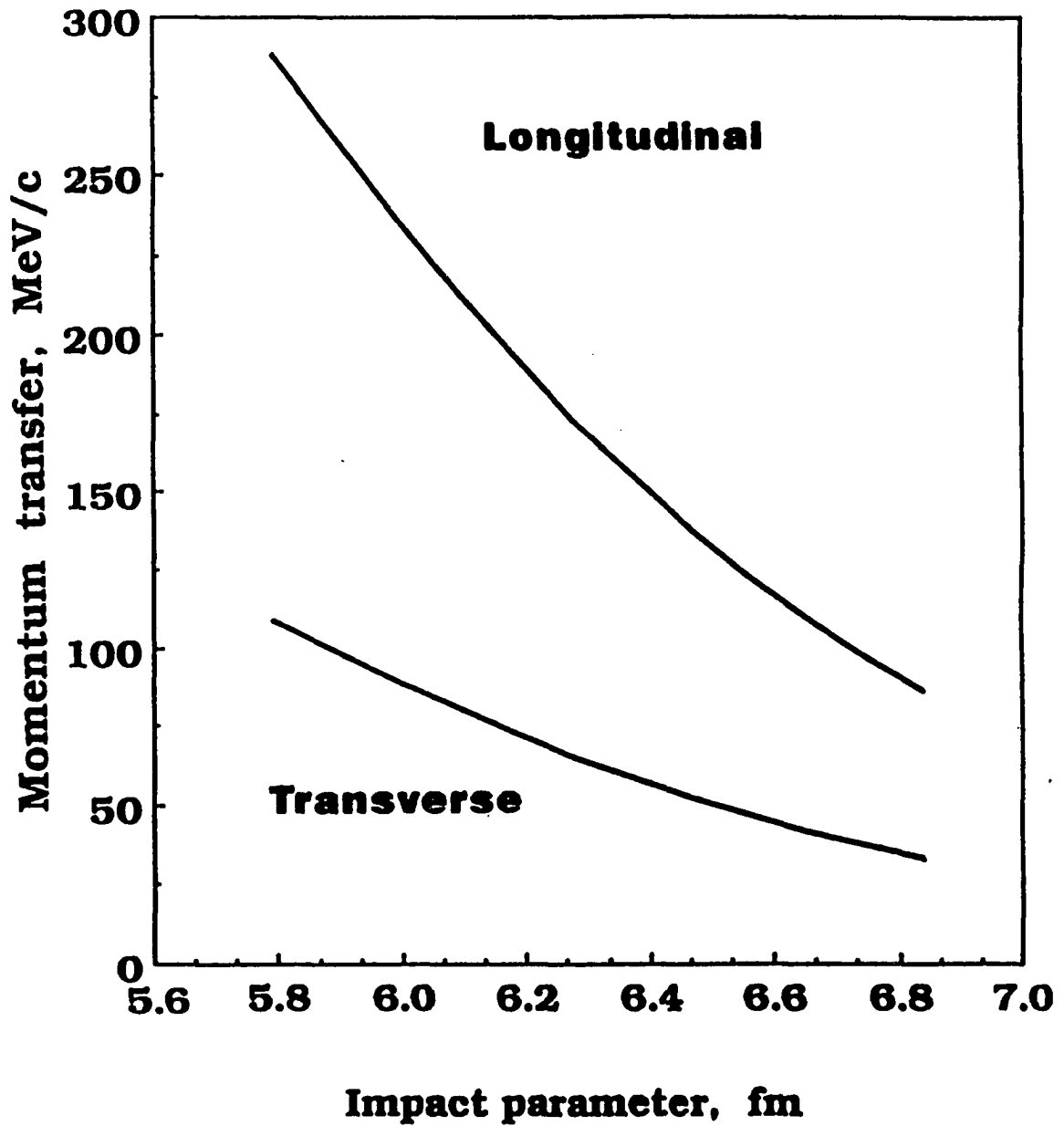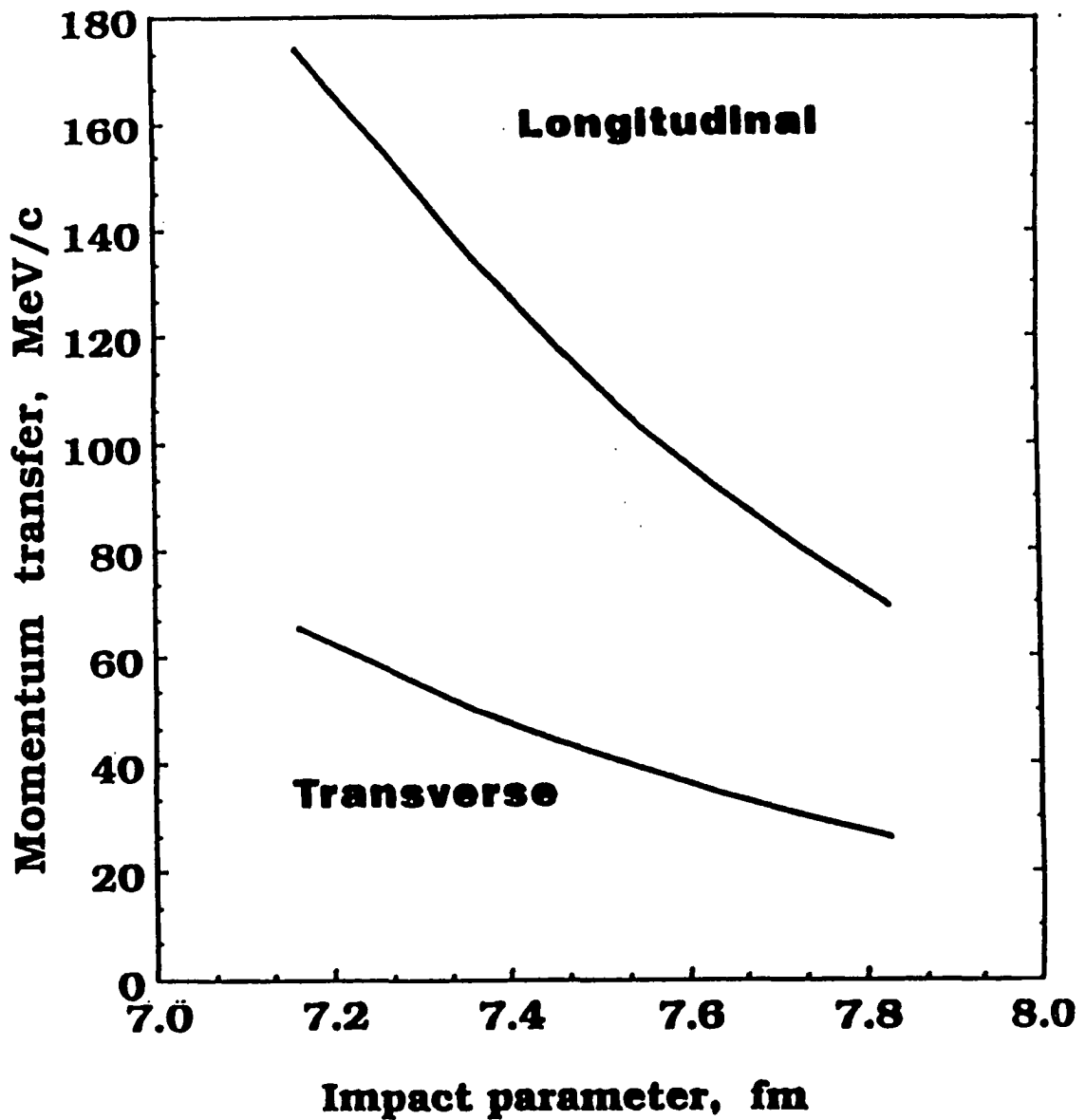
Figure 16: Momentum transfer (MeV/c) to ^{12}C projectile by the Cu target as a function of impact parameter (fm) in the reaction ^{12}C (2.1 AGeV) + Cu → Projectile Fragment + X, where X is unidentified. Harmonic-well density was used for the projectile, and Woods-Saxon was used for the target.
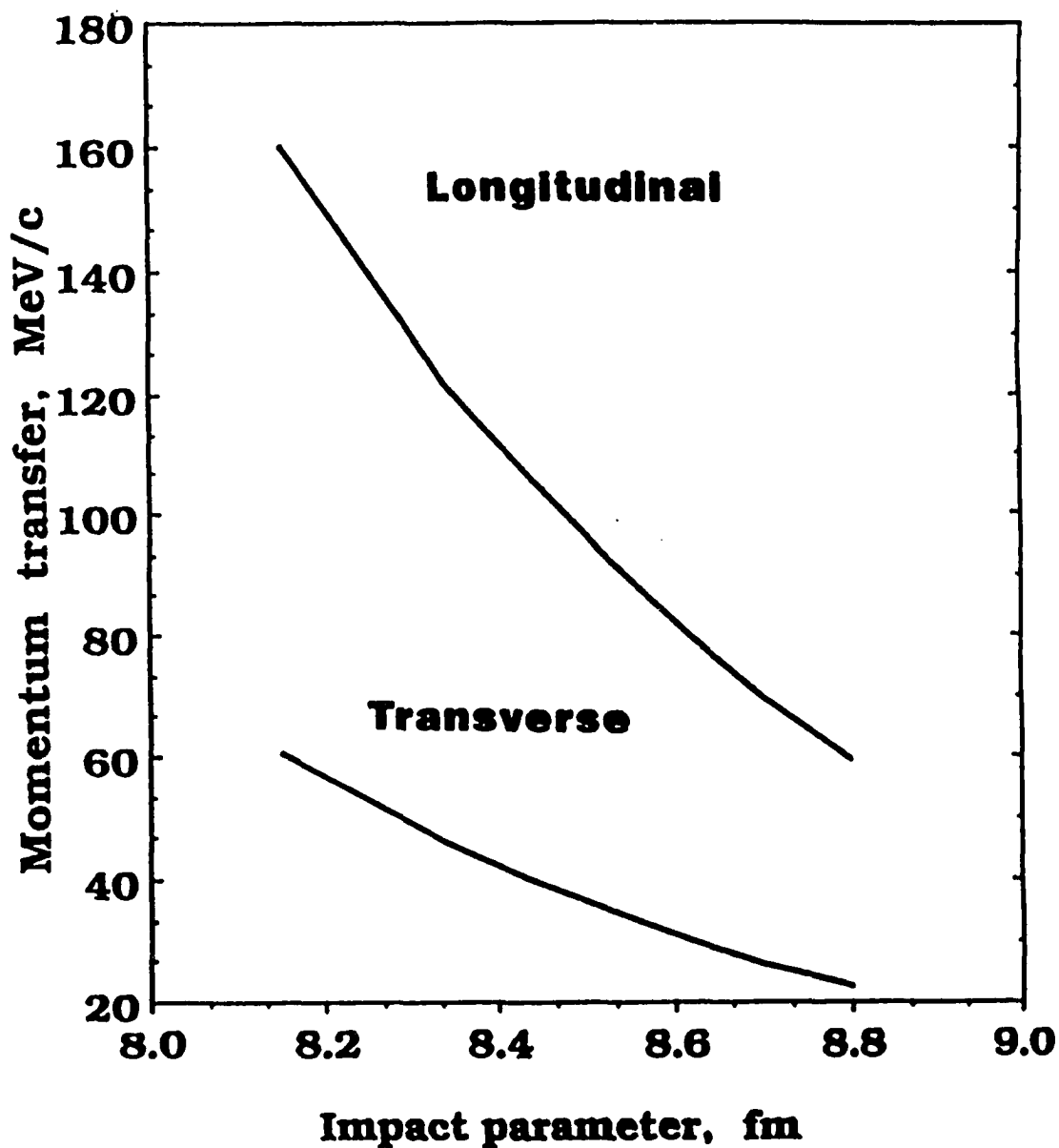
Fig. 17   Momentum transfer (MeV/c) to ^{12}C projectile by the Ag target as a
function of impact parameter (fm) in the reaction ^{12}C (2.1 AGeV) + Ag
→ Projectile Fragment + X, where X is unidentified. Harmonic-well
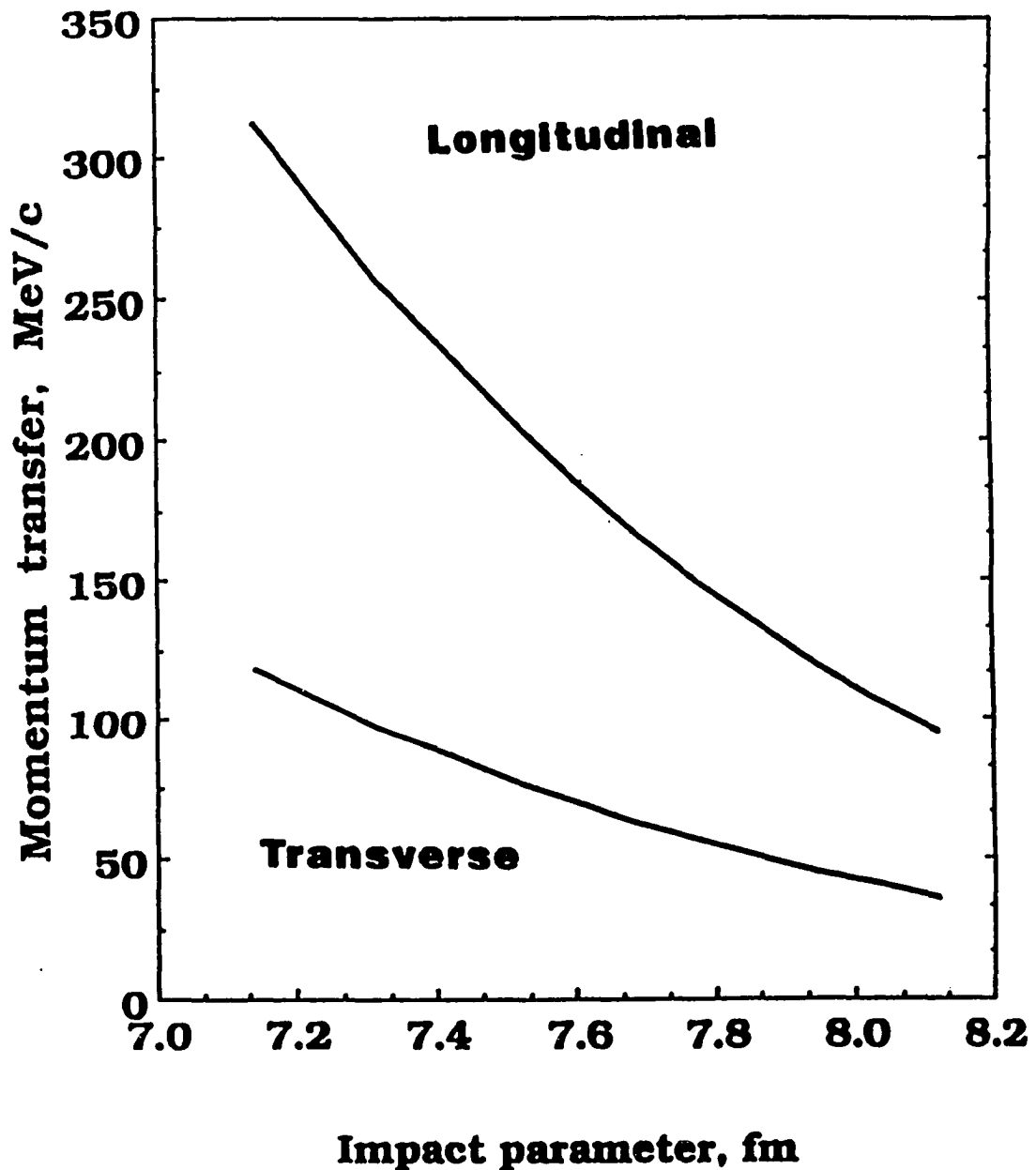density was used for the projectile, and Woods-Saxon was used for the
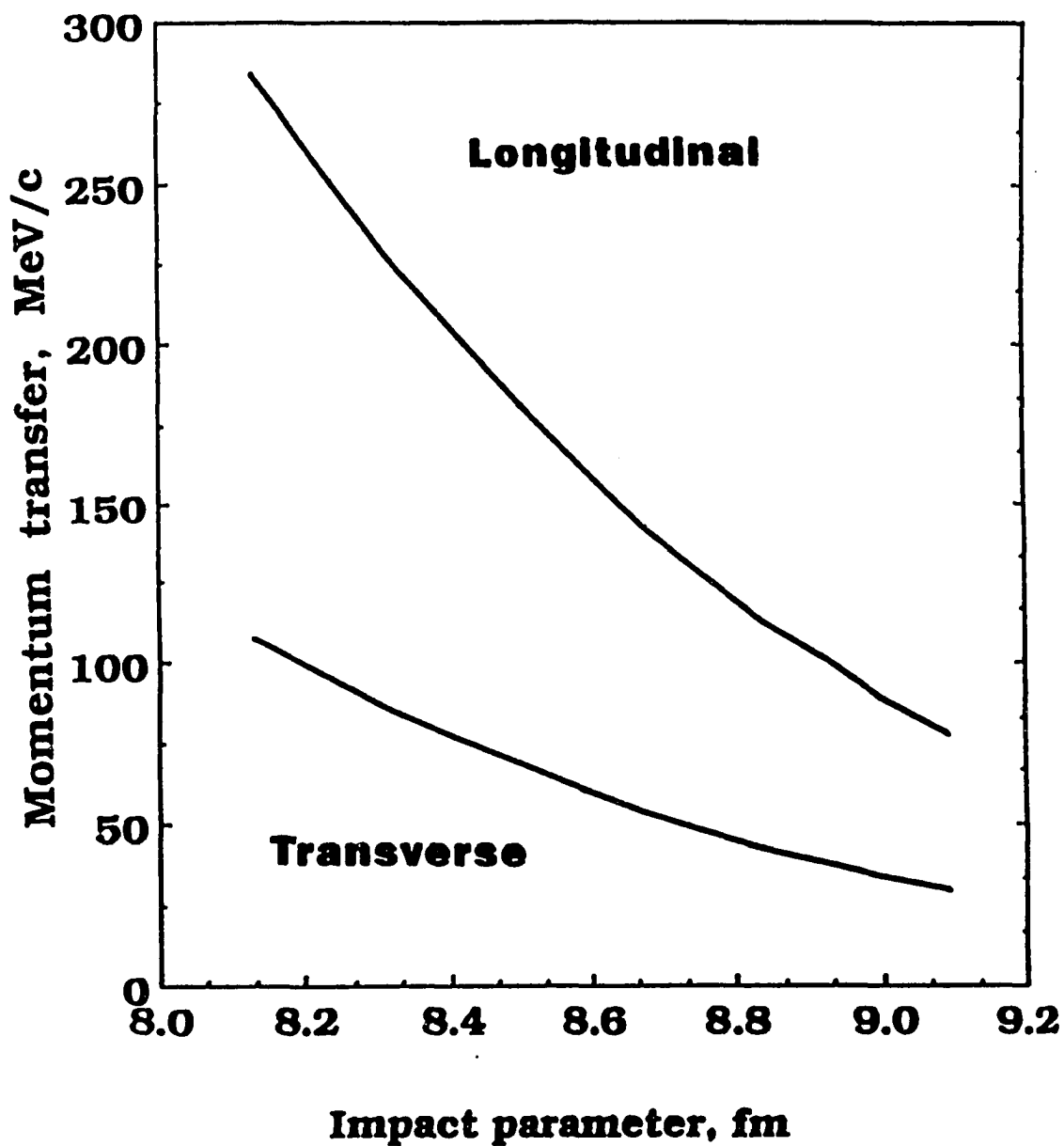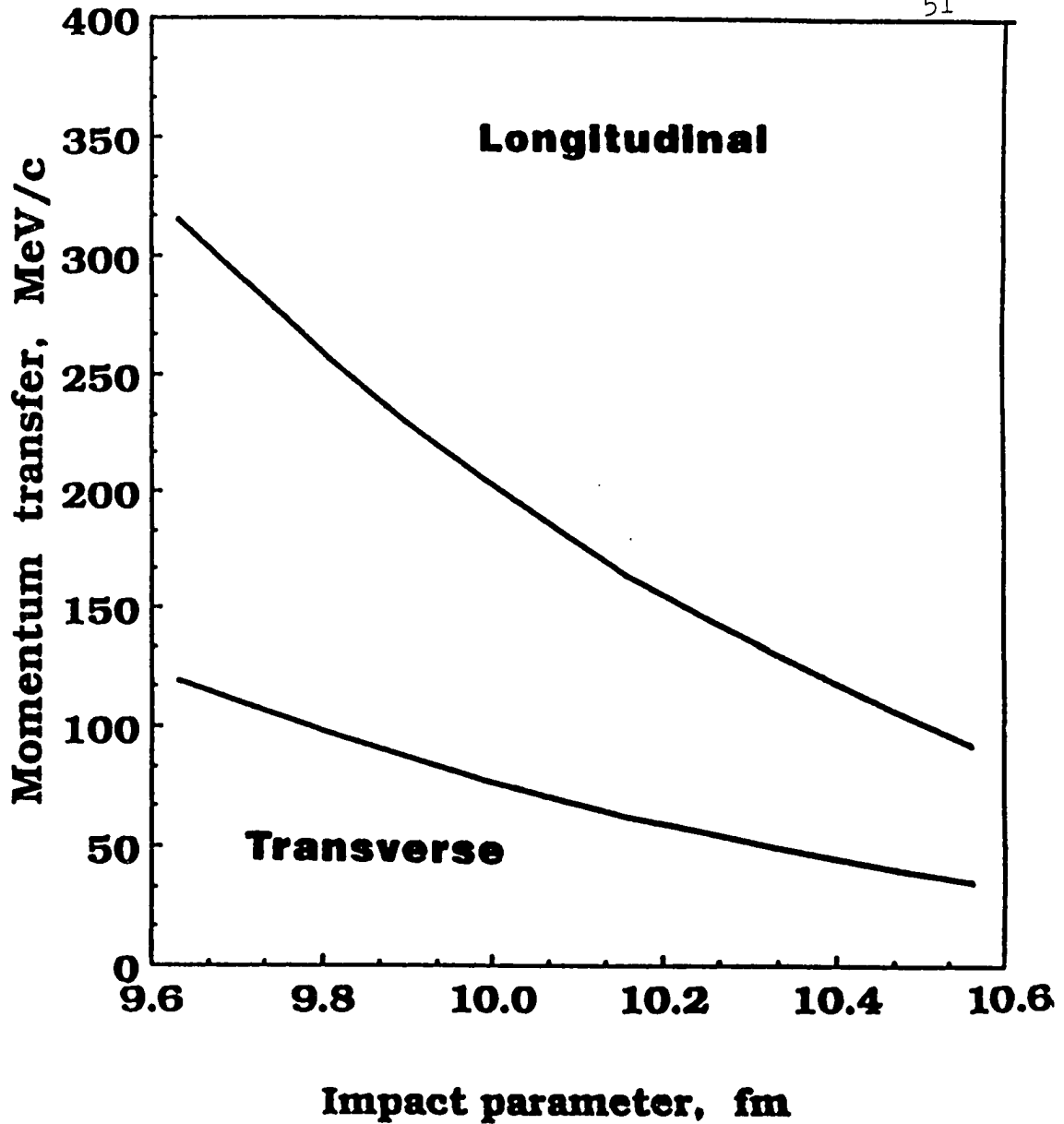target.
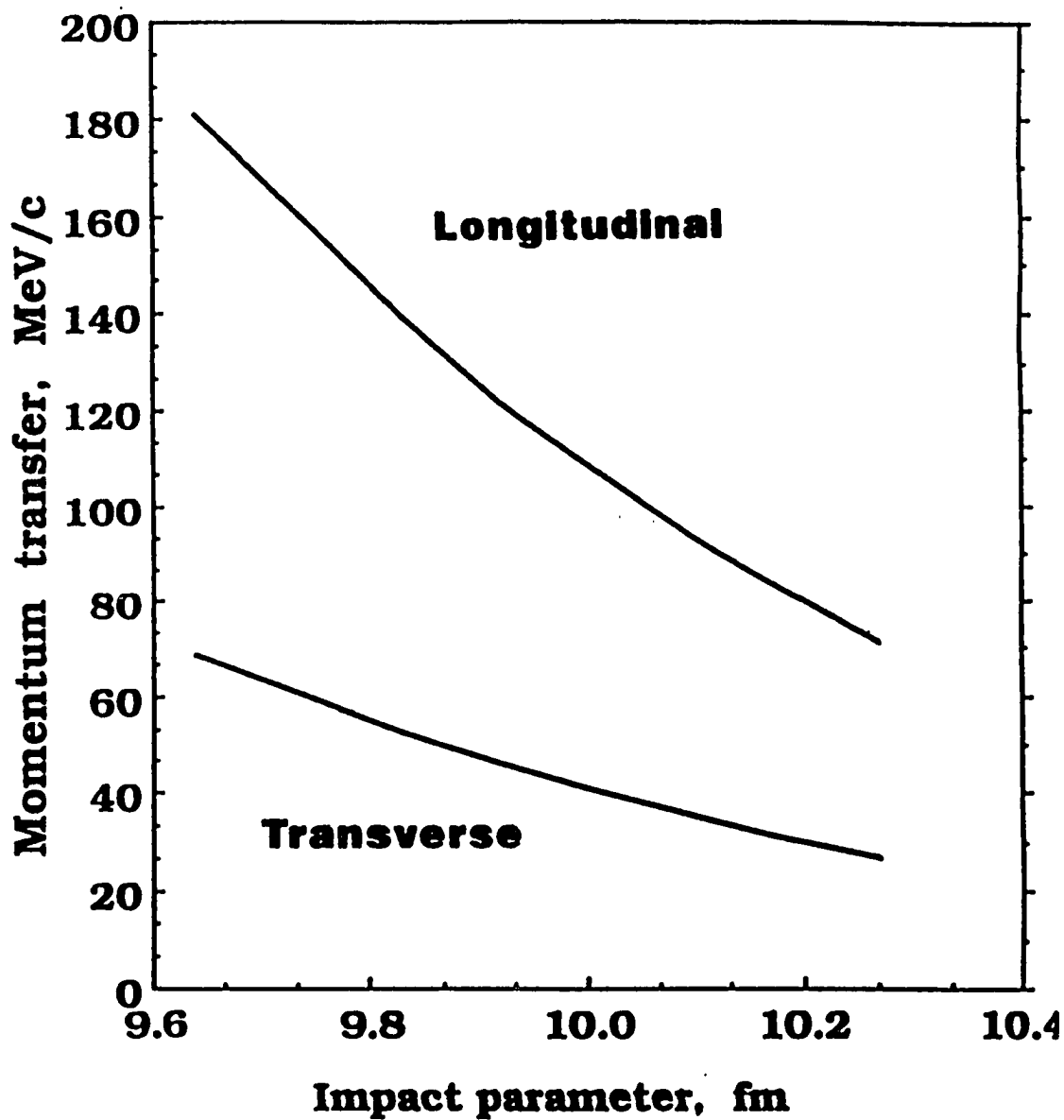
Fig. 18   Momentum transfer (MeV/c) to ^{12}C projectile by the Pb target as a function of impact parameter (fm) in the reaction ^{12}C (2.1 AGeV) + Pb → Projectile Fragment + X, where X is unidentified. Harmonic-well density was used for the projectile, and Woods-Saxon was used for the target.

From the figures, two features are readily apparent. First the longitudinal momentum transfer is larger than the transverse, indicating the primarily absorptive nature of nuclear collisions at this energy. Second, the predicted momentum transfers decrease rapidly with increasing impact parameter.

Another feature that stands out is that momentum transfers are only slightly target dependent. The choice of the impact parameters was of consequence in this and will be discussed shortly. The longitudinal momentum transfer to ^{16}O rises from ~230 MeV/c for ^{9}Be target to ~320 MeV/c for ^{208}Pb target at the closest impact parameters (see figures 1 and 6). The transverse momentum transfer increase is only ~90 MeV/c to ~120 MeV/c. The projectile dependence is more noticeable, however. The longitudinal momentum transfer to ^{12}C (at 1.05 A GeV) is ~155 MeV/c (figure 7) for ^{9}Be and rises to ~180 MeV/c (figure 12) for ^{208}Pb. Transverse momentum transfer is ~25 MeV/c - 30 MeV/c only for all targets. At incident energy of 2.1 A GeV, however, the energy dependence of transverse momentum transfer is noticeable. It ranges from ~60 MeV/c for the ^{9}Be target (figure 13) to ~70 MeV/c for ^{208}Pb (figure 18). Longitudinal momentum transfer hardly changes between 1.05 A GeV and 2.1 A GeV. The increase in transverse momentum transfer is related to $\alpha(e)$ which is the energy-dependent ratió of real to the imaginary part of the NN forward scattering amplitude. These trends show that while the longitudinal momentum transfer remains fairly constant at high energies, the transverse momentum transfer is highly energy-dependent.

In Figures 19-21 and Tables 3-5, our results on momentum down-shifts are reported. Experimental data[19] have been averaged over isotopes using

$$\langle P_\| \rangle_{exp}^{ave} = \frac{\sigma_{F1} \langle P_\| \rangle_{F1} + \sigma_{F2} \langle P_\| \rangle_{F2} + \cdots}{\sigma_{F1} + \sigma_{F2} + \cdots} \qquad (4.14)$$

where σ_{F1}, σ_{F2} are the fragmentation cross sections for isotopes 1 and 2, respectively, and $\langle P_\| \rangle_{F1}$, $\langle P_\| \rangle_{F2}$ are their corresponding downshifts (experimentally observed). These calculations are presented in Figures 19-21. To translate the calculated longitudinal momentum transfers into "Momentum downshifts," we follow the following prescriptions.

(1) The semi-empirical fragmentation code NUCFRAG[89] developed at NASA Langley is used to assign a range of impact parameters b_1 - b_2, b_2 - b_3, for each fragment A_F = 1,2,3...(A_p-1) where A_F, A_p are the fragment and parent mass numbers, respectively. This range is divided into ~ 30 intervals and corresponding longitudinal momentum transfer calculated for these values of impact parameters. An arithmetic average is done and the average is multiplied by the Goldhaber factor. This is the "momentum downshift" for fragment A_F. Standard deviation of the mean is computed following standard procedures.

(2) An impact parameter b is uniquely assigned by NUCFRAG for each fragment A_F where A_F = 1,2...(A_p-1). The corresponding longitudinal momentum transfer is calculated. The average longitudinal momentum transfer is taken as the same as the above. This average, multiplied by the Goldhaber factor (Eq. (4.7)) is the "momentum downshift" for that fragment. The results are compared from the two approaches.
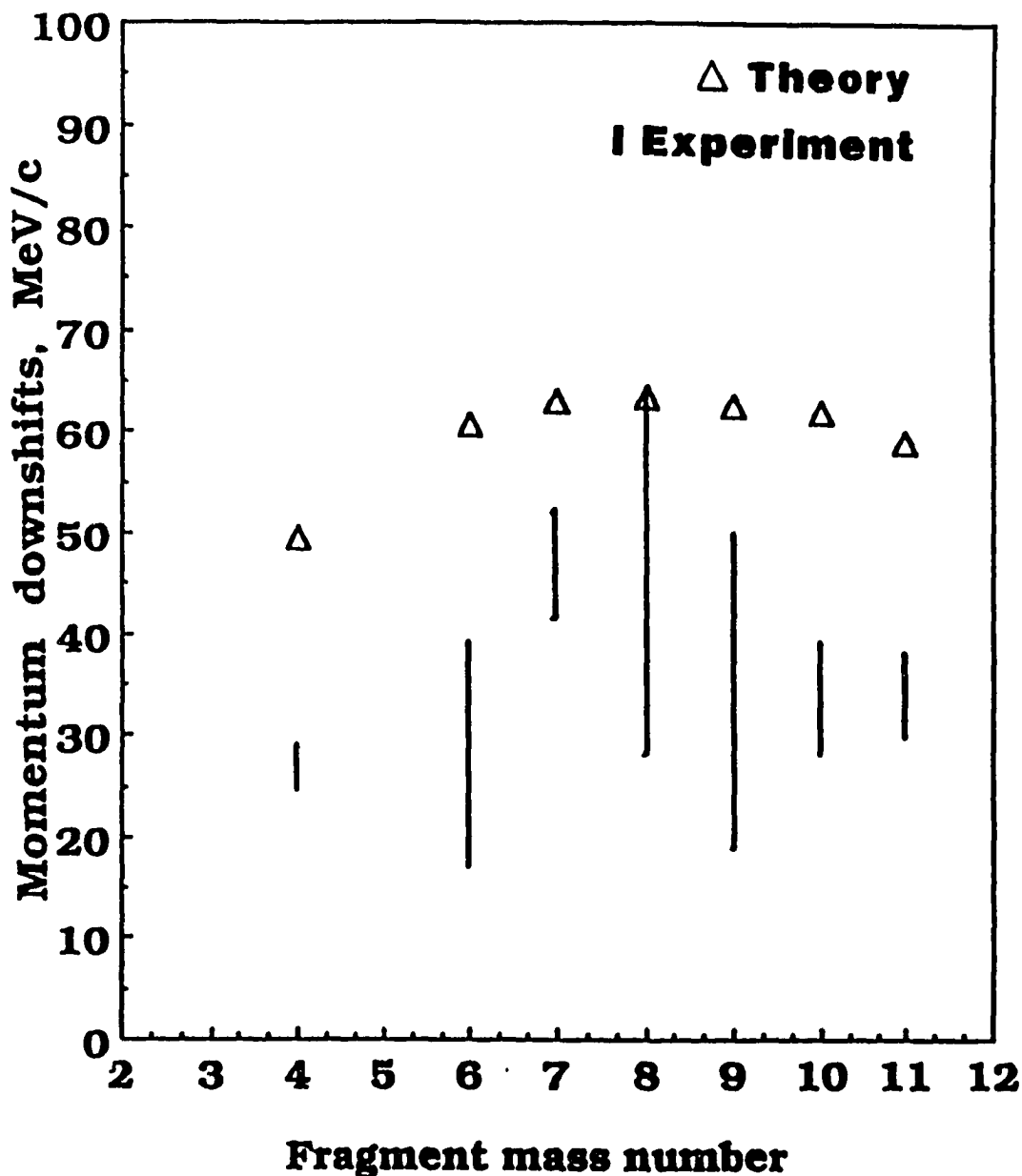
Figure 19: Momentum downshifts of projectile fragments in the reaction ^{12}C (1.05 AGeV) + Target → Projectile Fragment + X, where X is unidentified and targets are ^{9}Be, ^{12}C, ^{27}Al, Cu, Ag and Pb. Harmonic-well densities were used for A < 20, Woods-Saxon for A > 20.
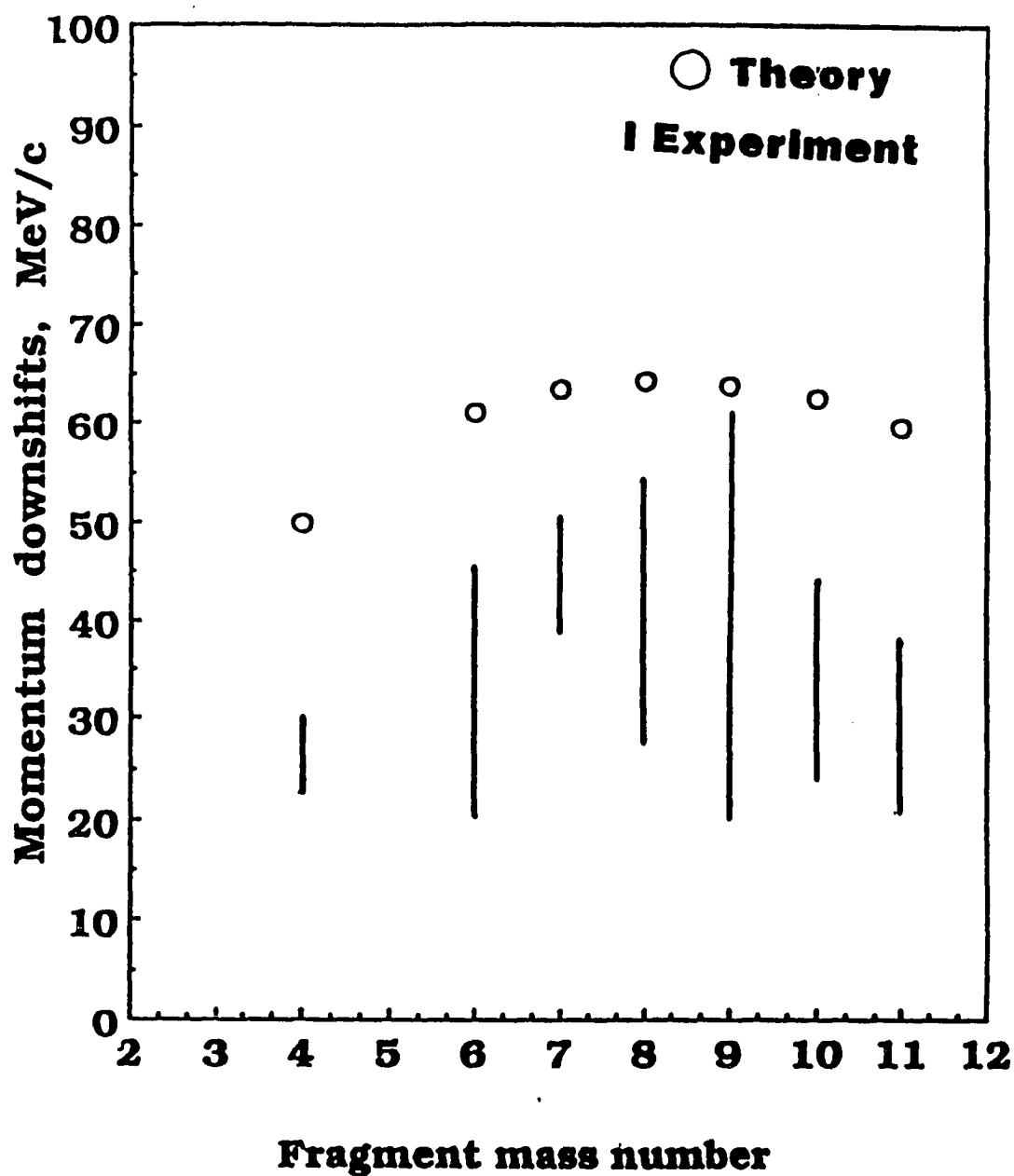
Fig. 20   Momentum downshifts of projectile fragments in the reaction ^{12}C
(2.1 AGeV) + Target → Projectile Fragment + X, where X is unidentified
and targets are ^{9}Be, ^{12}C, ^{27}Al, Cu, Ag and Pb. Harmonic-well densities
were used for A < 20, Woods-Saxon for A > 20.
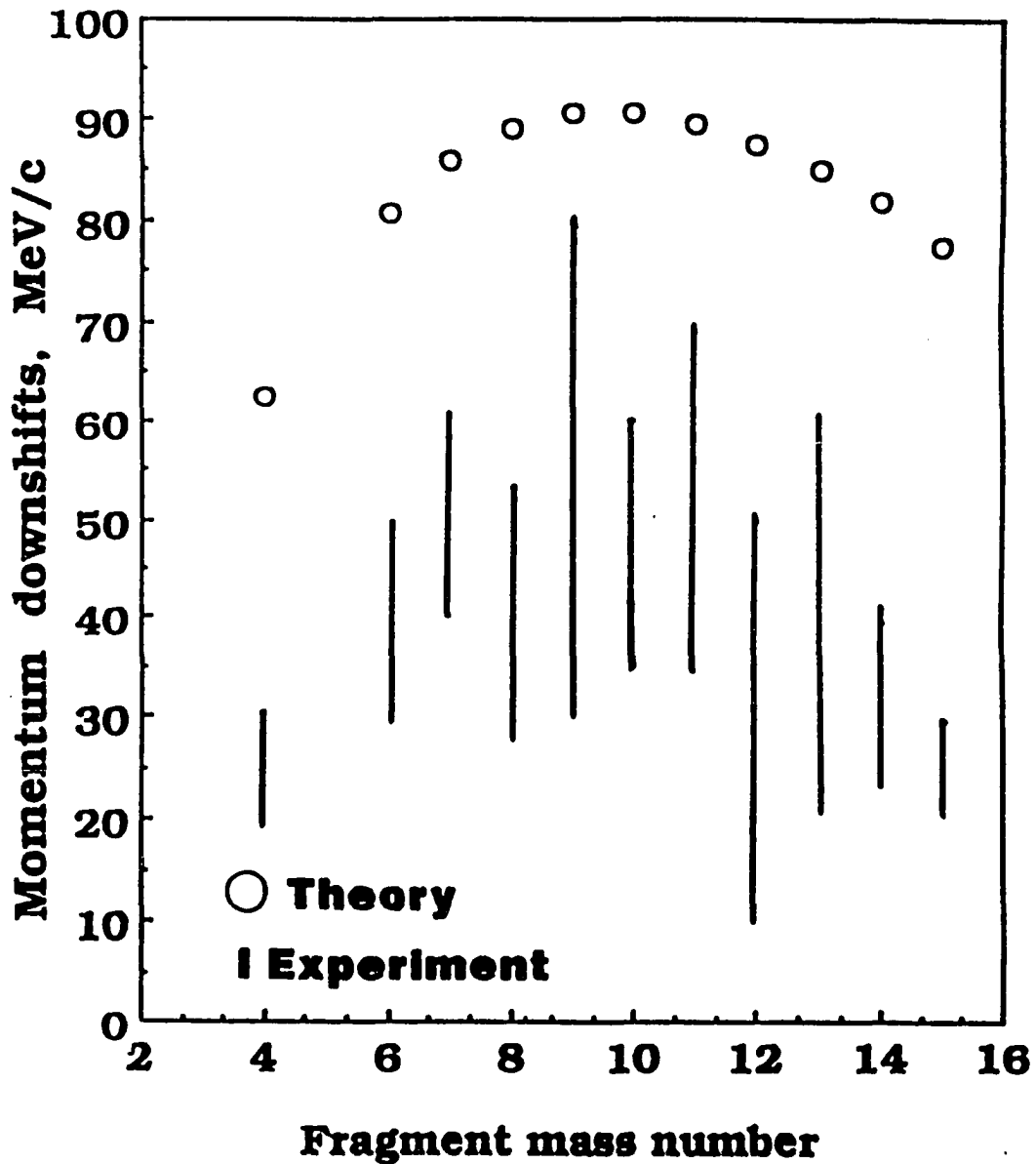
Figure 21: Momentum downshifts of projectile fragments in the reaction ^{16}O
(2.1 AGeV) + Target → Projectile Fragment + X, where X is unidentified
and targets are ^{9}Be, ^{12}C, ^{27}Al, Cu, Ag and Pb. Harmonic-well densities
were used for A < 20, Woods-Saxon for A > 20.

Table 3: Momentum downshifts - $\langle P_{||} \rangle$ in MeV/c of projectile fragments in the reaction $^{12}C(1.05\ AGeV)$ + Target → Projectile Fragment + X where X is not identified. Last column shows target averaged downshift. Realistic densities (Harmonic-well for ^{12}C, ^{9}Be; Woods-Saxon for Al, Cu, Ag, and Pb) were used. Standard deviations correspond to impact parameter averaging for each fragment (see text).

Projectile Fragment	^{9}Be	^{12}C	^{27}Al	^{64}Cu	^{108}Ag	^{208}Pb	$-\langle P_{||} \rangle_{ave}$
11 (C,B)	54.24 ± 2.16	45.0 ± 2.04	57.0 ± 2.46	56.3 ± 2.4	62.4 ± 2.8	57.70 ± 2.4	55.4 ± 2.4
10 (C,B,Be)	54.66 ± 2.88	46.2 ± 2.76	58.32 ± 3.12	57.52 ± 3.0	63.96 ± 3.4	59.20 ± 3.0	56.6 ± 3.0
9 (C,Be,Li)	56.8 ± 2.9	48.9 ± 2.88	60.6 ± 3.24	59.6 ± 3.2	66.24 ± 3.5	60.5 ± 3.7	58.77 ± 3.2
8 (B,Li)	56.54 ± 3.24	49.6 ± 3.2	60.7 ± 3.72	59.9 ± 3.6	66.5 ± 4.13	61.7 ± 4.2	59.2 ± 3.7
7 (Be,Li)	55.2 ± 3.6	49.44 ± 3.72	59.9 ± 4.2	58.9 ± 4.2	65.67 ± 4.7	62.1 ± 4.7	58.5 ± 4.2
6 (Li,Ne)	52.64 ± 3.96	47.99 ± 4.2	57.77 ± 4.7	56.76 ± 4.9	63.5 ± 5.3	60.4 ± 5.7	56.5 ± 4.8
4 (He)	41.3 ± 4.3	39.74 ± 5.16	46.8 ± 5.88	46.7 ± 6.24	51.84 ± 7.14	51.0 ± 6.9	46.3 ± 6.0

Table 4: Momentum downshifts — $<P_{||}>$ in MeV/c of projectile fragments in the reaction ^{12}C(2.1 AGeV) + Target → Projectile Fragment + X where X is not identified. Last column shows target averaged downshift. Realistic densities (Harmonic-well for ^{9}Be, ^{12}C; Woods-Saxon for Al, Cu, Ag, Pb) were used. Standard deviations correspond to impact parameter averaging for each fragment (see text).

Projectile Fragment	^{9}Be	^{12}C	^{27}Al	^{64}Cu	^{108}Ag	^{208}Pb	$- <P_{||}>_{ave}$
11	53.44 ± 2.15	44.48 ± 2.1	56.32 ± 2.4	55.7 ± 2.4	61.76 ± 2.7	57.1 ± 2.4	54.8 ± 2.35
10	53.92 ± 2.82	45.6 ± 2.72	57.55 ± 3.04	56.9 ± 2.94	63.2 ± 3.3	58.5 ± 3.0	55.99 ± 2.96
9	55.84 ± 2.82	48.31 ± 2.72	59.84 ± 3.2	58.9 ± 3.15	65.44 ± 3.5	59.84 ± 3.6	58.03 ± 3.2
8	55.68 ± 3.2	48.32 ± 3.2	60.0 ± 3.7	59.14 ± 3.52	65.7 ± 4.0	60.96 ± 4.21	58.4 ± 3.7
7	54.38 ± 3.51	48.72 ± 3.68	59.04 ± 4.16	58.24 ± 4.16	64.8 ± 4.64	61.34 ± 4.70	57.76 ± 4.16
6	51.84 ± 3.84	47.36 ± 4.16	56.96 ± 4.6	55.98 ± 4.8	62.65 ± 5.3	59.58 ± 5.6	55.73 ± 4.75
4	40.67 ± 4.16	39.2 ± 5.12	46.08 ± 5.76	46.06 ± 6.08	51.12 ± 7.04	50.38 ± 6.7	45.6 ± 5.9

Table 5: Momentum downshifts - $\langle P_{||} \rangle$ in MeV/c of projectile fragments in the reaction $^{16}O(2.1\ AGeV) + Target \rightarrow Projectile\ Fragment + X$. Last column shows target averaged downshift. Realistic densities (Harmonic-well for Be, C, O; Woods-Saxon for Al, Cu, Ag and Pb) were used. Standard deviations correspond to impact parameter averaging for each fragment (see text).

Projectile Fragment	^{9}Be	^{12}C	^{27}Al	^{64}Cu	^{108}Ag	^{208}Pb	$-\langle P_{||} \rangle_{ave}$
15 (O,N)	65.28 ± 2.24	56.56 ± 2.18	72.16 ± 2.56	74.72 ± 2.67	81.92 ± 2.99	77.12 ± 2.72	71.28 ± 2.56
14 (O,N,C)	66.72 ± 2.88	58.66 ± 2.86	74.48 ± 3.28	77.31 ± 3.2	84.94 ± 3.6	79.84 ± 3.33	73.66 ± 3.2
13 (O,N,C,B)	70.38 ± 2.88	62.94 ± 2.88	78.72 ± 3.33	81.07 ± 3.36	89.12 ± 3.78	83.68 ± 3.52	77.65 ± 3.3
12 (N,C,B)	72.0 ± 3.2	65.31 ± 3.2	80.99 ± 3.74	83.28 ± 3.84	91.68 ± 4.24	85.92 ± 4.0	79.84 ± 3.73
11 (C,B,Be)	73.12 ± 3.84	67.2 ± 3.68	82.72 ± 4.16	84.89 ± 4.32	93.68 ± 4.8	87.68 ± 4.48	81.58 ± 4.16
10 (B,Be)	73.44 ± 3.84	68.51 ± 4.0	83.68 ± 4.64	85.92 ± 4.75	94.88 ± 5.34	88.96 ± 5.0	82.56 ± 4.64
9 (Be,Li)	72.8 ± 4.0	68.96 ± 4.46	83.74 ± 5.12	85.92 ± 5.3	95.04 ± 5.9	89.04 ± 5.6	82.56 ± 5.12
8 (B,Li)	71.04 ± 4.48	63.32 ± 4.88	82.56 ± 5.7	84.64 ± 5.86	93.76 ± 6.51	88.09 ± 6.18	81.41 ± 5.6
7 (Be,Li)	68 ± 4.64	66.30 ± 5.3	79.77 ± 6.192	81.92 ± 6.4	90.56 ± 7.2	85.22 ± 6.9	78.62 ± 6.08
6 (Li,He)	63.10 ± 4.96	62.49 ± 5.71	75.04 ± 6.72	77.12 ± 7.04	85.6 ± 7.84	80.64 ± 7.57	74.0 ± 6.72
4 (He)	47.7 ± 5.12	48.70 ± 6.0	58.32 ± 7.12	60.16 ± 7.46	66.72 ± 8.32	63.2 ± 8.0	57.44 ± 7.08

Extensive numerical work revealed that the second approach, while being more efficient yields results comparable to the first approach, not differing by more than 7 MeV/c. When accuracy was desired, the first approach was always preferred over the second.

It may now be worthwhile to discuss the experimental results and theoretical calculations. It is clear from figures 19-21 that the momentum downshifts are overpredicted in all cases except for a few. The source of this discrepancy is the impact parameters obtained from the geometrical, semi-empirical code NUCFRAG. The projectile and target densities are approximated in the above code as uniform spheres with $R \simeq 1.26 A^{1/3}$ (fm). This is obviously an oversimplification. Electron scattering[87] from nuclei reveal that nuclei possess diffuse surfaces. Realistic charge distributions (Woods-Saxon for example) take the diffuseness into account through skin thickness t(fm), which is a measure of the distance where nuclear density falls from 90% to 10% of its value. A sharp cut-off of the density thus neglects the extended, diffuse nuclear surface. Since realistic nuclear densities were used in the calculations of longitudinal and transverse momentum transfer, it is likely that the impact parameters from NUCFRAG are not very realistic. An alternate procedure would be to make our calculations compatible with uniform density calculations from NUCFRAG.

This was accomplished in two steps. Realistic densities were replaced by uniform densities $[R = 1.26 A^{1/3}]$ in the momentum transfer calculations. The zero-range of the two-body interaction in NUCFRAG was implemented in our calculation by reducing the range arbitrarily by

a factor of five   i.e. $B'(e) = \dfrac{B(e)}{5}$ where $B(e)$ was given previously by

equation (4.9) all projectile-target combinations. This amounted to

$B'(e) \sim .08$ fm^{-2} at 2.1 A GeV, for example. The effect on our calcula-

tion can be seen in figures 22-24. In figure 22, the imaginary part of

the optical potential $V_{opt}(r)$ for ^{16}O - ^{9}Be collision at 2.1 A GeV is

plotted using Harmonic-well densities as well as uniform densities with

variable slope parameter $B(e)$. The first-order optical potential

follows closely the density distribution of the nuclei (actually ex-

tends beyond due to finite range of the interaction). As uniform

density was substituted and the range of the interaction reduced by a

factor of 5, the shape of the potential became steeper, thus approxi-

mating a sphere with a sharp cutoff. The effect on the longitudinal

momentum transfer to ^{16}O in the collision of the ^{16}O-^{9}Be pair ($E_{inc} =$

2.1 A GeV) can be seen in figure 23. Compared with the realistic

density calculations (see also figure 1), the magnitude of the momentum

transfer is reduced. Setting $B(e) = 0$ outright involved numerical

difficulties.

The momentum downshifts of Oxygen fragments are plotted and

compared with experimental data[19] in figure 24. The experimental data

have been averaged according to (4.14). Notice the significant agree-

ment between theory and experiment. Similar results obtain for ^{12}C

fragmentation at 2.1 A GeV and 1.05 A GeV.

It may be appropriate to point out that the above procedure can be

reversed and theoretical calculations utilized as an impact parameter

"gauge". With experimentally observed downshifts as inputs, one can

calculate with realistic densities the impact parameters where the same
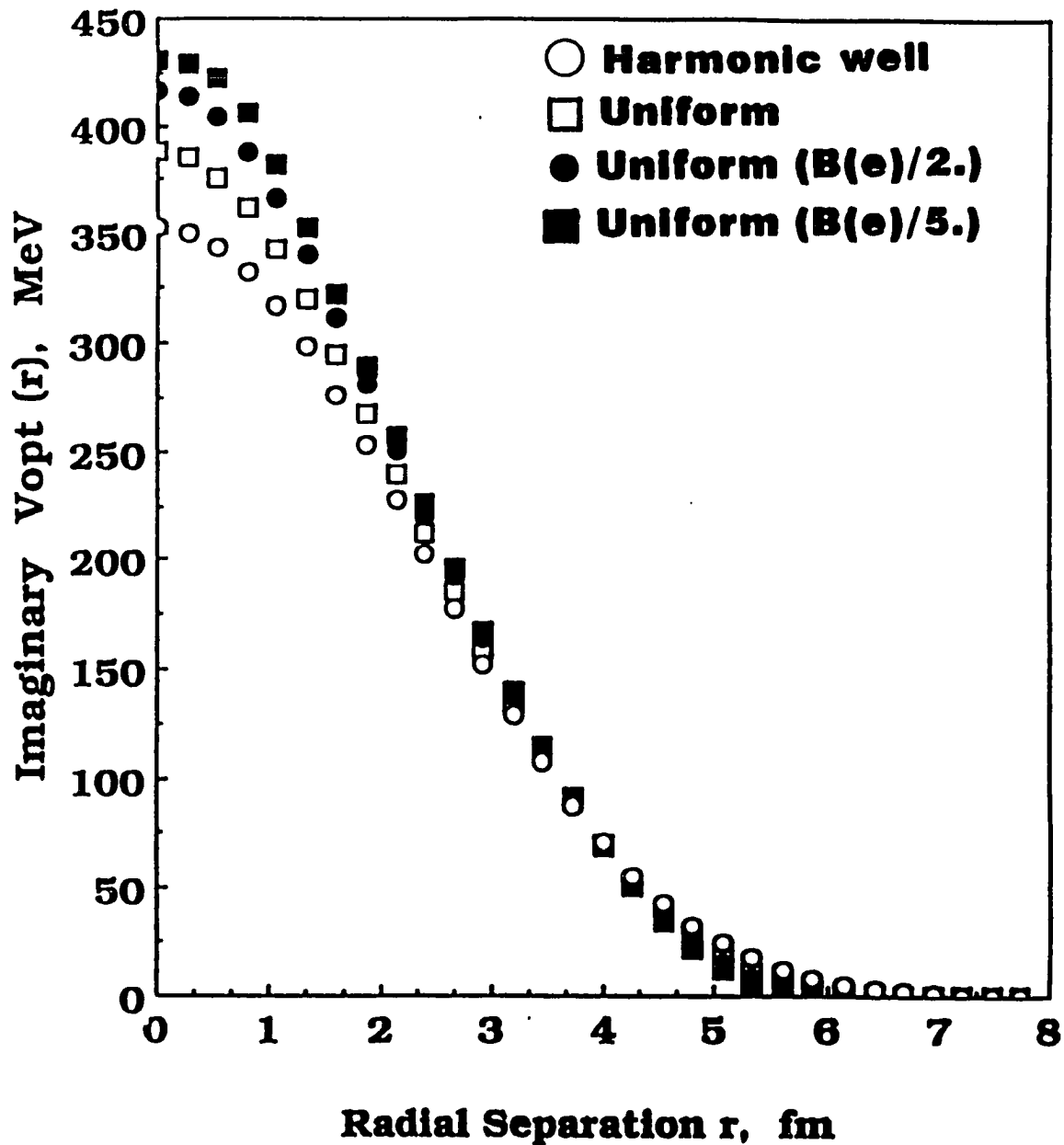
Fig. 22 Imaginary part of the optical potential Vopt(r) in MeV as a function of separation r in fm for Oxygen with Beryllium at 2.1 A GeV. Harmonic well densities were used for both the projectile and the target and compared with uniform density calculations. Slope parameter was modified to B'(e)=B(e)/2 and B'(e)=B(e)/5 respectively to simulate a zero-range interaction.
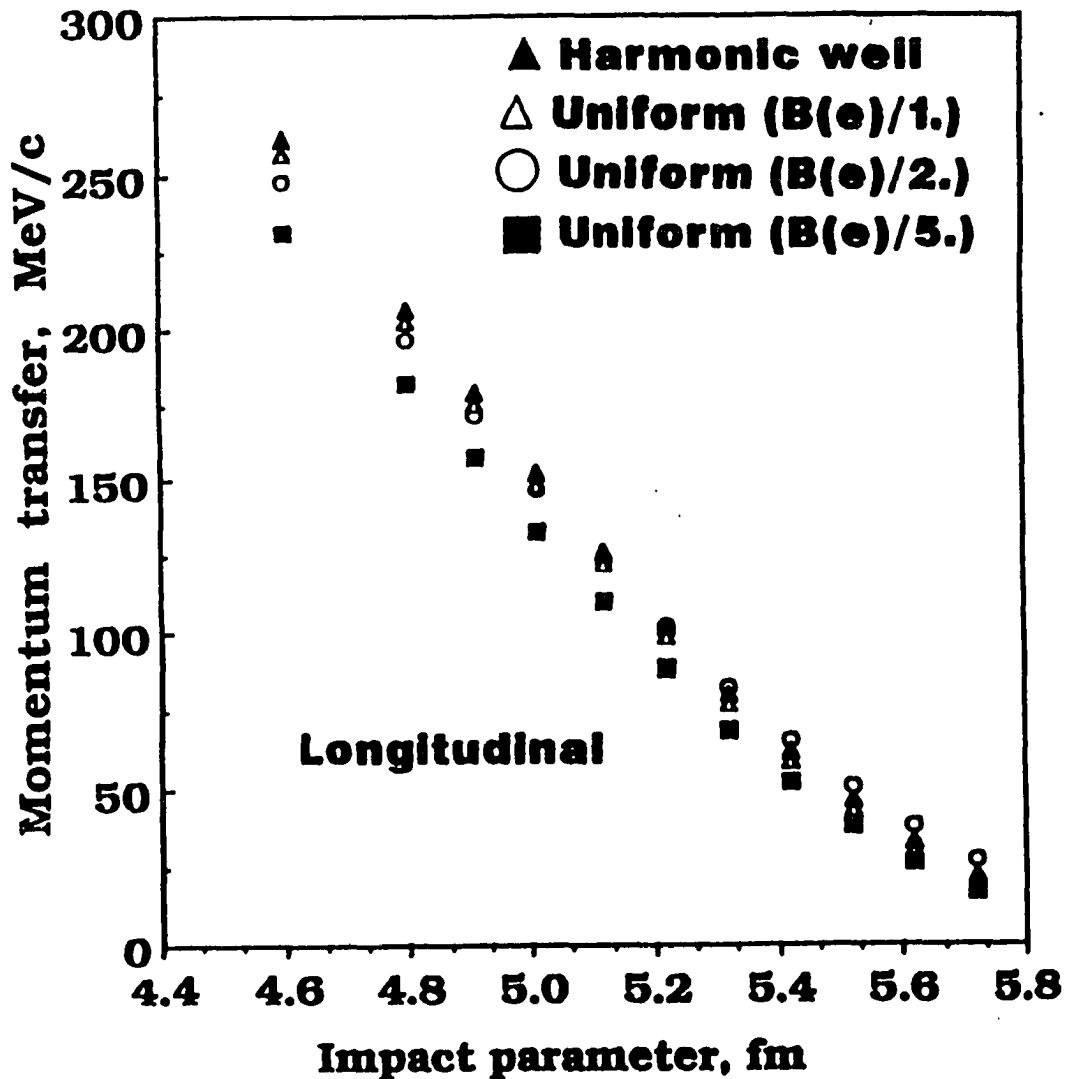
Fig. 23   Longitudinal momentum transfer in MeV/c to Oxygen by the Beryllium target as a function of impact parameter in fm. Harmonic well densities were used for both the projectile and the target and compared with uniform density calculations. Slope parameter was modified to B'(e)=B(e)/2 and B'(e)=B(e)/5 respectively to simulate a zero-range interaction.
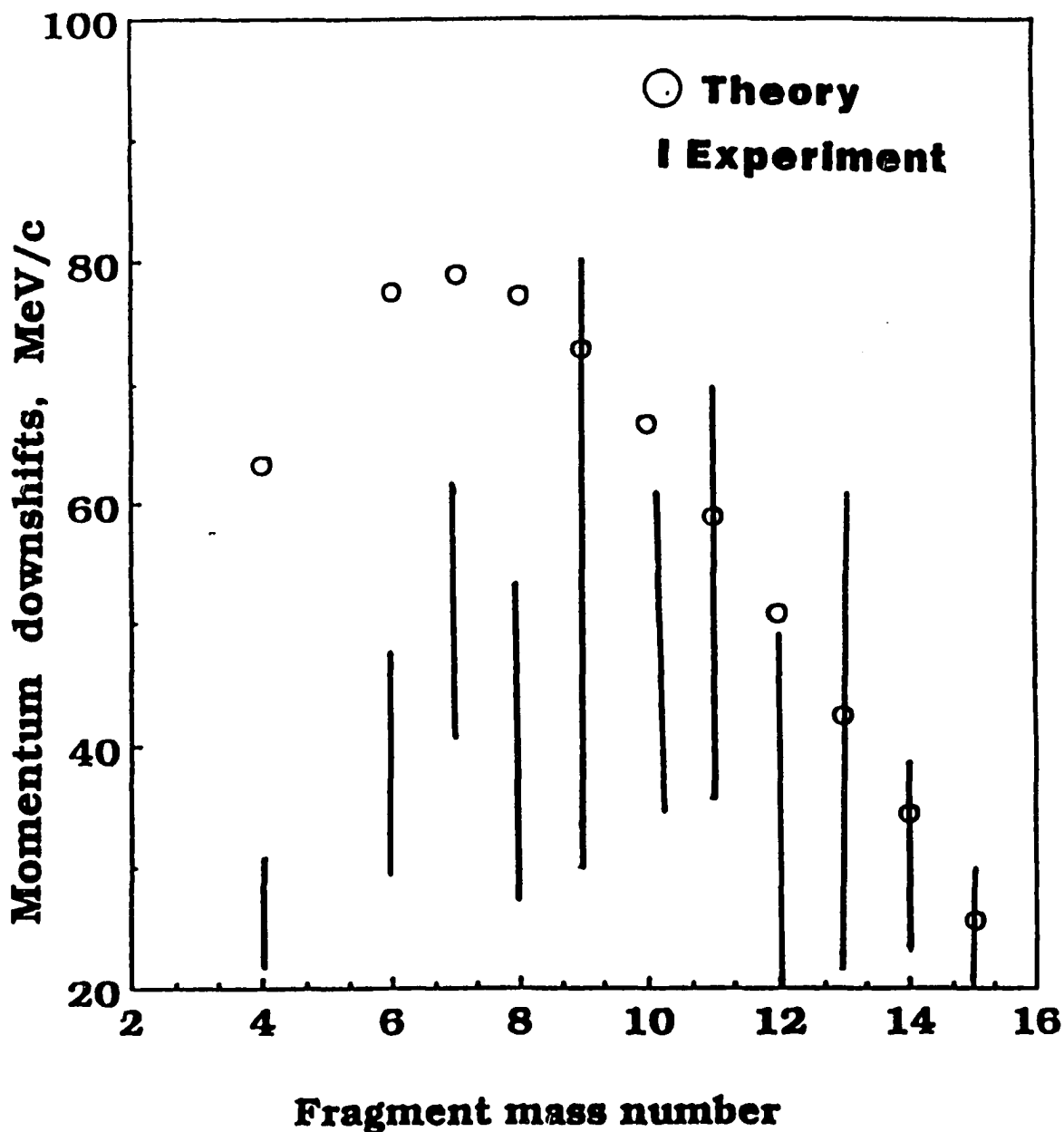
Fig. 24   Momentum downshifts of projectile fragments in the reaction ^{16}O
(2.1 AGeV) + Target → Projectile Fragment + X, where X is unidentified
and targets are ^{9}Be, ^{12}C, ^{27}Al, Cu, Ag and Pb. Uniform densities were
used for the projectile and the targets. Slope parameter was modified
(B'(e) = B(e)/5) to approximate a zero-range interaction.

downshifts obtain. The practical advantage of these impact parameters
is that they can be utilized in localizing a reaction event as well as

used as guides to other calculations such as those of transverse
momentum transfer, fragmentation cross-sections, and Coulomb dissocia-
tion cross-sections.

The energy dependence of the momentum transfer is a quantity of
fundamental interest. As noted previously, the NN input parameters are
energy dependent. Longitudinal and transverse momentum transfers have
been plotted for ^{16}O - ^{9}Be pair at incident energies E_{inc} = 0.2, 0.4,
0.6, 0.8, 1.05 and 2.1 A GeV in figures 25 and 26, respectively. Note
the gradual increase of longitudinal momentum transfer as the bom-
barding energy increases, attaining a "limiting" value at $E_{inc} \geq 1$
A GeV. The transverse momentum transfer can be readily obtained from
the longitudinal momentum transfer by multiplying the latter by $\alpha(e)$,
where $\alpha(e)$ is the ratio of the real to the imaginary part of the NN
forward scattering amplitude. As is well-known, $\alpha(e) < 0$ at 2.1 A GeV
which implies a repulsive, real part of the optical potential. The
corresponding transverse momentum transfer is from a repulsive mean
field and is positive (according to our sign convention). At lower
bombarding energies, $V_{opt}(r)$ = -$(V_{Real} + iV_{Imag})$ holds and the corre-
sponding mean field is attractive. Transverse momentum transfer is
negative indicating that deflection to negative scattering angles is
feasible. Coulomb effects have been ignored in our calculations. The
above predictions should be verifiable in sophisticated experiments in
the future.
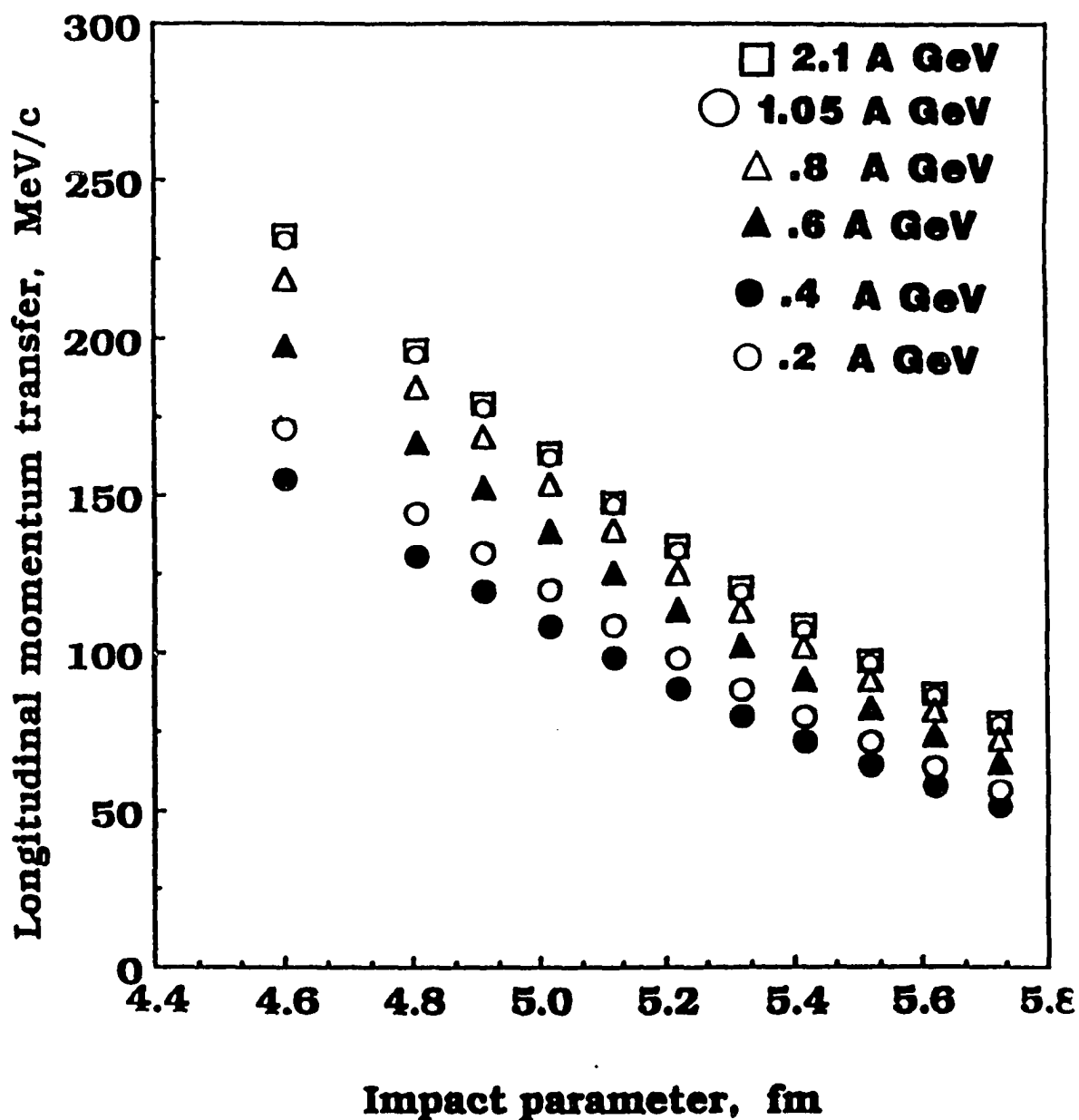
Figure 25: Longitudinal momentum transfer (MeV/c) to ^{16}O projectile by the ^9Be target as a function of impact parameter (fm) in the reaction $^{16}O(E_{inc})+^9Be$—>Projectile Fragment+X. Incident energies E_{inc}=2.1,1.05,.8,.6,.4 and .2 A GeV were used.
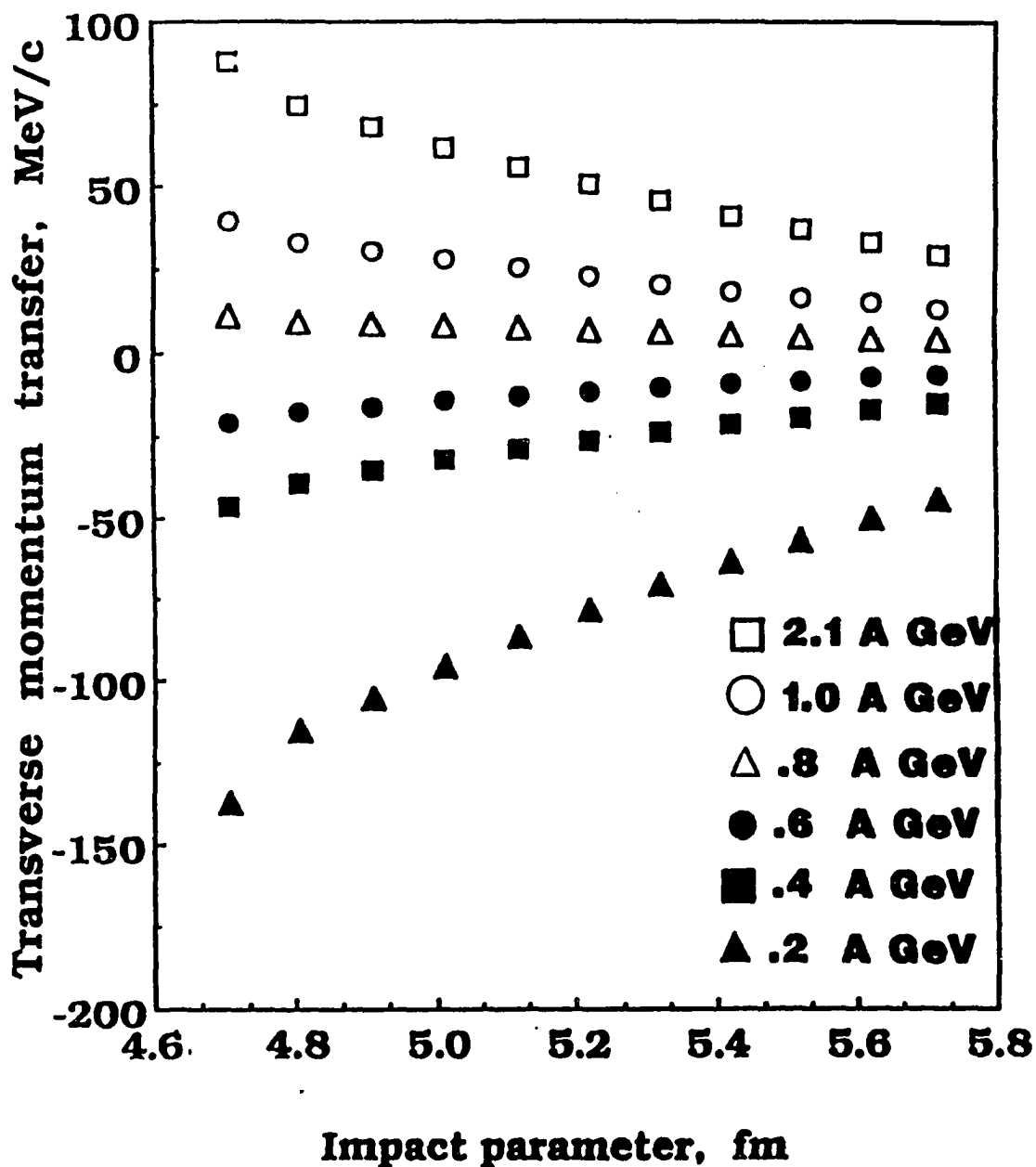
Figure 26: Transverse momentum transfer (MeV/c) to ^{16}O projectile by the ^9Be target as a function of impact parameter (fm) in the reaction ^{16}O (E_{inc}) + $^9Be \rightarrow$ Projectile Fragment + X. Incident energies $E_{inc} = 2.1, 1.05, .8, .6, .4, .2$ AGeV were used.

B. Momentum Widths

Equation (4.5a) is Goldhaber's result for the modification of the fragment momentum width due to collisional momentum transfer. Specifically, the following equations can be derived from (4.5a)

$$\sigma_{\parallel}^{\prime 2} = \frac{F(A-F)}{A}\,\sigma_o^2 + \frac{F^2}{A^2}\,Q_{\parallel}^2 \qquad (4.15a)$$

$$\sigma_{x}^{\prime 2} = \frac{F(A-F)}{A}\,\sigma_o^2 + \frac{F^2}{A^2}\,Q_x^2 \qquad (4.15b)$$

where $\sigma_{\parallel}^{\prime 2}$, $\sigma_{x}^{\prime 2}$ are the modified widths, $Q_{\parallel}$, Q_x are the momentum transfers, and F and A are the fragment and parent mass numbers. The first terms in (4.15a) and (4.15b) are the unmodified widths in the longitudinal and transverse directions given in terms of Fermi momentum as

$$\sigma_{\parallel}^2 = \frac{F(A-F)}{A}\,\sigma_o^2 \quad ; \quad \sigma_o^2 = \frac{P_F^2}{5} \qquad (4.16a)$$

$$\sigma_{\perp}^2 = 2\,\frac{F(A-F)}{A}\,\sigma_o^2 \qquad (4.16b)$$

The extra factor of 2 in (4.16b) is due to summing over x and y directions.

Moniz et al.[90] measured the Fermi momentum of a range of nuclei via electron scattering. We have developed in the last chapter the theory of longitudinal and transverse momentum transfer. The expressions for the longitudinal and transverse momentum transfer in nucleus-nucleus collisions are given in equations (3.39) and (3.40).

Experimental data on the widths of longitudinal momentum distributions of projectile fragments were measured by Greiner et al.[19] The widths of the transverse momentum distributions, when resolved onto the detector plane were found to be similar to the longitudinal widths

$$\sigma(P_{11}) \simeq \sigma(P_x) \simeq \sigma(P_y) \qquad (4.17)$$

within 10% suggesting isotropy of fragment production in the projectile frame.

Brady et al.[26] measured the widths of transverse momentum distributions of projectile fragments in the reaction $^{139}_{57}La$ (1.2 A GeV) + ^{12}C → Projectile Fragment + X. These measurements were made at the Bevalac Heavy Ion Super-conducting Spectrometer (HISS) with the MUSIC detector. Fragment momentum widths $\sigma(P_x)$ were measured in the detector plane and fit to the expression

$$\sigma(P_x) = \sigma_0 \sqrt{\frac{F(A-F)}{(A-1)}} \quad (MeV/c) \qquad (4.18)$$

with variable σ_0. It was found that Goldhaber theory, based on interpolated value of Fermi momentum $P_F \simeq 250$ MeV/c $(=\sqrt{5} \ \sigma_0)$ underpredicted the widths. Values of $\sigma_0 \simeq 169$ MeV/c was necessary, implying an unreasonable value for the Fermi momentum of 377 MeV/c for ^{139}La. Based on our theory of transverse momentum transfer, we show in Table 6 and Figure 27 a much improved agreement with the experiment. This shows that collisional momentum transfer is substantially responsible for increased transverse widths.

These calculations were done using the following steps based on our expression for transverse momentum transfer. In Equation (3.39) we used a Woods-Saxon density for ^{139}La and Harmonic-well density for ^{12}C

‹

Table 6: Transverse momentum widths $\sigma_\perp$ ($Q_\perp$) in MeV/c of projectile fragments in the reaction ^{139}La(1.2 AGeV) + ^{12}C → Projectile Fragment + X, calculated from equations (4.15b and (4.16b). The last column lists the modified widths. When squared, the third column yields the modifications due to momentum transfer.

Projectile Fragment (mass no.)	$\sigma(P_x)$ Goldhaber (MeV/c)	$\sigma_t(b)$ ours (MeV/c)	$\sigma(P_x)$ expt fit (MeV/c) (ref. 26)	$\sigma_\perp(Q_\perp)$ ours (MeV/c)
138	112.0	15.6	169	159.2
137	157.8	16.5	238	223.8
136	192.6	18.0	290	272.9
135	221.5	19.5	334	313.8
134	246.8	21.0	372	349.6
133	269	22.6	406	381.0
132	289.8	24.36	437	410.5
131	308.6	26.23	465	437.2
130	326	28.2	492	462.0
129	342	30.2	517	484.6
128	357.8	32.6	540	507
127	372	35.05	561	527.2
126	386.8	37.6	582	548.3
125	398.8	40.3	602	565.4
124	411	43.15	620	582.8
123	423	46.16	638	599.9
122	434	49.3	655	615.7
121	445	52.6	671	631.5
120	455	56.04	687	646

Table 6 (Continued)

Projectile Fragment (mass no.)	$\sigma(P_x)$ Goldhaber (MeV/c)	$\sigma_t(b)$ ours (MeV/c)	$\sigma(P_x)$ expt fit (MeV/c) (ref. 26)	$\sigma_\perp(Q_\perp)$ ours (MeV/c)
119	465	59.60	702	660.3
118	475	63.34	716	674.7
117	483.7	67.03	730	687.3
116	492.5	75.7	743	700.3
115	501	79.78	756	713
114	509	84.14	768	724.7
113	517	88.46	780	736.5
112	524.3	92.9	791	747.3
111	531.5	97.3	802	757.6
110	538.5	102	812.5	768.3
109	545	106.4	822	778.0
108	551.6	111	832.4	78?
107	558	115.6	842	797.5
106	564	125.7	851	807.5
105	569.6	119	859.6	814.3
104	575	123.5	868	822.5
103	580	127.9	876	830
102	586	132.2	884	839
101	590.6	136.7	891	846
100	595.4	141	898	854
99	600	145	905	861
98	604.3	149.2	912	867.5
97	608.5	153	918	874
96	612.5	157	924	880.3

Table 6 (Continued)

Projectile Fragment (mass no.)	$\sigma(P_x)$ Goldhaber (MeV/c)	σ_t(b) ours (MeV/c)	$\sigma(P_x)$ expt fit (MeV/c) (ref. 26)	$\sigma_\perp(Q_\perp)$ ours (MeV/c)
95	616	160.5	930	886
94	620	164.2	936	892
93	623.6	167.5	941	897.6
92	627	170.9	946	903
91	630	173.8	951	908
90	633	176.7	955	912
89	636	179.5	960	917
88	638.7	182.0	964	921
87	641	184.5	968	925
86	643.6	186.7	971	929
85	645.9	188.7	974.6	932.7
84	648	190.6	978	936
83	650	192.2	980.8	939
82	651.8	193.6	983.5	942
81	653.5	195	986	944.5
80	655	196	988	947
79	656.4	197	990	949
78	657.6	197.7	992	951
77	658.7	198.3	994	952
76	659.7	198.7	995.5	954
75	660.5	198.9	996.7	955
74	661	198.9	997.7	955
73	661.7	198.8	998.6	956.6
72	662.2	198.6	999.2	957.3

Table 6 (Concluded)

Projectile Fragment (mass no.)	$\sigma(P_x)$ Goldhaber (MeV/c)	$\sigma_t(b)$ ours (MeV/c)	$\sigma(P_x)$ expt fit (MeV/c) (ref. 26)	$\sigma_\perp(Q_\perp)$ ours (MeV/c)
71	662.5	198.0	999.6	957.6
70	662.6	197.6	999.8	957.6
69	662.6	196.8	999.8	957.5
68	662.5	196	999.6	957.2
67	662.2	195	999.2	956.6
66	661.8	193.8	998.6	955.8
65	661.2	192.5	997.7	954.7
64	660.5	191.15	996.7	953.4
63	659.7	189.7	995.5	952
62	658.7	188.0	994	950
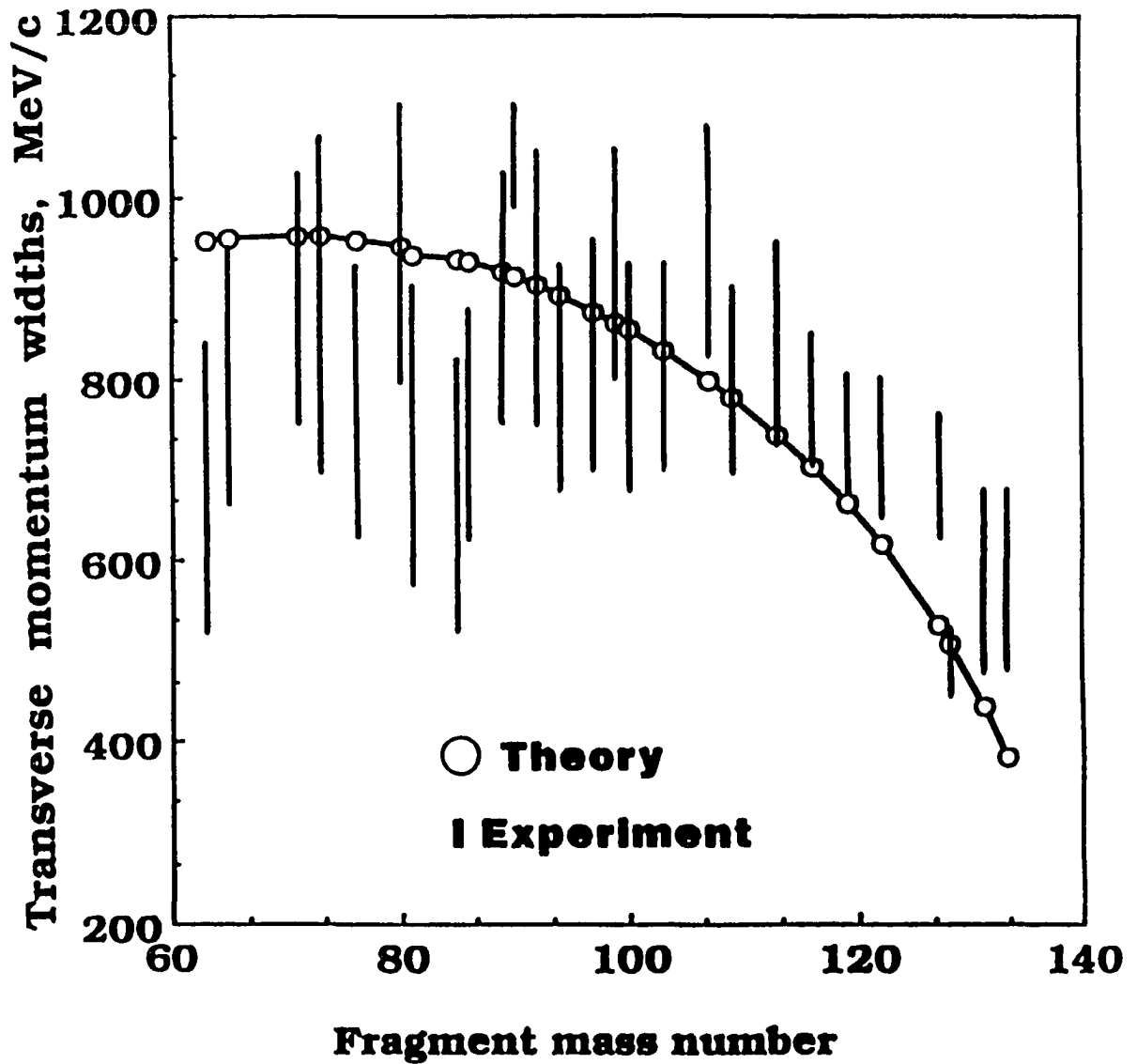
Figure 27: Transverse momentum widths of projectile fragments in the reaction
^{139}La (1.2 AGeV) + ^{12}C → Projectile Fragment + X, where X is
unidentified. Harmonic-well density was used for ^{12}C, Woods-Saxon
for Lanthanum.

where the parameters have been listed before in table 2. Root mean square momentum transfer $Q_\perp$ and squared rms momentum transfer $Q_\perp$ were calculated, and widths $\sigma_\perp(Q_\perp)$ were calculated using (4.15b). Since the experimental widths are in the detector plane and momentum transfer is calculated in the reaction plane, information on the azimuth of the reaction plane is necessary. Since such information is not available, we assumed that the momentum transfer in the reaction plane and detector plane are identical.

CHAPTER V

CORRECTIONS

Modifications to the above formalism will be addressed in this chapter. These are called (i) The Deceleration correction and (ii) The Coulomb correction. In theoretical calculations, the assumption of constant velocity is frequently made. Momentum transfer introduces an asymmetry into the problem; the assumption of constant velocity of beam nucleons is then strictly not valid. Our evaluation of momentum transfer in Chapter IV can only be correct if the corrections to our calculations are small. As will become apparent, this correction, related to deceleration of the projectile due to momentum transfer is indeed small at high energies (but not necessarily so at lower bombarding energies). Modification of the expressions derived previously will be made first. Numerical evaluation will be carried out for these corrections, labelled collectively as "The Deceleration corrections".

Coulomb repulsion of the charges in heavy-ions will be treated next. Ever since the beginning of the science of heavy-ions, the interplay of nuclear and Coulomb effects has unveiled new insights. This is also true for the problem treated here. An analysis of electromagnetic dissociation cross-sections at high energy reveals the importance of electromagnetic (EM) fields generated. The Weizsacker-Williams method of virtual quanta will be used to show the importance of the EM fields. Momentum transfer calculations will be performed and compared with the nuclear contribution. Finally, modifications to the

88

point-Coulomb assumption will be made in favor of a more realistic charge distribution.

V.a Deceleration Correction

The assumption of constant velocity (per nucleon) is frequently made in intermediate and high energy nucleus-nucleus as well as hadron-nucleus collision calculations. The change in velocity is assumed small at these energies. Momentum transfer to the projectile, as evaluated in this work will enable us to evaluate the change in velocity (per nucleon) thus testing the assumption of constant velocity. We shall develop, in addition a self consistent framework for evaluating momentum transfer.

Consider a beam with kinetic energy per nucleon of T/A GeV. Then the velocity per constituent nucleon is

with
$$v = \beta c = c \ (1 - 1/\gamma^2)^{1/2} \qquad (5.1)$$

$$\gamma = 1 + \frac{T/A}{M_n} \ ; \ M_n = \text{rest energy of nucleon} \qquad (5.2)$$

Momentum transfer $\Delta P \ \frac{MeV}{c}$ to the beam implies a change in velocity

$$\Delta v = \Delta \beta c = \frac{\Delta P \ c}{M_n \cdot A_p} \ \text{per nucleon.} \qquad (5.3)$$

We parametrize the changed velocity as follows

$$v(z) = v + \delta(z) \qquad (5.4)$$

where $\delta(z)$ is a path-dependent correction with $\delta(z) \ll v$.

Previous expressions for longitudinal and transverse momentum transfer read (with $\Delta P_{\parallel} = Q_{\parallel}$, $\Delta P_{\perp} = Q_{\perp}$)

$$\Delta P_{\parallel} = -(A_p A_T) \int d^3\vec{\xi_p}\; \rho_p(\vec{\xi_p}) \int d^3\vec{\xi_T}\; \rho_T(\vec{\xi_T})$$

$$\left[\vec{\nabla}_{\xi_p} \int_{-\infty}^{\infty} Im\tilde{t}\;(\vec{x'},\vec{\xi_p},\vec{\xi_T})\;\frac{dz'}{v} \right] \tag{5.5}$$

and

$$\Delta P_{\perp} = -(A_p A_T) \int d^3\vec{\xi_p}\; \rho_p(\vec{\xi_p}) \int d^3\vec{\xi_T}\; \rho_T(\vec{\xi_T})$$

$$\left[\vec{\nabla}_{\xi_p} \int_{-\infty}^{\infty} Re\;\tilde{t}\;(\vec{x'},\vec{\xi_p},\vec{\xi_T})\;\frac{dz'}{v} \right] \tag{5.6}$$

The bracketed expressions were z-integrable with a suitable choice the two-body amplitude $\tilde{t}$. Now because of (5.4), this is not so. For $\delta(z) \ll v$, the following expansion can be used

$$\frac{dz}{v(z)} = \frac{dz}{v + \delta(z)} = \frac{dz}{v}\left[1 - \frac{\delta(z)}{v} + \left(\frac{\delta(z)}{v}\right)^2 - \right] \tag{5.7}$$

Equation (5.5) now can be written as

$$\Delta P_{\parallel} = -(A_p A_T) \int d^3\vec{\xi_p}\; \rho_p(\vec{\xi_p}) \int d^3\vec{\xi_T}\; \rho_T(\vec{\xi_T})$$

$$\left[\vec{\nabla}_{\xi_p} \int_{-\infty}^{\infty} Im\;\tilde{t}\;(\vec{x'},\vec{\xi_p},\vec{\xi_T})\frac{dz'}{v} \right.$$

$$\left. -\vec{\nabla}_{\xi_p} \int_{-\infty}^{\infty} Im\;\tilde{t}\;(\vec{x'},\vec{\xi_p},\vec{\xi_T})\frac{dz'}{v} \cdot \frac{\delta(z')}{v} + \ldots \right] \tag{5.8}$$

Note that we have obtained a series that takes into account corrections to our previous expressions, (5.5) and (5.6). The first term in (5.8) is (5.5), as expected. Successive terms are corrections to (5.5) due to the asymmetry introduced as a result of momentum transfer. For $\delta(z)$

$\ll$ v, the higher order corrections should be small at high energies, and the series should converge rapidly.

A reasonable ansatz for $\delta(z)$ is

$$\frac{d}{dz} \delta(z) \, \alpha \, V(b,z) \tag{5.9}$$

The above equation (5.9) implies

$$\delta(z) \, \alpha \int_{-\infty}^{z} V(b,z) \, dz \tag{5.10}$$

$$\begin{aligned} &\alpha \; \chi(b,z) \\ &= \frac{\chi(b,z)}{\chi(b)} \cdot \Delta v \end{aligned} \tag{5.11}$$

with Δv as in (5.3) and the phase shift operator is

$$\chi(b,z) \; = \; - \frac{\mu}{k} \int_{-\infty}^{z} V(b,z) dz \; = \; - \frac{1}{v_{rel}} \int_{-\infty}^{z} V(b,z) dz \tag{5.12}$$

Also note that

$$\frac{\delta(z)}{v} \underset{z \to \infty}{\to} \frac{\delta(\infty)}{v} = \frac{\Delta v}{v} \; , \; \text{as expected.} \tag{5.13}$$

Equation (5.8) can now be written as

$$\Delta P_{\parallel}' = \Delta P_{\parallel} - \Delta P_{\parallel}^{corr} + \dots \tag{5.14}$$

where the correction, $O(\frac{\Delta v}{v})$ is

$$\Delta P_{\parallel}^{corr} = -(A_p A_T) \int d^3\vec{\xi}_p \; \rho_p(\vec{\xi}_p) \int d^3\vec{\xi}_T \; \rho_T(\vec{\xi}_T)$$
$$\left[\vec{\nabla}_{\xi_p} \int_{-\infty}^{\infty} \text{Im} \; \bar{t} \; (\vec{x}',\vec{\xi}_p,\vec{\xi}_T) \; \frac{\chi(b,z)}{\chi(b)} \; \frac{dz'}{v} \frac{\Delta v}{v} \right] \tag{5.15}$$

Numerical evaluation of the ratio appearing in (5.11), $\chi(b,z)/\chi(b)$

has been carried out for various projectile target combinations for

impact parameters ranging from 0-15 fm. The energy dependence of this

ratio has also been checked. This ratio has been compared for ^{16}O +

^9Be (fig. 28) and ^{16}O + ^{208}Pb at incident energy of 2.1 A GeV. Two

extreme values of impact parameter (b - 0,7 (fm) for ^9Be and b - 0,11

(fm) for ^{208}Pb) were chosen. The ratio is almost impact parameter

independent for the Be target whereas differences of 15-20% are

observed for the Pb target. Since the ratio $\dfrac{\chi(b,z)}{\chi(b)} - \dfrac{\delta(z)}{\Delta v}$, the above

indicates that the z-dependent change in velocity $\delta(z)$ is more pro-

nounced for a heavier target (^{208}Pb) than a lighter one (^9Be) at the

same impact parameter. This is in accord with our physical understand-

ing since ^9Be matter density is roughly Gaussian so that the ratio is

independent of b. For a heavy target such as ^{208}Pb, matter density is

more appropriately of the Woods-Saxon type so that the ratio depends on

the impact parameter. Thus the ansatz (5.9) is physically reasonable.

The resulting asymmetry $\Delta P_{\parallel}^{corr}$ was evaluated for ^{16}O (2.1 A GeV) + ^9Be

and is plotted in figure 29 (the correction $\Delta P_{\parallel}^{corr}$ has been multiplied

been multiplied by 10 for display). It can be seen that the correction

at impact parameters 4.52 - 5.53 fm is merely 3% or less. At smaller

impact parameters, however, the magnitude of the longitudinal momentum

transfer as well as the correction to it are slightly greater, indi-

cating the impact parameter dependence of these quantities.

Another question that we can investigate is the energy dependence

of the correction $\Delta P_{\parallel}^{corr}$. The energy dependence of longitudinal
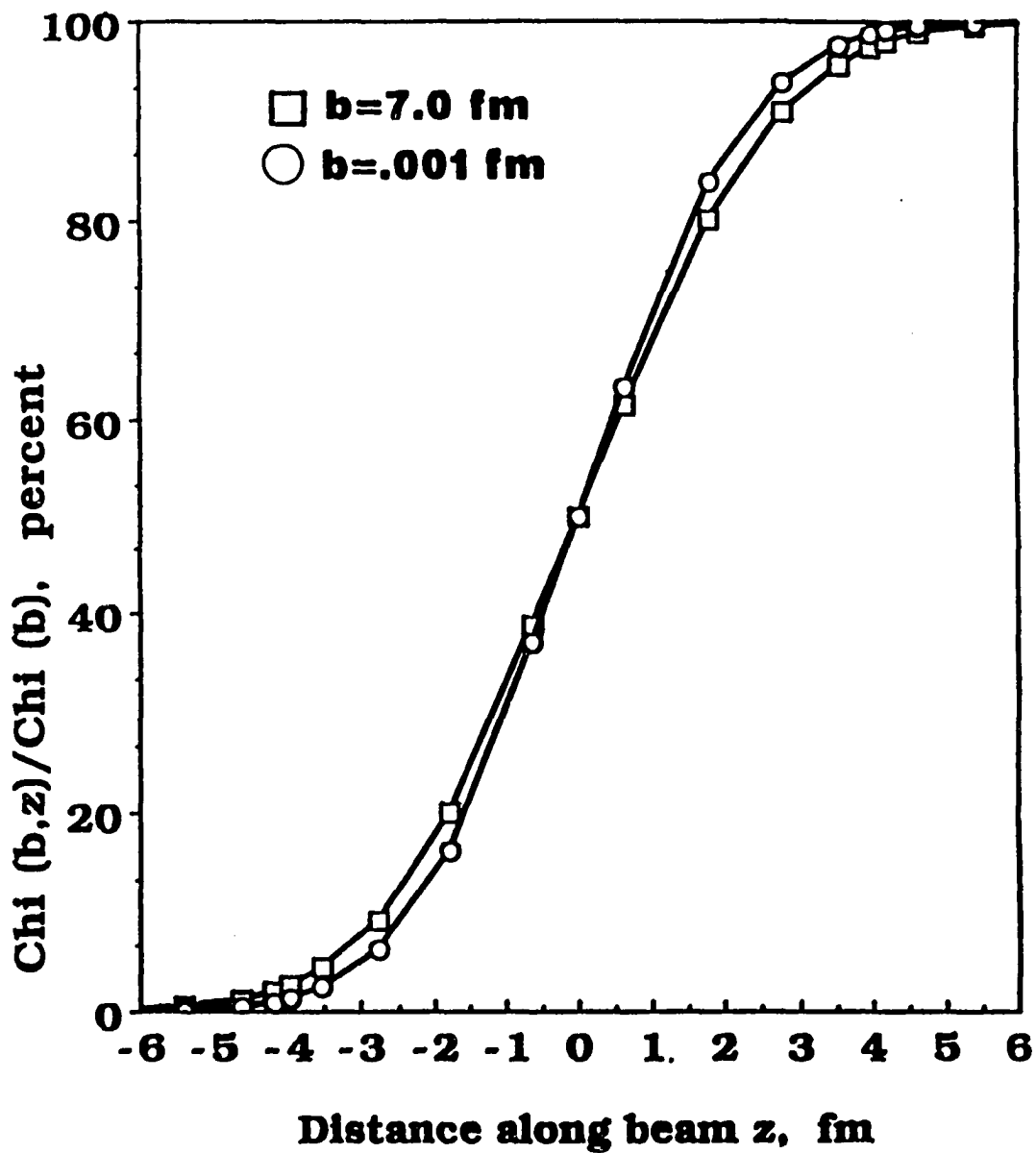
Figure 28: The ratio of phase-shift parameter χ (b, z)/χ (b) as a function of b and z (where z is the distance along the beam direction and b is the impact parameter) in the reaction ^{16}O (2.1 AGeV) + $^9Be \rightarrow$ Projectile Fragment + X.
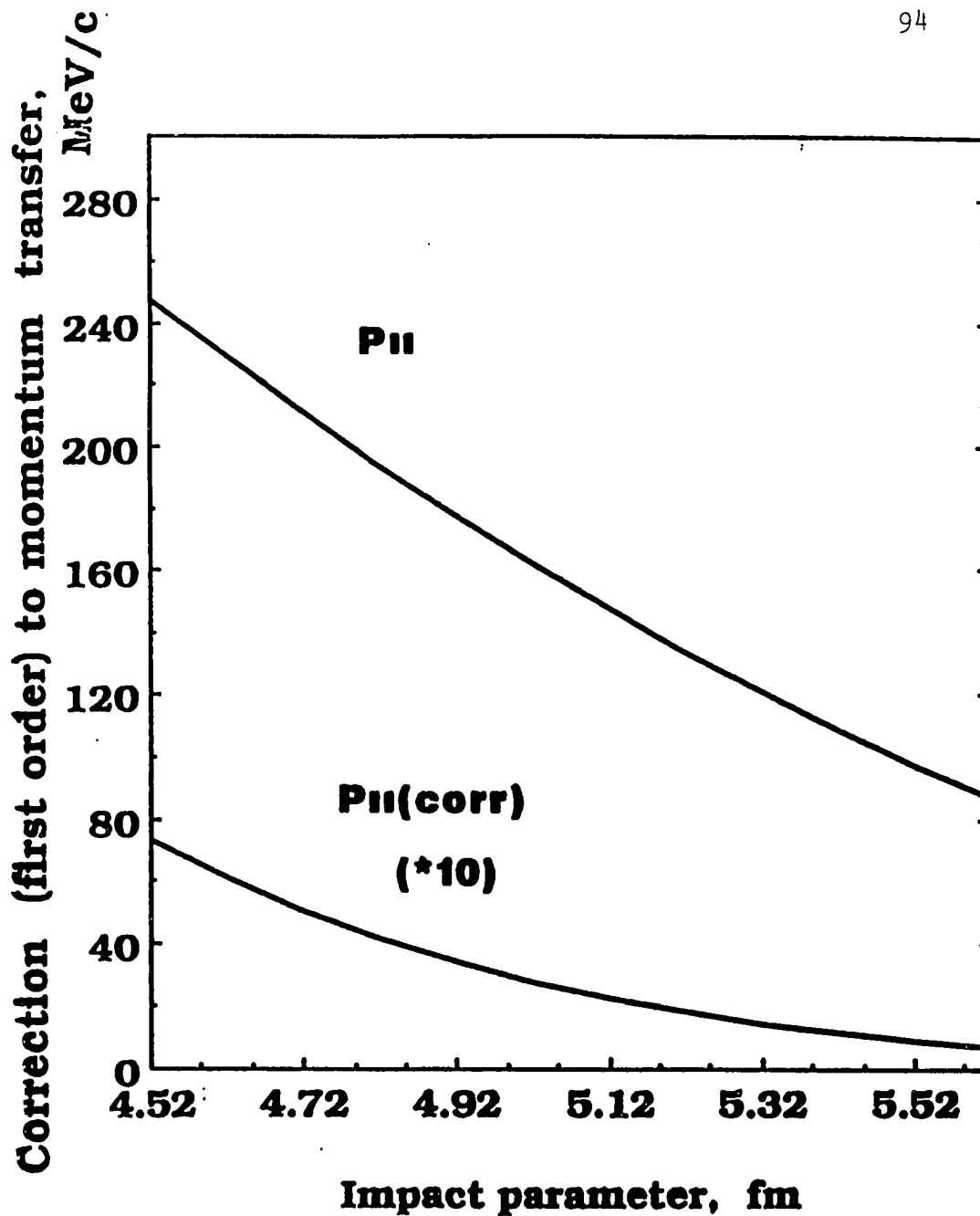
Figure 29: First order correction to calculated longitudinal momentum transfer as a function of impact parameter for $^{16}O(2.1 \text{ A GeV})+^{9}Be \rightarrow$ Projectile Fragment +X. The correction P_{11}^{corr} has been multiplied by 10 for comparison purposes.
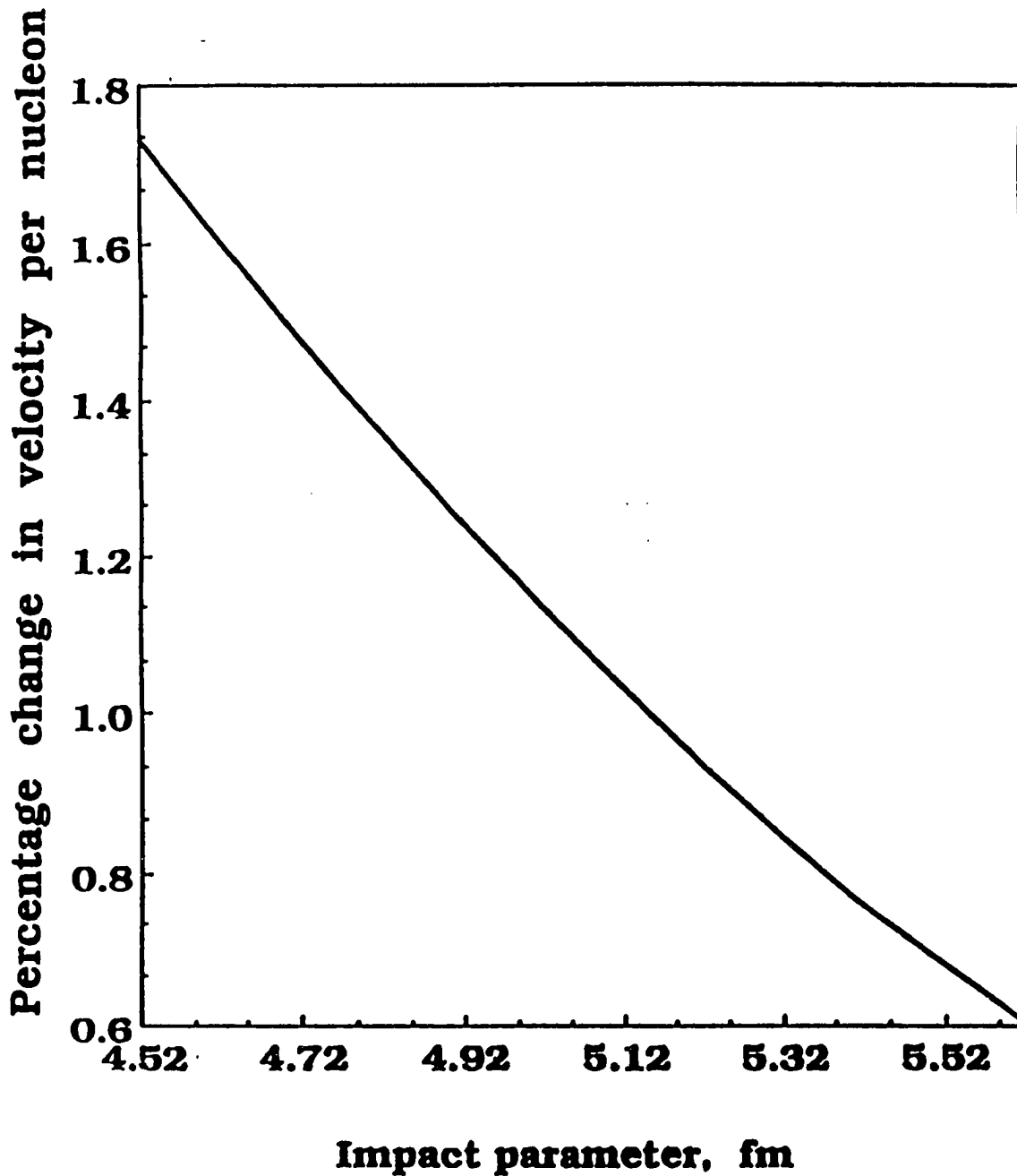
Fig. 30 Ratio of change in velocity per nucleon to incident velocity per nucleon (as determined by the incident beam energy) for ^{16}O (2.1 A GeV)+^{9}Be—>Projectile Fragment+X due to momentum transfer as a function of impact parameter.

momentum transfer has previously been displayed in figure 25. It was

observed that longitudinal momentum transfer saturates around -1 A GeV.

At 0.2 A GeV, for example, Longitudinal Momentum Transfer (LMT) is -160

MeV/c at 4.52 fm for $^{16}O + ^9Be$. At 3 fm, the correction $\Delta P_{\parallel}^{corr}$ is -100

MeV/c, which is -27% of the longitudinal momentum transfer of 370

MeV/c. At 2.1 A GeV, there is only a -10% correction at 3 fm.

Finally the ratio $\frac{\Delta v}{v}$ is plotted as a percentage at 2.1 A GeV for

$^{16}O + ^9Be$. Note that Δv has been defined in (5.3). The ratio is -1.6%

at these impact parameters and higher at 3-4 fm. At 0.2 A GeV, this

ratio is higher as expected, again indicating that momentum transfer

introduces relatively greater change of velocity (per nucleon) at .2

A GeV than at 2.1 A GeV.

These effects should be experimentally observable at intermediate

energy heavy ion collisions. Note that the higher order corrections in

(5.7) have not been evaluated because their magnitude is expected to be

small at high energies. At intermediate energy, these may not be small

so that all the higher order terms may need to be taken into account.

V.b Coulomb Corrections

A complete treatment of the problem of momentum and energy trans-

fer in relativistic heavy ion collisions must take into account Coulomb

effects. In low-energy heavy ion collisions, Coulomb effects play a

significant role. At relativistic energies, the importance of the

electromagnetic fields generated can be understood by analyzing the

Coulomb dissociation cross-sections in the fragmentation reactions[91].

It was found that these electromagnetic dissociation cross-sections are

sometimes comparable to the nuclear contribution and may overwhelm the latter for high Z (where Z is the charge number) targets such as Lead or Uranium. This is specially true of single-nucleon knockout reactions[92] of the type A_p + Target → (A_p-1) + X for projectiles such as ^{12}C(2.1 A GeV), ^{16}O(2.1 A GeV) and ^{12}C(1.05 A GeV) on targets ^{27}Al, ^{64}Cu, ^{108}Ag and ^{208}Pb. Excitation of the giant resonances[93] such as the Giant Dipole Resonance (GDR) and to some extent the Giant Quadrupole Resonance (GQR) and their decay contribute primarily to the one-nucleon knockout cross-sections, although the contribution of magnetic M1 resonance has also been pointed out.[93] The common procedure for the analysis of such Electromagnetic Dissociation cross-sections is due to Fermi, Weizsacker and Williams; it is known as the Weizsacker-Williams method of virtual quanta[94]. The EM fields generated by a relativistic projectile are equivalent to two plane wave pulses of radiation P_1 and P_2 impinging on the target, P_1 along the beam direction and P_2 transverse to it. The equivalent photon spectrum has been derived in many texts including Jackson; it is included in the Appendix for completeness. It can be seen that the photon number spectrum scales as Z_T^2 where Z_T is the charge number of the target; hence the overwhelming contribution for high Z targets can be understood.

We shall treat Coulomb corrections at various levels beginning with the proton-proton interaction. This will be generalized, via the Weizsacker-Williams approach to heavy-ion collisions at relativistic energies.

Consider the two-body transition amplitude of this work for pp

interaction. This was given by

$$t_{pp} \ (e,\vec{y}) = -\sqrt{\frac{e}{m}} \ \sigma_{pp}(e) \ [\alpha_{pp}(e) + i] \ [2\pi B_{pp}(e)]^{-3/2} exp \left(- \frac{\vec{y}^2}{2B_{pp}(e)} \right) \quad (5.16)$$

$$= - t(o) \ exp \ (-K\vec{y}^2) \qquad (5.17)$$

with $K = 1/2B_{pp}(e)$ and $t(o)$ is understood to be

$$t(o) = \sqrt{e/m} \ \sigma_{pp}(e) \ [\alpha_{pp}(e) + i] \ [2\pi B_{pp}(e)]^{-3/2} \qquad (5.18)$$

where $\sigma_{pp}(e)$, $\alpha_{pp}(e)$ and $B_{pp}(e)$ are the pp cross-section, ratio of the

real to the imaginary part of the forward scattering amplitude and the

slope parameter respectively; $\vec{y}$ is the relative separation between the

charges. With the parameters in Table 1 (with $\alpha_{pp}(e) = -.374$), the

transition amplitude at 2.1 A GeV is

$$t_{pp}(e,\vec{Y}) = (35 - 94i) \ exp(-1.19 \ \vec{Y}^2) \ MeV \qquad (5.19)$$

Momentum transfer to the target proton is semiclassically

$$\vec{\Delta P} = \int_{-\infty}^{\infty} \vec{\nabla} t_{pp}(\vec{Y}^2) \ \frac{dz}{v}; \quad dz = vdt, \quad v = \beta c$$

$$= - \int_{-\infty}^{\infty} \left[\frac{\partial}{\partial b} \hat{b} + \frac{\partial}{\partial z} \hat{z} \right] \ t(o) \ exp(-1.19 \ (\vec{b}^2 + z^2)) \ \frac{dz}{v}$$

$$\propto (143 - 382 \ i) \ b \ e^{-(\vec{b}^2 + z^2)(1.19)} \ \hat{b} \ \frac{MeV}{c} \qquad (5.20)$$

For $| \ b \ | = 1$ fm, $z = 1$ fm,

$$\Delta P \cong -13.2 \ \frac{MeV}{c} \ \hat{b} + 35.4 \ \frac{MeV}{c} \ i \ \hat{b}$$

$$= (-13.2 \ \hat{b} - 35.4 \ \hat{z}) \ \frac{MeV}{c} \quad with \ i\hat{b} = -\hat{z} \qquad (5.21)$$

At a separation of ~1.4 fm, an incoming proton imparts ~13 $\frac{MeV}{c}$ of

transverse momentum due to strong interactions. The Coulomb repulsion

of the protons contributes only

$$\Delta P = \frac{2e^2}{bv} \simeq 3 \ \frac{MeV}{c} \tag{5.22}$$

of transverse momentum to the target. However, as the separation grows

large, the nuclear and Coulomb contributions become comparable. The

above calculation of the Coulomb effect was performed by evaluating

the z-integrated force in an impulsive collision. Only the transverse

electric field contributes, the longitudinal field's contribution

vanishes due to symmetry.

For heavy-ions, the above method for treating the Coulomb repul-

sion can be generalized via the Weizsäcker-Williams method.

Consider the collision of heavy-ions with charge numbers Z_p, Z_T

respectively, with relative velocity $v = \beta c$ per nucleon. The EM

fields generated at the projectile by the target (and vice-versa) can

be found from equation (D.1) of Appendix D with $q = Z_T e$. The momentum

transfer in an impulsive collision is

$$\Delta P = Z_p \ e \int_{-\infty}^{\infty} E_{tran} \ (t) \ dt = 2 \ Z_p Z_T \ e^2/bv \ \hat{b} \tag{5.23}$$

with the longitudinal contribution vanishing due to symmetry.

The above equation is the basis of our calculations. For ^{12}C and

^{16}O projectiles (at 2.1 AGeV) on various targets ranging from Be

through Pb, we have previously calculated the transverse and longitudi-

nal momentum transfer in Chapter IV. Coulomb contribution is now shown

in Figures 31-33 and compared with the nuclear contribution. As can be
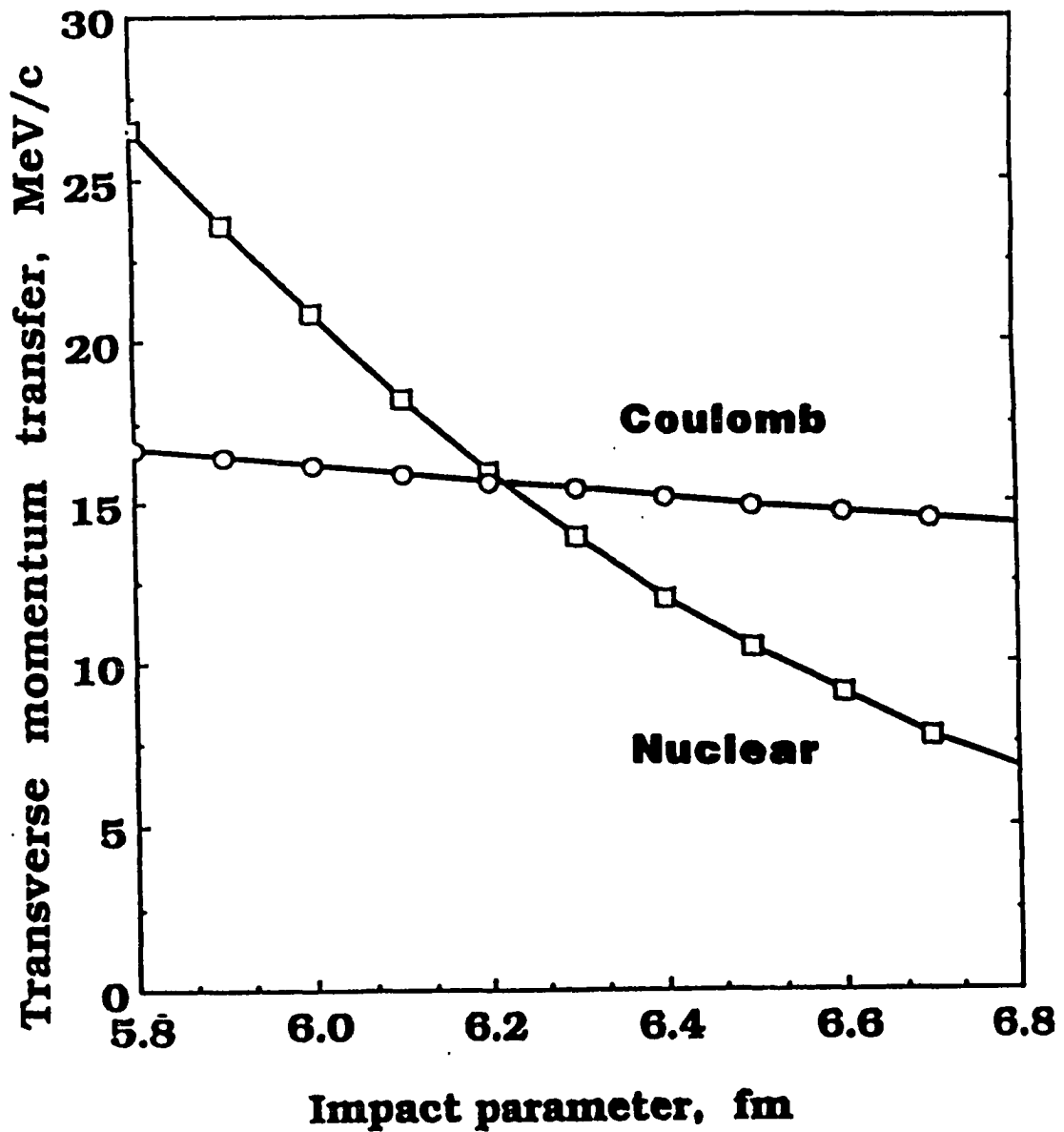
Figure 31: Transverse momentum transfer (MeV/c) to [16] O Projectile by the [9]Be target due to Coulomb interaction compared with the nuclear contribution as a function of impact parameter (fm) at B_{inc}=2.1 A GeV.
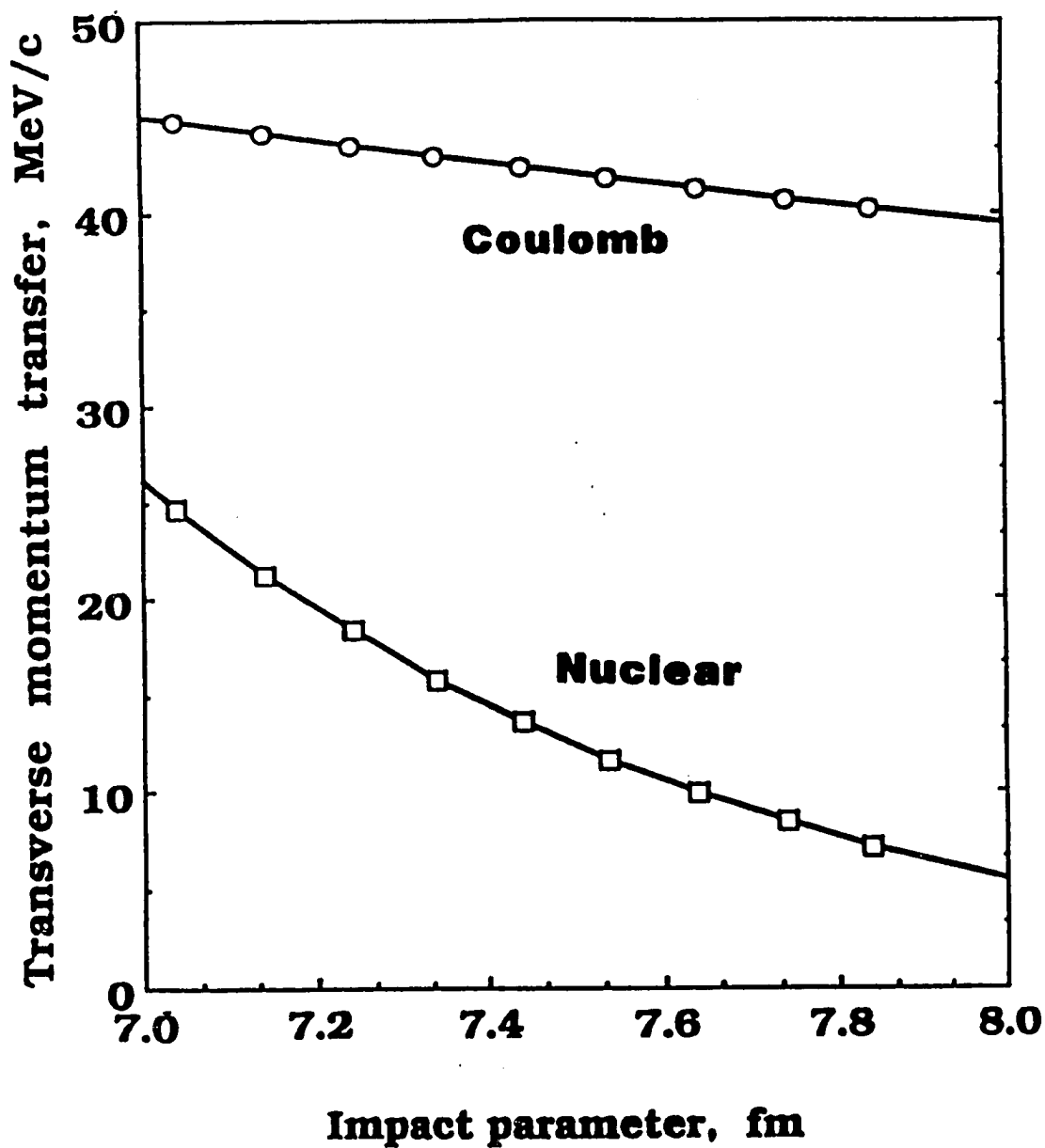
Figure 32: Transverse momentum transfer (MeV/c) to ¹⁶O Projectile by the ²⁷Al target due to Coulomb Interaction compared with the nuclear contribution as a function of Impact parameter (fm) at E_{Inc}=2.1 A GeV.
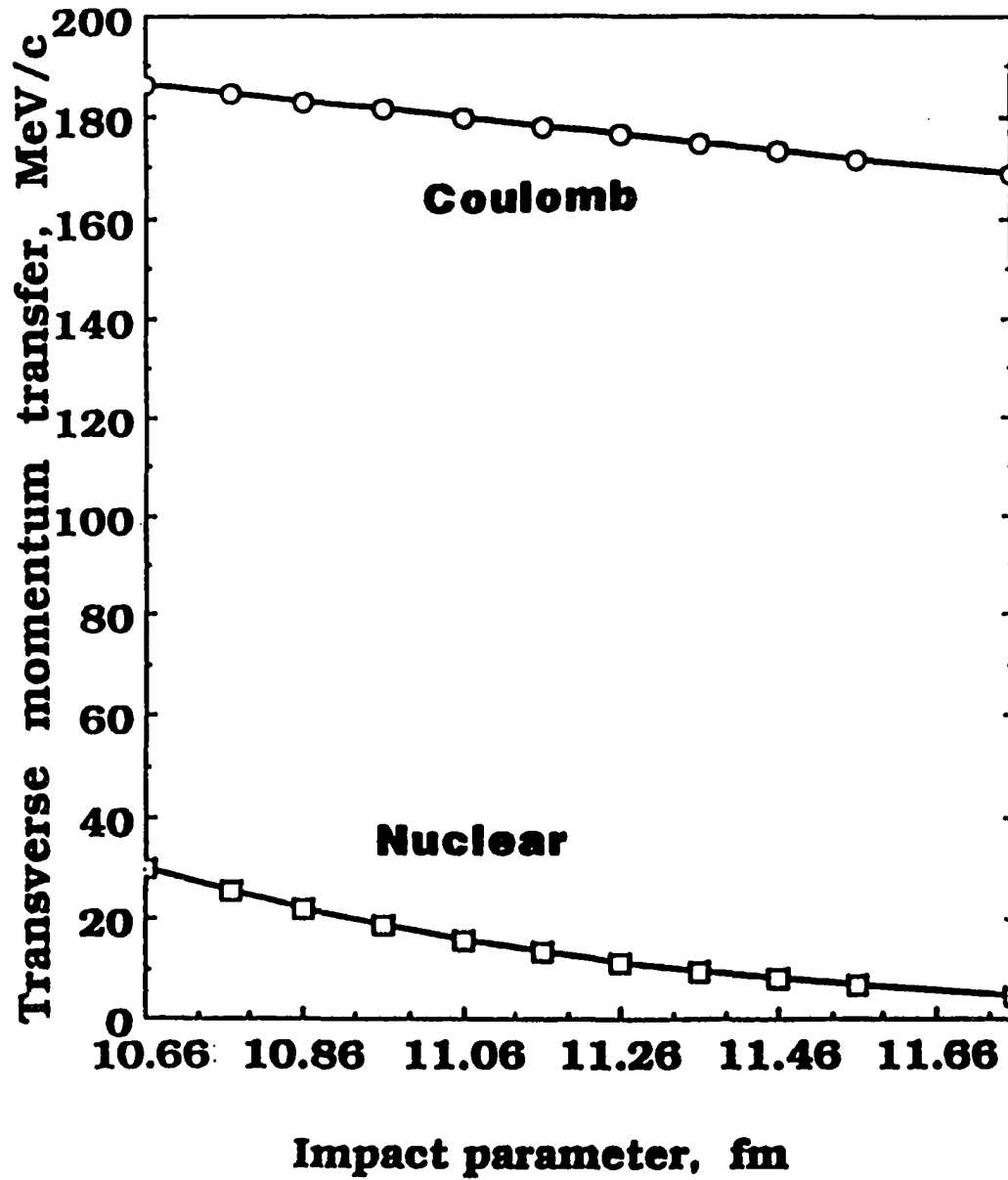
Figure 33: Transverse momentum transfer (MeV/c) to ^{16}O Projectile by the Pb target due to Coulomb interaction compared with the nuclear contribution as a function of impact parameter (fm) at E_{inc}=2.1 A GeV.

readily seen for heavier targets, Coulomb effects are non-negligible and may modify the transverse momentum spectra of fragments substantially. Note that an impact parameter cutoff b_{min} was included in the calculations. This was done to separate the strong interaction effects from the Coulomb.

Inherent in the Weizsacker-Williams approach is the point-Coulomb assumption for the heavy-ions. For impact parameters $b > b_{min}$ this is a reasonable assumption. However, for collisions with $b < b_{min}$ where $b_{min} = R_{0.1}$ (Projectile) $+ R_{0.1}$ (Target) (i.e. the sum of 10% charge radii of the projectile and target), the point Coulomb assumption becomes questionable. This can be seen in the departure of the potential for a unit charge in a uniform charge distribution from that of the point-Coulomb potential[95] i.e.

$$V(\tilde{r}) = \frac{Ze^2}{R} \left[\frac{3}{2} - \frac{1}{2} \left(\frac{r}{R} \right)^2 \right] \quad , \quad r < R$$

$$= \frac{Ze^2}{r} \quad , \quad r > R \tag{5.24}$$

with R the uniform charge radius of the distribution. This departure in the potential has been plotted in figure 34. The corresponding momentum transfer is reduced in magnitude as the overlap increases. For heavy ions described as two uniform charge distributions, extension of the above argument throws into doubt, for $b < b_{min}$, the Weizsäcker-Williams approach based on the point-Coulomb field.
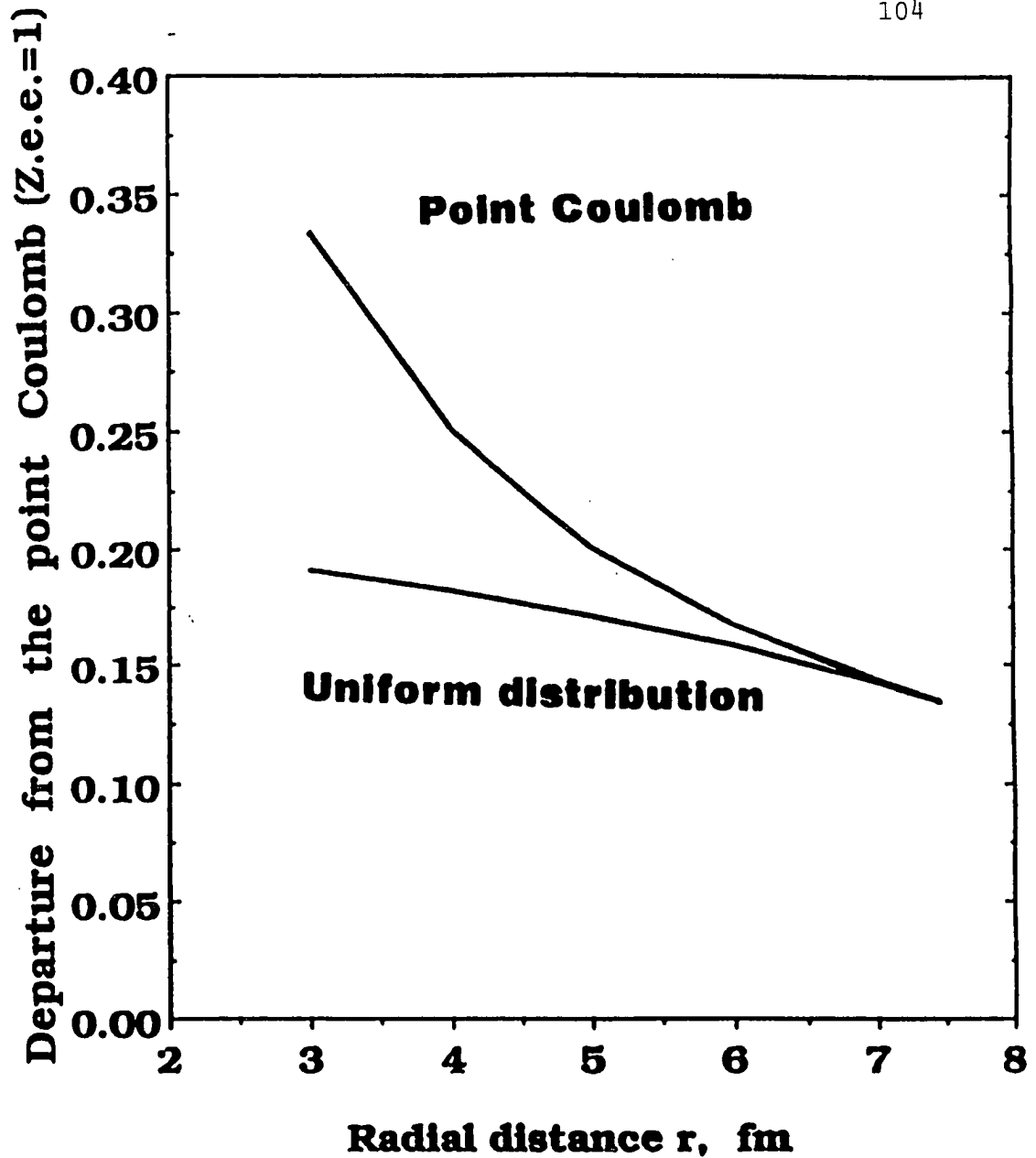
Figure 34: Departure of the Coulomb potential felt by an incident charge within a uniform charge distribution (^{208}Pb, Z=82) of radius R=1.26(A**(1/3)) from the point Coulomb field. The constant C in $V_{coul}(r)$=C/r has been set to unity.

CHAPTER VI

SUMMARY

In this work, an optical model description of momentum (longitudinal and transverse) transfer and energy deposition in relativistic heavy-ion collisions has been presented within the multiple scattering theory framework. Longitudinal and transverse momentum transfer have been evaluated and compared with experiment for various projectile-target combinations. Momentum "downshifts" of projectile fragments in the collision of ^{12}C (2.1 AGeV), ^{16}O (2.1 AGeV) and ^{12}C (1.05 AGeV) with targets ranging from ^{9}Be through ^{208}Pb have been evaluated using the above theory and compared with target-averaged data from experiments. Transverse momentum widths of Lanthanum fragments in the reaction of ^{139}La (1.2 AGeV) with ^{12}C have also been calculated. Quantitative as well as qualitative agreement has been found with experiment. Thus the theory of this work can account for many features of heavy ion momentum spectra in a comprehensive fashion.

Energy transfer calculations can also be undertaken using the optical model description along the above lines. Such calculations are significant because energy transfer determines the various channels available for de-excitation (in the two stage Abrasion-Ablation model of relativistic heavy ion collisions). Sophisticated experiments in the future will hopefully address this question. Theoretical calculations are already in progress in this respect and await comparisons with future experimental measurements.

We have provided, through "The Deceleration correction," a method for investigating and correcting the oft-used constant velocity assumption. Momentum transfer to the projectile could invalidate such an assumption. Based on our calculations, we find at relativistic speeds, that this change is minor. Specifically, we found that the first-order correction to our calculations were small at high energies ($v \simeq c$). These corrections, however, were found to be substantial at lower bombarding energies, provided the impulse approximation remains valid at these energies.

The very important question of Coulomb effects has also been addressed. This has been done within the Weizsacker-Williams method of virtual quanta. We find a substantial momentum transfer (transverse) due to repulsion of the charges. Use of more realistic charge distributions in place of the point-Coulomb assumption made in the Weizsacker-Williams approach resulted in reduction of the magnitude of momentum transfer as the collision impact parameters grew smaller.

The future directions for research in this area remain open. Only the single scattering term of the multiple scattering series has been utilized so far. The importance of the double-scattering term and its physical meaning within the context of our work remains to be explored in detail. A comprehensive theory of energy-momentum transfer within the framework of energy-momentum conservation requires the relativistic theory of nucleus-nucleus interactions. Although a satisfactory theory of proton-nucleus multiple scattering formalism (Dirac phenomenology) already exists, similar approaches have had limited success for heavy-ions. An alternate approach may be the theory currently known as "Quantum Hadrodynamics"[96] which is a relativistic field theory of

strongly interacting mesons and baryons. Semi-classical solutions for energy-momentum transfer can be obtained from the above theory for the collision of heavy-ions. Such approaches already show substantial promise. Future work should definitely proceed along these lines.

REFERENCES

1. P. Freier, E.J. Lofgren, E.P. Ney, F. Oppenheimer, H.L Bradt and G. Peters, Phys. Rev. 74, 213 (1948).

2. P. Freier, E.J. Lofgren, E.P. Ney, and F. Oppenheimer, Phys. Rev. 74, 1818 (1948).

3. H. Alfven, Nature 143, 435 (1939).

4. M.M. Shapiro and R. Silberberg, Ann. Rev. Nucl. Sci. 20, 323 (1970).

5. C.J. Waddington, Prog. Nucl. Phys. 8, 1 (1960).

6. C.F. Powell, P.H. Fowler, D.H. Perkins, "The Study of Elementary Particles by the Photographic Method," (Pergamon, London, 1959).

7. H.L. Bradt and B. Peters, Phys. Rev. 74, 1828 (1948); H.L. Bradt and B. Peters, Phys. Rev. 75, 1779 (1949); H.L. Bradt and B. Peters, Phys. Rev. 80, 943 (1950).

8. Y. Eisenberg, Phys. Rev. 96, 1378 (1954).

9. G. Alexander and G. Yekutieli, Nuovo Cimento 19, 103 (1961).

10. G.Alexander, J. Avidan, A. Anvi, G. Yekutieli, Nuovo Cimento 20, 648 (1961).

11. P.L. Jain, E. Lohrmann, M. Teucher, Phys. Rev. 115, 643 (1959).

12. Y. Tsuzuki, J. Phys Soc. Jpn., 16, 2131 (1961).

13. K. Rybicki, Nuovo Cimento 28, 1437 (1963).

14. F. Abraham, J. Gierula, R. Levi-Setti, K. Rybicki and C.H. Tsao, Phys. Rev. 159, 1110 (1967).

15. B. Andersson, I. Otterlund and K. Kristiansson, Ark. Phys. 31 527 (1966).

16. M.G. White, M. Isaila, K. Prelec and H.L Allen, Science 174, 1121 (1971); H.A. Grunder, W.D. Hartsough and E.J. Lofgren, Science 174, 1128 (1971).

17. F.J.M. Farley, "Speculations on Nucleus-Nucleus Collisions with the ISR," CERN NP Intern. Rep. 70-26 (1970), unpublished.

18. A. Ghiorso, H. Grunder, W. Hartsough, G. Lambertson, E. Lofgren, K. Lou, R. Main, R. Mobley, R. Morgado, W. Salsig and F. Selph, IEE Trans. Nucl. Sci. NS-20 (3), 155 (1973).

19. D.E. Greiner, P.J. Lindstrom, H.H. Heckman, B. Cork and F.S. Bieser, Phys. Rev. Lett. 35, 152 (1975).

20. H. Feshbach and K. Huang, Phys. Lett. B 47, 300 (1973).

21. J.V. Lepore and J.R. Riddell Jr., Lawrence Berkeley Laboratory Report No. 3086 (1974), unpublished.

22. A.S. Goldhaber, Phys. Lett. B 53, 306 (1974).

23. N. Masuda and F. Uchiyama, LBL Report 4263 (1975), unpublished.

24. G.F. Bertsch, Phys. Rev. Lett. 46, 472 (1981).

25. M.J. Murphy, Phys. Lett. B 56, 23 (1975).

26. F.P. Brady, W.B. Christie, J.L. Romero, C.E. Tull, b. McEachern, M.L. Webb, J.C. Young, H.J. Crawford, D.E. Greiner, P.J. Lindstrom and H. Sann, Phys Rev. Lett. 60, 1699 (1988).

27. W. A. Friedman, Phys. Rev. C, 27(#2), 569 (1983).

28. J. Hufner, K. Schafer and B. Schurman, Phys. Rev. C. 12, 1888 (1975).

29. S.H. Fricke, Ph.D. Thesis, University of Minnesota (1984), unpublished; B.J. Bayman, P.J. Ellis and Y.C. Tang, Phys Rev. Lett. 53, 1322 (1984).

30. J.D. Bowman, W.J. Swiatecki and C.F. Tsang, LBL Report No. LBL-2908 (1973), unpublished.

31. K.M. Watson, Phys. Rev. 89, 575 (1953).

32. M.L. Goldberger and K.M. Watson, "Collision Theory," (John Wiley and Sons, N.Y.), pp. 749 (1964).

33. R.J. Glauber, Phys. Rev. 100, 242 (1955).

34. V. Franco and R.J. Glauber, Phys. Rev. 142, 1195 (1966).

35. L. Zamick, Ann. Phys. 21, 550 (1963).

36. V. Franco, Phys. Rev. 175, 1376 (1968).

37. O. Kofoed-Hansen, Nuovo Cimento 60A, 621 (1969).

38. W. Czyz and L.C. Maximon, Ann. Phys. 52, 59 (1969).

39. J.W. Wilson, Phys. Lett. 52B, 149 (1974).

40. J.W. Wilson, Ph.D. Thesis, College of William and Mary (1975), unpublished.

41. J.W. Wilson and L.W. Townsend, Can. Journal of Physics 59, 1569 (1981).

42. J.W. Wilson and C.M. Costner, NASA Technical Note D-8107 (1975).

43. L.L. Foldy and J.D. Walecka, Ann. Phys. (NY), 54, 447 (1969).

44. R.J. Glauber, "Lectures in Theoretical Phys.," Vol. I, Ed. W.E. Brittin and L.G. Dunham, (Interscience Publishers, Inc., N.Y.), pp. 364 (1959).

45. E. Merzbacher, "Quantum Mechanics," (John Wiley & Sons, Inc., New York), pp. 167 (1970).

46. K. Gottfried, "Quantum Mechanics," Vol. I, (W.A. Benjamin, Mass.), pp. 240 (1966).

47. P.M. Morse and H. Feshbach, "Methods of Theoretical Physics," (McGraw-Hill, New York) Part I, pp. 349 (1953).

48. H.H. Heckman, D.E. Greiner, P.J. Lindstrom and F.S. Bieser, Phys. Rev. Lett. 28, 926 (1972).

49. P.J. Lindstrom, D.E. Greiner, H.H. Heckman, B. Cork and F.S. Bieser, LBL Report No. 3650 (1975).

50. D.E. Greiner, P.J. Lindstrom, F.S. Beiser and H.H. Heckman, Nucl. Inst. Methods 116, 21 (1974).

51. H.H. Heckman, Heavy Ion Fragmentation Experiments at the Bevatron, NASA CR-142589 (1975).

52. D.L. Olson, B.L. Berman, D.E. Greiner, H.H. Heckman, P.J. Lindstrom and H.J. Crawford, Phys. Rev. C. 28, 1602 (1983).

53. J. Jaros, Ph.D. Thesis, Univ. of Calif., Berkeley (1975), unpublished; LBL Report No. 3849 (1975), unpublished.

54. H.H. Heckman, D.E. Greiner, P.J. Lindstrom, H. Shwe, Phys. Rev. C 17 1735 (1978).

55. G.M. Chernov, K.G. Gulamov, U.G. Gulyamov, S.Z. Nasyrov, L.N. Svechnikova, Nucl. Phys. A 280, 478 (1977).

56. B. Jakobsson and R. Kullberg, Phys. Ser. 13, 327 (1976).

57. B. Judek, Proc. Int. Conf. Cosmic Rays, 14th Munchen, 2342 (1975).

58. R. Kullberg, K. Kristiansson, B. Lindkvist and I. Otterland, Nucl. Phys. A 280, 431 (1977).

59. H.L. Bradt and B. Peters, Phys. Rev. 77, 54 (1950).

60. S. Barshay, C.B. Dover, J.P. Vary, Phys. Rev. C 11, 360 (1975).

61. P.J. Karol, Phys. Rev. C 11, 1203 (1975).

62. J.W. Wilson and C.M. Costner, NASA Technical Note No. D-8107 (1975), unpublished.

63. J.W. Wilson and L.W. Townsend, Can. Journal of Physics 59, 1569 (1981).

64. L. Anderson, Ph.D. Thesis, Univ. of Calif., Berkeley (1977), unpublished.

65. J. Papp, J. Jaros, L. Schroeder, J. Staples, H. Steiner, A. Wagner and J. Wiss, Phys. Rev. Lett. 10, 601 (1975).

66. R.K. Bhaduri, Phys. Lett. 50B, 211 (1974).

67. M. Buenerd, C.K. Gelbke, B.G. Harvey, D.L. Hendrie, J. Mahoney, A. Menchaca-Roca, C. Olmer, D.K. Scott, Phys. Rev. Lett. 37, 1191 (1976).

68. C.K. Gelbke, M. Buenerd, D.L. Hendrie, J. Mahoney, M.C. Mermaz, C. Olmer, D.K. Scott, LBL Report No. 5826 (1977).

69. C.K. Gelbke, D.K. Scott, M. Bini, D.L. Hendrie, J.L. Laville, J. Mahoney, M.C. Mermaz, C. Olmer, Phys. Lett. B 70, 415 (1977).

70. V. Franco and G.K. Varma, Phys. Rev. C 15, 1375 (1977); V. Franco and A. Tekou, Phys. Rev. C 16, 658 (1977); V. Franco and W.T. Nutt, Phys. Rev. C 17, 1347 (1978).

71. T.F. Cleghorn, MS. Thesis, Univ. of Minnesota (1967); Report No. CR-104.

72. T.F. Cleghorn, P.S. Freier and C.J. Waddington, Can. J. Phys. 46, 572 (168).

73. R. Serber, Phys. Rev. 18, 304 (1949).

74. J. Gosset, H.H. Gutbrod, W.G. Meyer, A.M. Poskanzer, A. Sandoval, R. Stock and G.D. Westfall, Phys. Rev. C 16, 629 (1977).

75. L.F. Oliveira, R. Donangelo and J.O. Rasmussen, Phys. Rev. C 19 826 (1979).

76. M. Bleszynski and C. Sander, Nucl. Phys. A 326, 525 (1979).

77. L.W. Townsend, Can. J. Phys. 61, 93 (1983).

78. L.W. Townsend, J.W. Wilson and J.W. Norbury, Can. J. Phys. 63, 135 (1985).

79. L.W. Townsend, J.W. Wilson, F.A. Cucinotta and J.W. Norbury, Phys. Rev. C 34, 1491 (1986).

80. M.P. Guthrie, Oak Ridge National Laboratory Technical Memorandum #3119 (1970).

81. H.W. Bertini, R.T. Santoro and O.W. Hermann, Phys. Rev. C 14, 590 (1976).

82. R.K. Smith and M. Danos, Proc. Meeting Heavy-Ion Collisions, 363 (1977).

83. C.Y. Wong, Proc. 5th High Energy Heavy Ion Study, p. 61 (Lawrence Berkeley Laboratory Report No. LBL-12652), 1981.

84. F. Reif, "Statistical and Thermal Physics," p. 39 (McGraw-Hill, N.Y. 1965).

85. A.I. Khinchin, "Mathematical Foundations of Statistical Mechanics," p. 166 (Dover, NY 1949).

86. L.W. Townsend and J.W. Wilson, NASA Reference Publication No. RP-1134 (1985).

87. R. Hofstadter and H.R. Collard, "Landolt-Bornstein Numerical Data and Functional Relationships in Science and Technology," Group I, Vol. 2, 21 (ed. H. Schopper, Springer-Verlag, 1967).

88. C.W. DeJaeger, H. DeVries and C. DeVries, "Atomic Data & Nucl. Data," Vol. 14, No. 5/6, 479 (1974).

89. J.W. Wilson, L.W. Townsend and F.F. Badavi, Nucl. Inst. Methods in Phys. Res., B18, 225 (1987).

90. E.J. Moniz, I. Sick, R.R. Whitney, J.R. Ficence, R.D. Kephart and W.P. Trower, Phys. Rev. Lett. 26, 445 (1971).

91. J.W. Norbury and L.W. Townsend, NASA TP-2527, 1986.

92. H.H. Heckman and P.J. Lindstrom, Phys. Rev. Lett. 36, 193 (1976).

93. C.A. Bertulani and G. Baur, Phys. Rep. 163 (5 & 6), 1988.

94. A.D. Jackson, "Classical Electrodynamics," p. 719 (John Wiley & Sons, New York, 1975).

95. M.A. Preston and R.K. Bhaduri, "Structure of the Nucleus," p. 89 (Addison-Wesley, Mass., 1975).

96. B.D. Serot and J.D. Walecka, "The Relativistic Nuclear Many-Body Problem," Vol. 16, Advances in Nuclear Physics (Plenum, N.Y. 1986).

APPENDIX A

DERIVATIONS (OF MOMENTUM AND ENERGY TRANSFER FORMULAE)

In this Appendix, we shall go through the derivation of the final

result for momentum transfer $p^{\alpha j}{}_{tran}$ between the $\alpha\underline{th}$ target constituent

and $j\underline{th}$ projectile constituent (equation (3.31)),

$$\vec{p}^{\alpha j}_{tran} = -\int d^3\xi_p \; \rho_j(\bar{\xi}_p) \int d^3\xi_T \; \rho_\alpha(\xi_T) \left[\vec{\nabla}_{\xi_p} \int_{-\infty}^{\infty} \tilde{t}_{\alpha j} (\vec{x},'\bar{\xi}_p,\bar{\xi}_T) \; \frac{dz'}{v} \right]$$

(A.1)

and the total momentum transfer (equation (3.32)),

$$\vec{P}_{tot} = \sum_{\alpha=1}^{A_T} \sum_{j=1}^{A_p} \vec{p}^{\alpha j}_{tran}$$

$$= -(A_p A_T) \int d^3\xi_p \; \rho_p(\bar{\xi}_p) \int d^3\xi_T \; \rho_T(\bar{\xi}_T) \left[\vec{\nabla}_{\xi_p} \int_{-\infty}^{\infty} \tilde{t}(\vec{x},'\bar{\xi}_p,\bar{\xi}_T) \; \frac{dz'}{v} \right]$$

(A.2)

where the symbols have been explained in the text in Chapter 3.

Equation (A.1) was derived from the expression

$$\sum_{\alpha=1}^{A_T} \sum_{j=1}^{A_p} p^{\alpha j}_{tran} = -<g_{p,o}(\bar{\xi}_p) \; g_{T,o}(\bar{\xi}_T) \left| -\sum_{j=1}^{A_p} \vec{\nabla}_{\xi_{p,j}} \right.$$

$$\int_{-\infty}^{\infty} \sum_{j=1}^{A_T} \sum_{\alpha=1}^{A_p} t_{\alpha j} (\vec{x},\bar{\xi}_p,\bar{\xi}_T) \; \frac{dz}{v} \left| g_{p,o}(\bar{\xi}_p) g_{T,o}(\bar{\xi}_T) \right.>$$

(A.3)

where the projectile and target many-body wave functions $\left| g_{p,o} \right>$ and

$\left| g_{T,o} \right>$ are written in terms of single particle states in a Slater

determinant as follows

114

$$|g_{P,0}(\bar{\xi}_p)\rangle = \frac{1}{\sqrt{A_p!}} \begin{bmatrix} \phi_{j1}(\bar{\xi}_{P1}) & \phi_{j2}(\bar{\xi}_{P1}) & \cdots & \phi_{jAp}(\bar{\xi}_{P1}) \\ \phi_{j1}(\bar{\xi}_{P2}) & \phi_{j2}(\bar{\xi}_{P2}) & \cdots & \phi_{jAp}(\bar{\xi}_{P2}) \\ \vdots & \vdots & & \vdots \\ \phi_{j1}(\bar{\xi}_{p\,A_p}) & \phi_{j2}(\bar{\xi}_{p\,A_p}) & \cdots & \phi_{jAp}(\bar{\xi}_{p\,A_p}) \end{bmatrix}$$

(A.4)

and where the single particle states have been orthonormalized. The ground state single-particle densities are defined as

$$\rho(\bar{\xi}_p) = \langle g_{p,0}(\bar{\xi}_p) \mid \sum_{j=1}^{A_p} \delta(\bar{\xi}_p - \bar{\xi}_{pj}) \mid g_{p,0}(\bar{\xi}_p)\rangle$$

$$= \frac{1}{A_p!} \int d^3\bar{\xi}_{p1} \ldots d^3\bar{\xi}_{P,Ap} \sum_{j=1}^{A_p} \delta(\bar{\xi}_p - \bar{\xi}_{pj})$$

$$\times \sum_{Perm} \left| \phi_{j1}(\bar{\xi}_{p1}) \right|^2 \ldots \left| \phi_{jAp}(\bar{\xi}_{P,A}) \right|^2$$

$$= \sum_{j=1}^{A_p} \left| \phi_j(\bar{\xi}_p) \right|^2$$

(A.5)

where $\sum_{Perm}$ means all permutations of ξ_{Pj} have to be taken. For $\alpha = 1,2\ldots A_T$ target and $j = 1,2\ldots A_p$ projectile nucleons, momentum transfer due to collision of αj pair is $\bar{P}^{\alpha j}_{tran}$ and the total momentum is obtained by summing over all such pairs.

Explicitly, we can write

$$\overline{P}^{\alpha j}_{tran} = - \frac{1}{A_p!} \frac{1}{A_T!} \int d^3\overline{\xi}_{P1} \ldots d^3\overline{\xi}_{P'A_p} \sum_{Perm} \left| \phi_{j1}(\overline{\xi}_{P1}) \right|^2 \ldots \left| \phi_{jAp}(\overline{\xi}_p A_p) \right|^2$$

$$\int d^3\overline{\xi}_{T1} \ldots d^3\overline{\xi}_{T'A_T} \sum_{Perm} \left| \phi_{k1}(\overline{\xi}_{T1}) \right|^2 \ldots \left| \phi_{kA_T}(\overline{\xi}_{T}A_T) \right|^2$$

$$\left[\sum_{j=1}^{A_p} \overline{\nabla}_{\xi p,j} \quad \sum_{j=1}^{A_p} \sum_{\alpha=1}^{A_T} \int_{-\infty}^{\infty} t_{\alpha j} (\overline{x}', \overline{\xi}_{P_j}, \overline{\xi}_{T_\alpha}) \frac{dz'}{v} \right] \qquad \text{(A.6)}$$

$$\overline{P}^{\alpha j}_{tran} = - \frac{1}{A_p!} \frac{1}{A_T!} \sum_{j=1}^{A_p} \sum_{\alpha=1}^{A_T} \int \int d^3\overline{\xi}_{pj} \; d^3\overline{\xi}_{T\alpha} \left[\sum_{\ell=1}^{A_p} \left| \phi_{\partial\ell} (\overline{\xi}_{pj}) \right|^2 \right]$$

$$\cdot \left[\sum_{m=1}^{A_T} \left| \phi_{\beta m}(\overline{\xi}_d) \right|^2 \right] \cdot \left[\overline{\nabla}_{\xi_{Pj}} \int_{-\infty}^{\infty} t_{\alpha j} (\overline{x}', \overline{\xi}_{P}, \overline{\xi}_{T}) \frac{dz'}{v} \right]$$

$$\text{(A.7)}$$

$$= - \int d^3\overline{\xi}_P \; \rho_j(\overline{\xi}_P) \int d^3\overline{\xi}_T \; \rho_\alpha(\overline{\xi}_T) \left[\overline{\nabla}_{\xi_P} \int_{-\infty}^{\infty} t_{\alpha j} (\overline{x}', \overline{\xi}_P, \overline{\xi}_T) \frac{dz'}{v} \right] \quad \text{(A.1)}$$

$$\therefore \overline{P}_{tot} = \sum_{j=1}^{A_p} \sum_{\alpha=1}^{A_T} \overline{P}^{\alpha j}_{tran}$$

$$= - (A_p A_T) \int d^3\overline{\xi}_P \; \rho_p(\overline{\xi}_P) \int d^3\overline{\xi}_T \; \rho_T(\overline{\xi}_T) \left[\overline{\nabla}_{\xi_P} \int \hat{t}(\overline{x}', \overline{\xi}_P, \overline{\xi}_T) \frac{dz'}{v} \right]$$

$$\text{(A.2)}$$

as claimed.

The derivation of the energy transfer in relativistic heavy-ion collisions is analogous to the above derivation for momentum transfer.

We assume that the energy of the projectile can be evaluated by taking the expectation value of the sum of projectile energy operators between the full state vector (i.e. equation (3.14))

$$E = < \bar{\psi}_I (\infty) \mid H_p \mid \bar{\psi}_I (\infty) > \qquad (A.8)$$

where H_p = Internal Hamiltonian of the projectile

$$H_p = - \frac{1}{2m_n} \sum_{j=1}^{A_p} \bar{\nabla}^2_{\xi P_j} + \sum_{i<j} V_{ij} \qquad (A.9)$$

Explicitly, the above (A.8) can be written as

$$E = <g_{p,o}(\xi_P) \; g_{T,o}(\xi_T) \mid e^{-i\bar{k}\cdot\bar{x}} \exp\left(i/v \sum_{j=1}^{A_p} \sum_{\alpha=1}^{A_T} \int_{-\infty}^{\infty} t_{\kappa j}(\bar{x}', \bar{\xi}_p, \bar{\xi}_T) \; dz'\right)$$

$$\left[- \frac{1}{2m_n} \sum_{j=1}^{A_p} \bar{\nabla}^2_{\xi P_j} + \sum_{i<j} V_{ij} \right] \exp\left(-i/v \sum_{j=1}^{A_p} \sum_{\alpha=1}^{A_T} \int_{-\infty}^{\infty} t_{\kappa j}(\bar{x}', \bar{\xi}_p, \bar{\xi}_T) \; dz'\right)$$

$$e^{i\bar{k}\cdot\bar{x}} \mid g_{p,o}(\bar{\xi}_p) g_{T,o}(\bar{\xi}_T> \qquad (A.10)$$

Using the identity

$$e^{iA} B e^{-iA} = B + i \; [A,B] + \frac{i^2}{2!} \; [A,[A,B]] + \ldots \qquad (A.11)$$

yields

$$\exp[\,iS]\left[-\frac{1}{2m_n}\sum_{j=1}^{A_p}\overline{\nabla}_{\xi_{pj}}^2 + \sum_{i<1}v_{ij}\right]\exp[-iS]$$

$$-\left[-\frac{1}{2m_n}\sum_{j=1}^{A_p}\overline{\nabla}_{\xi_{pj}}^2 + \sum_{i<j}v_{ij}\right] - \frac{i}{2m_n}\left[S,\sum_{j=1}^{A_p}\overline{\nabla}_{\xi_{pj}}\right]$$

$$- \frac{i^2}{2}\left[S,\left[S,\sum_{j=1}^{A_p}\overline{\nabla}_{\xi_{pj}}^2\right]\right] \qquad (A.12)$$

$$S = \sum_{\alpha=1}^{A_T}\sum_{j=1}^{A_p}\int_{-\infty}^{\infty}t_{\alpha j}(\bar{x}',\bar{\xi}_p,\bar{\xi}_T)\,\frac{dz'}{v} \qquad (A.13)$$

Using

$$[A,BC] = [A,B]C + B[A,C] \qquad (A.14)$$

One obtains the operator expression

$$\left[S,\sum_{j=1}^{A_p}\overline{\nabla}_{\xi_{pj}}^2\right] = \left[S,\sum_{j=1}^{A_p}\overline{\nabla}_{\xi_{pj}}\right]\overline{\nabla}_{\xi_{pj}}$$

$$+ \sum_{j=1}^{A_p}\overline{\nabla}_{\xi_{pj}}\left[S,\overline{\nabla}_{\xi_{pj}}\right] \qquad (A.15)$$

Similarly,

$$\left[S,\left[S,\sum_{j=1}^{A_p}\overline{\nabla}_{\xi_{pj}}^2\right]\right]$$ can be evaluated using (A.15).

Combining all the terms, one obtains

$$E = \langle g_{p,o}(\bar{\xi}_p)g_{T,o}(\bar{\xi}T) \mid H_p \mid g_{p,o}(\bar{\xi}_p)g_{T,o}(\bar{\xi}T) \rangle$$

$$+ \frac{i}{2m_n} \langle g_{p,o}(\bar{\xi}_p)g_{T,o}(\bar{\xi}T) \mid \sum_{j=1}^{A_p} \bar{\nabla}^2_{\xi_{pj}} \cdot S \mid g_{p,o}(\bar{\xi}_p)g_{T,o}(\bar{\xi}T) \rangle$$

$$+ \frac{1}{2m_n} \langle g_{p,o}(\bar{\xi}_p)g_{T,o}(\bar{\xi}T) \mid \sum_{j=1}^{A_p} \left(\bar{\nabla}_{\xi_{pj}} S \right)^2 \mid g_{p,o}(\bar{\xi}_p)g_{T,o}(\bar{\xi}T) \rangle$$

$$+ \frac{i}{2m_n} \langle g_{p,o}(\bar{\xi}_p)g_{T,o}(\bar{\xi}T) \mid \sum_{j=1}^{A_p} \bar{\nabla}_{\xi_{pj}} S \cdot \bar{\nabla}_{\xi_{pj}} \mid g_{p,o}(\bar{\xi}_p)g_{T,o}(\bar{\xi}T) \rangle$$

$$\tag{A.16}$$

The first term in (A.16) will be recognized as the initial energy of the projectile $E_{o,proj}$. This can be taken to the left hand side and energy transfer defined as

$$E_{tran} = E - E_o \tag{A.17}$$

The second and the fourth terms can be combined. The first term in the resulting expression can be converted into a surface integral by use of the divergence theorem. This will vanish if the single particle states vanish sufficiently fast at infinity. The remaining expression can be shown to contribute nothing to the excitation energy for even-even nuclei such as ^{12}C, ^{16}O considered in this work. For odd-even nuclei, this contribution is $O(\frac{1}{A_p})$, therefore this has been ignored. The final result for energy transfer is then

$$E_{tran} = E - E_o$$

$$= \frac{1}{2m_n} \langle g_{p,o}(\bar{\xi}_p)g_{T,o}(\bar{\xi}T) \mid \sum_{j=1}^{A_p} \left(\bar{\nabla}_{\xi_{pj}} S \right)^2 \mid g_{p,o}(\bar{\xi}_p)g_{T,o}(\bar{\xi}T) \rangle$$

$$\tag{A.18}$$

The rest of the calculation is analogous to the momentum transfer calculations i.e. one obtains

$$E_{tran}^{tot} = \sum_{j=1}^{A_P} \sum_{\alpha=1}^{A_T} E_{tran}^{\alpha j} \tag{A.19}$$

where

$E_{tran}^{\alpha j}$ = Energy transfer in the collision of the α-j pair

$$= \frac{1}{2m_n} \int d^3\bar{\xi}_p \; \rho_j(\bar{\xi}_p) \int d^3\bar{\xi}_T \; \rho_\alpha(\bar{\xi}_T) \left[\bar{\nabla}_{\xi_p} \int_{-\infty}^{\infty} \bar{t}_{\alpha j}(\bar{x}',\bar{\xi}_p,\bar{\xi}_T) \frac{dz'}{v} \right]^2 \tag{A.20}$$

and

$$E_{tran}^{tot} = \frac{1}{2m_n} (A_P A_T) \int d^3\bar{\xi}p \; \rho_p(\bar{\xi}_p) \int d^3\bar{\xi}_T \; \rho_T(\bar{\xi}_T) \left[\bar{\nabla}_{\xi_p} \int_{-\infty}^{\infty} \bar{t}(\bar{x}',\bar{\xi}p,\bar{\xi}_T) \frac{dz'}{v} \right]^2 \tag{A.21}$$

where $\rho_j(\bar{\xi}p)$ and $\rho_\alpha(\xi T)$ are the single particle density of the jth projectile and α^{th} target nucleon and $\rho_p(\bar{\xi}p)$, $\rho_T(\bar{\xi}_T)$ are the nuclear densities of the projectile and the target, as before.

APPENDIX B

$$V_{m\mu, m'\mu'} \text{ and } P_{m\mu, m'\mu'}$$

We want to discuss how our expression for momentum, equation (3.20) relates to Wilson's expression for potential, equation (2.41). We expect an analogy on physical grounds because momentum transfer in a collision is directly related to the gradient of the interaction in a one to one fashion. The coupled equations in (2.40)

$$(\vec{\nabla}_x^2 + \vec{K}^2)\, \psi_{m\mu}\, (\vec{x}) - \frac{2M_n A_p A_T}{(A_p + A_T)}\, \sum_{m'\mu'}\, V_{m\mu, m'\mu'}\, (\vec{x})\, \psi_{m'\mu'}(\vec{x}) \qquad (B.1)$$

define a potential matrix $\bar{V}$ with matrix elements

$$V_{m\mu, m'\mu'}(\vec{x}) - \langle g_{p,m}(\vec{\xi}_p)\, g_{T,\mu}(\vec{\xi}_T) \mid V_{opt}(\vec{x}, \vec{\xi}_p, \vec{\xi}_T) \mid g_{p,m'}(\vec{\xi}_p) g_{T,\mu'}(\vec{\xi}_T) \rangle \qquad (B.2)$$

with

$$V_{opt}(\vec{x}, \vec{\xi}_p, \vec{\xi}_T) = \sum_{\alpha j}\, t_{\alpha j}(\vec{x}_\alpha, \vec{x}_j) \qquad (B.3)$$

so that the matrix looks like (2.44) with

$$\bar{V}(\vec{x}) - \begin{bmatrix} V_{00,00}(\vec{x}) & V_{00,01}(\vec{x}) & V_{00,10}(\vec{x}) \cdots \\ V_{01,00}(\vec{x}) & V_{01,01}(\vec{x}) & V_{01,10}(\vec{x}) \cdots \\ V_{10,00}(\vec{x}) & V_{10,01}(\vec{x}) & V_{10,10}(\vec{x}) \cdots \end{bmatrix} \qquad (B.4)$$

121

We introduced in (3.20) similar expressions for the momentum of the projectile and its matrix elements were defined in (3.20). Equation (3.20) defines a coupled problem because the approximate wave operator

$$\phi(\vec{x}, \vec{\xi}_p, \vec{\xi}_T) \simeq \exp\left[-\frac{i}{v} \int_{-\infty}^{\infty} V_I(\vec{x}', \vec{\xi}_p, \vec{\xi}_T)\, dz'\right] \qquad (B.5)$$

induces transition in the internal eigenstates $g_{p,m}$ and $g_{T,\mu}$ of the projectile and target, respectively. Equation (3.20) defines a matrix $\bar{P}(x)$.

$$\bar{P}(\vec{x}) = \begin{bmatrix} P_{00,00}(\vec{x}) & P_{00,01}(\vec{x}) & P_{00,10}(\vec{x})\ldots \\ P_{01,00}(\vec{x}) & P_{01,01}(\vec{x}) & P_{01,10}(\vec{x})\ldots \\ P_{10,00}(\vec{x}) & P_{10,01}(\vec{x}) & P_{10,10}(\vec{x})\ldots \end{bmatrix} \qquad (B.6)$$

This expression for momentum

$$P_{m\mu,m'\mu'}(\vec{x}) = <g_{p,m}(\vec{\xi}_p)\, g_{T,\mu}(\vec{\xi}_T)|\, e^{+\frac{i}{v}\int_{\infty}^{\infty} V_I(\vec{x}', \vec{\xi}_p, \vec{\xi}_T)dz'} \begin{bmatrix} A_p \\ -i\sum_{j=1}^{p} \vec{\nabla}_{\xi_{p,j}} \end{bmatrix}$$

$$x \quad e^{-\frac{i}{v}\int_{\infty}^{\infty} V_I(\vec{x}', \vec{\xi}_p, \vec{\xi}_T)dz'} |\, g_{p,m'}(\vec{\xi}_p)\, g_{T,\mu'}(\vec{\xi}_T)> \qquad (B.7)$$

can be compared to Wilson's expression, (B.2) above.

One can recognize that there is a close connection between the two expressions. This connection should be one to one, since for each channel defined by the eigenstates m,m' of the projectile and μ,μ' of the target, an interaction $V_{m\mu,m'\mu'}$ induces a momentum transfer $P_{m\mu,m'\mu'}$.

The Sudden Approximation

The connection between our derivation and the more familiar formalism of time-dependent Schrodinger theory will be discussed briefly.

Consider

$$i \frac{\partial}{\partial t} \left| \psi_S(t) \right> = \hat{H} \left| \psi_S(t) \right> = (\hat{H}_0 + \hat{H}_1) \left| \psi_S(t) \right> \qquad \hbar = 1 \qquad (B.8)$$

where $\psi_S(t)>$ is the time dependent Schrodinger state vector and where $\hat{H}_0$ and $\hat{H}_1$ are the unperturbed Hamiltonian and the interaction, respectively. In the "Interaction Representation" the above reads[45,46,47]

$$i \frac{\partial}{\partial t} \left| \psi_S(t) \right> = e^{i \hat{H}_0 t} (-H_0 + H_0 + H_1) e^{-i \hat{H}_0 t} \left| \psi_I(t) \right>$$

$$= \hat{H}_I(t) \left| \psi_I(t) \right> \qquad (B.9)$$

with

$$\left| \psi_I(t) \right> = e^{i\hat{H}_0 t} \left| \psi_S(t) \right> \qquad (B.10a)$$

$$\hat{H}_I(t) = e^{i\hat{H}_o t} \hat{H}_1 e^{-i\hat{H}_o t} \qquad (B.10b)$$

The time evolution operator is defined as

$$\left| \psi_I(t) \right> = \hat{U}(t,t_o) \left| \dot{\psi}_I(t_o) \right> \qquad (B.11)$$

Specifically,

$$\left| \psi_I(\infty) \right> = \hat{U}(\infty, -\infty) \left| \psi_I(-\infty) \right> \qquad (B.12)$$

where $\hat{U}$ must satisfy

$$i \frac{\partial}{\partial t} \hat{U}(t, t_o) = \hat{H}_I(t) \hat{U}(t, t_o) \quad ; \quad \hat{U}(t_o, t_o) = 1 \qquad (B.13)$$

Writing the above as an integral equation, one obtains

$$\hat{U}(t, t_o) = 1 - \frac{i}{\hbar} \int_{t_o}^{t} \hat{H}_I(t') \hat{U}(t', t_o) \, dt' + \ldots \qquad (B.14)$$

On iteration, the above yields

$$\hat{U}(t, t_o) = \sum_{n=0}^{\infty} \left(-\frac{i}{\hbar} \right)^n \int_{t_o}^{t_1} dt_1 \ldots \int_{t_o}^{t_{n-1}} \left[\hat{H}_I(t_1) \ldots \hat{H}_I(t_n) \right] \qquad (B.15)$$

The above is a formal solution to the time-development of the state vector from initial time t_o to final time t. It is a power series in the strength of the interaction $\hat{H}_I(t)$ and it is time-ordered, i.e., earlier times occur to the left of later times. Explicitly,

$$\hat{U}(t, t_o) = 1 - \frac{i}{\hbar} \int_{t_o}^{t} \hat{H}_I(t_1) \, dt_1 + \left\{ -\frac{i}{\hbar} \right\}^2 \int_{t_o}^{t} dt_2 \left[\hat{H}_I(t_1) \hat{H}_I(t_2) \right] + \ldots$$

$$(B.16)$$

Consider adiabatic switching of the interaction. Define[46]

$$\hat{H}_I(t) = e^{-\varepsilon|t|}\hat{H}_1 \qquad (B.17)$$

which implies that instead of turning on the interaction at $T = (t-t_0)$, turn it on and off slowly. As $t \to \pm \infty$

$$\hat{H}_1(t) \to 0 \qquad \text{and} \qquad \hat{H} \to \hat{H}_0 \qquad (B.18)$$

and the solutions to the Schrodinger equation take the form

$$|\psi(t)\rangle = e^{-i\hat{H}_0 t}|\psi\rangle = e^{-iE_0 t}|\psi\rangle \qquad (B.19)$$

with $\hat{H}_0|\psi\rangle = E_0|\psi\rangle$ for stationary states.

Then in this limit

$$\psi_I(t) = e^{i\hat{H}_0 t}|\psi(t)\rangle = |\psi\rangle \qquad (B.20)$$

which is independent of time. Therefore,

$$|\psi_I(\infty)| = |\phi_f\rangle$$
$$|\psi_I(-\infty)| = |\phi_i\rangle \qquad (B.21)$$

Next, the sudden approximation will be discussed to justify (3.19). We can write[46]

$$|\psi_I(\infty)> = \hat{U} (\infty, -\infty) \; | \; \psi_I (-\infty)>$$

$$= \sum_{n=0}^{\infty} \left\{ - \frac{i}{\hbar} \right\}^n \int_{-\infty}^{\infty} e^{-\epsilon|t_1|} dt_1 \int_{-\infty}^{t_1} e^{-\epsilon|t_2|} dt_2 \cdots \cdots \int_{-\infty}^{t_{n-1}} e^{-\epsilon|t_n|} dt_n$$

$$\left[\hat{H}_I(t_1) \; \hat{H}_I(t_2) \ldots \hat{H}_I(t_n) \right] \tag{B.22}$$

It has been shown in reference [47] that a necessary condition for the sudden approximation to be valid is that the interactions at two different times commute

$$\left[\hat{H}_I(t_1), \; \hat{H}_I(t_2) \right] = 0 \tag{B.23}$$

so that time-ordering is unimportant in (B.22). Following reference [47]

$$|\psi_I(\infty)> = \exp \left[-i \int_{-\infty}^{\infty} \hat{H}_1 (t') \; dt' \right] |\psi_I(-\infty)> \tag{B.24}$$

which is the desired result.

Having derived (B.24) it is necessary to relate these equations (B.22)-(B.24) to our previous discussion in equations in Chapter III. Essential to the derivation of equation (3.19) was the commutativity of interaction matrices at different points along a straight line trajectory

$$\left[\bar{V}_I(\vec{x}', \vec{\xi}), \; \bar{V}_I(\vec{x}'', \vec{\xi}) \right] = 0 \tag{B.25}$$

In the Interaction Representation, this is entirely equivalent to[47]

$$\left[\hat{H}_I(t'), \ \hat{H}_I(t'') \right] = 0 \qquad (B.26)$$

provided one identifies $dz' = vdt'$ and $dz'' = vdt''$ assuming constant velocity per nucleon. The latter can be justified on the basis of a high energy assumption.

The physical basis for the sudden approximation in the high energy context is as follows; the collision time $t_{coll} \ll t_{nuc}$ where t_{nuc} is the period associated with orbital motion of the nucleons in the nucleus. This condition

$$t_{coll} \ll t_{nuc} \qquad (B.27)$$

is met in relativistic heavy ion collisions. We shall argue this by calculating the ratio $\dfrac{t_{coll}}{t_{nuc}}$. For incident beam energies above 1 GeV/N the nucleon velocity $\simeq \beta c = c$. For the distance we shall take typical nuclear diameter $\simeq 6$ fm. Then $t_{coll} \simeq \dfrac{6 \ fm}{c}.$ For t_{nuc} we will consider the period of nucleons in a Fermi gas i.e.

$t_{nuc} = (E/h)^{-1} = \dfrac{1}{\nu} = t_{nuc}.$ For a typical nucleus with Fermi energy $\simeq$ 40 MeV, the ratio is

$$\frac{t_{coll}}{t_{nuc}} = \frac{6 \ fm \ x \ 40 \ MeV}{2\pi(\hbar c)} \simeq \frac{1}{5} \quad ; \qquad \hbar c \simeq 197.3 \ MeV.fm \qquad (B.28)$$

which is small enough to justify the Sudden Approximation. Although details of the nuclear diameter and Fermi energy may vary, at relativistic energies the ratio will be small. We have omitted the Lorentz factor in the above argument, but the conclusions remain unchanged because we have overestimated the Fermi energy (not all nucleons are at the surface) and have considered the diameter of the nucleus and not of the nucleons themselves.

APPENDIX C

ANALYTICAL RESULTS USING GAUSSIAN DENSITIES

Analytical results are useful in getting physical insights as well as establishing the validity of numerical calculations. We present in this section analytical calculations of momentum and energy transfer using Gaussian densities. We know from Chapter III that momentum transfer between αth constituent of the projectile and jth constituent of the target is

$$\vec{P}_{\alpha j} = - \int d^3\vec{\xi}_p \; \rho_j(\vec{\xi}_p) \int d^3\vec{\xi}_T \; \rho_k(\vec{\xi}_T) \left[\vec{\nabla}_{\xi_p} \int_{-\infty}^{\infty} \tilde{t}_{\alpha j}(\vec{x}' + \vec{\xi}_p - \vec{\xi}_T) \; \frac{dz'}{v} \right]$$

(C.1)

where the notation was explained following equation (3.32). The total momentum transfer is obtained by summing over α and j as

$$\vec{P}_{trans} = \sum_{\alpha} \sum_{j} \vec{P}_{\alpha j}$$

(C.2)

$$= - A_p A_T \int d^3\vec{\xi}_p \; \rho_p(\vec{\xi}_p) \int d^3\vec{\xi}_T \; \rho_T(\vec{\xi}_T) \left[\vec{\nabla}_{\xi_p} \int_{-\infty}^{\infty} \tilde{t}(\vec{x}', \vec{\xi}_p, \vec{\xi}_T) \; \frac{dz'}{v} \right]$$

Define a vector $\vec{G} = G_b \; \hat{b} + G_\perp \; \hat{\perp}$ with $(\hat{X}, \hat{Y}, \hat{Z}) = (\hat{b}, \hat{\perp}, \hat{z})$ (C.3)

with

$$\vec{G} = \left[\vec{\nabla}_{\xi_p} \int_{-\infty}^{\infty} \tilde{t}(\vec{x}' + \vec{\xi}_p - \vec{\xi}_T) \; \frac{dz'}{v} \right]$$

(C.4)

129

so that equation (C.1) be rewritten as

$$\vec{P}_{\alpha j} = - \int d^3\vec{\xi}_p \ \rho_j(\vec{\xi}_p) \int d^3\vec{\xi}_T \ \rho_\alpha(\vec{\xi}_T) \left[\vec{G} \ (\vec{x}' + \vec{\xi}_p - \vec{\xi}_T) \right] \tag{C.5}$$

and with

$$\tilde{t} = - t(o) \ e^{-\kappa(\vec{x}' + \vec{\xi}_p - \vec{\xi}_T)^2} \tag{C.6}$$

where t(o) is assumed to be real.

The components of $\vec{G}$ can be written with $\xi_{p,b}$ $(\xi_{p,\perp})$ as the

components of $\vec{\xi}_p$ along $\hat{b}$ (and perpendicular to $\hat{b}$) and $\xi_{T,b}$ $(\xi_{T\perp})$

the components of $\vec{\xi}_T$ along $\hat{b}$ (and perpendicular to $\hat{b}$).

$$G_b = \frac{t(o)}{v} \ \sqrt{\frac{\pi}{\kappa}} \ (2\kappa) \ (b + \xi_{p,b} - \xi_{T,b})$$

$$e^{-\kappa(b + \xi_{p,b} - \xi_{T,b})^2 -\kappa(\xi_{p,\perp} -\xi_{T,\perp})^2} \tag{C.7}$$

and

$$G_\perp = \frac{t(o)}{v} \ \sqrt{\frac{\pi}{\kappa}} \ (2\kappa) \ (\xi_{p,\perp} - \xi_{T,\perp})$$

$$e^{-\kappa(b + \xi_{p,b} - \xi_{T,b})^2 -\kappa(\xi_{p,\perp} -\xi_{T,\perp})^2} \tag{C.8}$$

Define the thickness function

$$F_T \ (\vec{\xi}_T) = \int_{-\infty}^{\infty} \rho_T \ (\vec{\xi}_{T,b} + z_T^2 \ ) \ dz_T \tag{C.9}$$

where

$$\rho_T(\vec{\xi}_T) = A_T \cdot \left[\frac{3}{2\pi \ a_T^2} \right]^{3/2} \ exp \ \left[- \frac{3\vec{\xi}_T^2}{2 \ a_T^2} \right] \tag{C.10}$$

$$F_T(\vec{\xi_T}) = A_T \cdot \left[\frac{3}{2\pi \, a_T^2} \right] \cdot \exp\left[-\frac{3\vec{\xi}_T^2}{2 \, a_T^2} \right] . \qquad (C.11)$$

Similarly

$$F_p(\vec{\xi_p}) = A_p \cdot \left[\frac{3}{2\pi \, a_p^2} \right] \cdot \exp\left[-\frac{3\vec{\xi}_p^2}{2 \, a_p^2} \right] \qquad (C.12)$$

where a_p, a_T are the root mean square radii of projectile and target, respectively. Therefore,

$$\vec{P} = -\int d^2\vec{\xi_T} \; F_T(\vec{\xi_T}) \int d^2\vec{\xi_p} \; F_p(\vec{\xi_p}) \left[\vec{G} \; (\vec{x}' + \vec{\xi_p} - \vec{\xi_T}) \right] \qquad (C.13)$$

or

$$\vec{P} = -\int d^2\vec{\xi_p} \; F_p(\vec{\xi_p}) \; \vec{Q} \; (b + \xi_{pb}) \qquad (C.14)$$

where

$$\vec{Q} = \int d^2\vec{\xi_T} \; F_T(\vec{\xi_T}) \left[\vec{G} \; (\vec{x}' + \vec{\xi_p} - \vec{\xi_T}) \right] = Q_b \; \hat{b} + Q_\perp \; \hat{\perp} \qquad (C.15)$$

with

$$Q_b = \int d^2\vec{\xi_T} \; F_T(\vec{\xi_T}) \; G_b \; (b + \xi_{p,b} - \xi_{T,b}) \qquad (C.16)$$

or

$$Q_b = 2kA_T \; \frac{t(o)}{v} \sqrt{\frac{\pi}{\kappa}} \; \frac{3}{2\pi \, a_T^2} \; I(b + \xi_{p,b}; \; \xi_{p\perp} \;)$$

where we have used (C.7), and

$$I(b + \xi_{p,b}; \xi_{p\perp}) = \int \int d\xi_{T,b} \, d\xi_{T\perp} \, (b + \xi_{p,b} + \xi_{T,b})$$

$$\times \quad e^{-\frac{3}{2a_T^2} \left[\xi_{Tb}^2 + \xi_{T\perp}^2 \right] -\kappa (b + \xi_{pb} - \xi_{Tb})^2}$$

$$e^{-\kappa \left[\xi_{P\perp} - \xi_{T\perp} \right]^2} \tag{C.17}$$

On evaluation this yields (with $a = 3/2a_T^2$),

$$I(b + \xi_{p,b}; \xi_{p\perp}) = \frac{\pi}{(a+\kappa)^2} \frac{a \left\{ b + \xi_{p,b} \right\}}{1}$$

$$\exp \left[- \frac{a\kappa}{(a+\kappa)} \left\{ \left\{ b + \xi_{p,b} \right\}^2 + \xi_{p,\perp}^2 \right\} \right] \tag{C.18}$$

substituting (C.18) into (C.16) yields

$$Q_b = (2k) \, A_T \frac{t(o)}{v} \sqrt{\frac{\pi}{\kappa}} \frac{3}{2\pi a_T^2} \frac{\pi \, a \, (b + \xi_{p,b})}{(a+\kappa)^2}$$

$$\exp \left[- \frac{a\kappa}{(a+\kappa)} \left\{ \left\{ b + \xi_{p,b} \right\}^2 + \xi_{p,\perp}^2 \right\} \right] \tag{C.19}$$

Similarly, using the same method as in (C.16)-(C.19), we obtain

$$Q_\perp = (2K) \, A_T \frac{t(o)}{v} \sqrt{\frac{\pi}{\kappa}} \frac{3}{2\pi a_T^2} \frac{\pi \, a}{(a+\kappa)^2} \xi_{p,\perp}$$

$$\exp \left[- \frac{a\kappa}{(a+\kappa)} \left\{ \left\{ b + \xi_{p,b} \right\}^2 + \xi_{p,\perp}^2 \right\} \right] \tag{C.20}$$

which yields the two components in (C.15).

Now we need to evaluate (C.14)

$$\vec{P}_{trans} - \sum_{\alpha}^{A_p} \sum_{j}^{A_T} \vec{P}_{\alpha j} - - \int d^2\vec{\xi}_p \ F_p(\vec{\xi}_p) \ \vec{Q}(b + \xi_{p,b}) \ - P_b \ \hat{b} + P_\perp \ \hat{\perp}$$

$$- P_b \ \hat{b} + P_\perp \ \hat{\perp} \qquad (C.21)$$

On evaluation this yields $(a' - 3/2a_p^2)$,

$$P_b \ \hat{b} - \hat{b} \ A_p A_T \ (2K) \ \frac{t(o)}{v} \ \sqrt{\frac{\pi}{\kappa}} \ \frac{3}{2\pi a_p^2} \ \frac{3}{2\pi a_T^2} \ \frac{\pi^2 aa'b}{(aa' + \kappa(a+a'))}$$

$$\exp\left[- \frac{aa'\kappa b^2}{(aa' + \kappa(a+a'))} \right] \qquad (C.22)$$

or,

$$P_b \ \hat{b} - \hat{b} \ (A_p A_T) \ \frac{2t(o)}{v} \ \sqrt{\frac{\pi}{\kappa}} \ (aa'b) \ \chi \ \exp\left[- \chi b^2 \right] \qquad (C.23)$$

where $\chi - \left[\dfrac{aa'\kappa}{aa' + \kappa(a+a')} \right]$

Thus, finally,

$$\vec{P}_{trans} - \sum_{\alpha j} \vec{P}_{\alpha j} - P_b \ \hat{b} + P_\perp \ \hat{\perp}$$

$$- P_b \ \hat{b} \quad \text{and} \quad P_\perp - 0 \ \text{due to symmetry}$$

$$- \hat{b} \ A_p A_T \ \sqrt{\frac{\pi}{\kappa}} \ \frac{2t(o)}{v} \ aa'b\chi \ \exp\left[- \chi b^2 \right] \qquad (C.27)$$

which is the analytical result for momentum transfer.

The above result holds for only real two-body amplitudes t(o). For complex t(o), there is a longitudinal component of momentum transfer as we have shown in Chapter III. The above result can be generalized to the latter case.

APPENDIX D

THE EQUIVALENT PHOTON SPECTRUM

In this Appendix, we shall derive via the Weizsäcker-Williams method of virtual quanta the equivalent photon spectrum generated by the target at the projectile.

For an incident particle of charge q, velocity $V = \beta(c)$ passing a system S at an impact parameter b, the spectrum of equivalent radiation is obtained from the electromagnetic fields[94]

$$E_2(t) = \frac{q\gamma b}{(b^2 + \gamma^2 v^2 t^2)^{3/2}} \, \hat{b}$$

$$E_1(t) = \frac{-q\gamma Vt}{(b^2 + \gamma^2 v^2 t^2)^{3/2}} \, \hat{z} \qquad (D.1)$$

$$B_3(t) = \beta E_2(t); \quad (1,2,3) = (\hat{z}, \hat{b}, \hat{1}_b)$$

where $E_1(t)$, $E_2(t)$ are the electric fields along the beam direction and transverse to it and $B_3(t)$ is the accompanying magnetic field. For $V \simeq c$, the fields $E_1(t)$, $E_2(t)$ and $B_3(t)$ are completely equivalent to plane wave pulses of radiation P_1 and P_2 incident on S, P_1 along beam direction, P_2 transverse to it. The equivalency is not exact for P_2, since there is no magnetic field accompanying $E_1(t)$. If the motion is nonrelativistic in the frame S, then the particles in this frame respond to electric forces only so that one can add an extra magnetic term to the fields without affecting the results. This field, $B_1(t) \simeq \beta E_1(t)$ will be shown to be of minor importance in calculations.

135

The equivalent frequency spectrum (energy per unit area per unit frequency interval) of the pulses P_1, P_2 are given by

$$\frac{dI_1(w,b)}{dw} = \frac{c}{2\pi} \left| E_2(w) \right|^2$$

$$\frac{dI_2(w,b)}{dw} = \frac{c}{2\pi} \left| E_1(w) \right|^2 \tag{D.2}$$

with

$$E_2(w) = \frac{1}{\sqrt{2\pi}} \int_{-\infty}^{\infty} E_2(t) e^{iwt} \, dt \tag{D.3}$$

and similarly for $E_1(w)$. Explicitly, these Fourier integrals are

$$E_2(w) = \frac{q\gamma b}{\sqrt{2\pi}} \int_{-\infty}^{\infty} \frac{e^{iwt} \, dt}{(b^2 + \gamma^2 v^2 t^2)^{3/2}} \tag{D.4}$$

$$= \frac{q}{\sqrt{2\pi}} \frac{1}{bV} \int_{-\infty}^{\infty} \frac{e^{i \, wbx/\gamma V} \, dx}{(1 + x^2)^{3/2}}; \quad x = \frac{\gamma Vt}{b} \tag{D.5}$$

$$= \frac{q}{bV} \frac{2}{\pi} \left[\frac{wb}{\gamma V} K_1 \left\{ \frac{wb}{\gamma V} \right\} \right] \tag{D.6}$$

and $\quad E_1(w) = - i \, \dfrac{q}{\gamma bV} \, \dfrac{2}{\pi} \left[\dfrac{wb}{\gamma V} K_0 \left\{ \dfrac{wb}{\gamma V} \right\} \right]$ \hfill (D.7)

where $K_0(K_1)$ are the modified Bessel functions of zeroth (first) order.

The frequency spectra are

$$\frac{dI_1(w,b)}{dw} = \frac{1}{\pi^2} \frac{q^2}{c} \left\{ \frac{c}{V} \right\}^2 \frac{1}{b^2} \left\{ \frac{wb}{\gamma V} \right\}^2 K_1^2 \left\{ \frac{wb}{\gamma V} \right\} \tag{D.8}$$

and

$$\frac{dI_2(w,b)}{dw} = \frac{1}{\pi^2} \frac{q^2}{c} \left\{\frac{c}{v}\right\}^2 \frac{1}{\gamma^2 b^2} \left\{\frac{wb}{\gamma v}\right\}^2 K_0^2 \left\{\frac{wb}{\gamma v}\right\} \qquad (D.9)$$

These have been plotted in reference 94 (Figure 15.7). The intensity of pulse P_2 involves a factor of $\dfrac{1}{\gamma^2}$ and is of minor importance for $V \simeq c$. To obtain the energy incident per unit frequency interval, one sums the frequency spectra over all impact parameters. This is

$$\frac{dI(w)}{dw} = 2\pi \int_{b_{min}}^{\infty} \left[\frac{dI_1(w)}{dw} + \frac{dI_2(w)}{dw} \right] b\,db \qquad (D.10)$$

where b_{min} is a minimum impact parameter beyond which other interactions take over (strong interactions in heavy ion collisions, for example). The result is

$$\frac{dI(w)}{dw} = \frac{2\pi}{\pi^2} \frac{q^2}{c} \left\{\frac{c}{v}\right\}^2 \frac{1}{b^2} \int_{b_{min}}^{\infty} \left[\xi^2 K_1^2 (\xi) + \frac{1}{\gamma^2} \xi^2 K_0^2 (\xi) \right] b\,db; \quad \xi = \frac{wb}{\gamma v}$$

$$= \frac{2}{\pi} \frac{q^2}{c} \left\{\frac{c}{v}\right\}^2 \left[x\, K_0(x)K_1(x) - \frac{1}{2} \beta^2 x^2 (K_1^2(x) - K_0^2(x)) \right] \qquad (D.11)$$

where $x = \dfrac{wb_{min}}{\gamma v}$.

For low frequencies $\quad w \ll \dfrac{\gamma v}{b_{min}}$, equation (D.11) reduces to

$$\frac{dI(w)}{dw} = \frac{2}{\pi} \frac{q^2}{c} \left\{\frac{c}{v}\right\}^2 \left[\ln\left\{\frac{1.123}{x}\right\} - \frac{1}{2} \beta^2\right] \qquad (D.12)$$

For high frequencies (w >> $\gamma V/b_{min}$), the result is an exponential fall-off

$$\frac{dI(w)}{dw} = \frac{q^2}{c} \left\{\frac{c}{v}\right\}^2 \left\{1 - \frac{1}{2} V^2/c^2\right\} e^{-2\frac{wb_{min}}{\gamma V}} \qquad (D.13)$$

The number spectrum of virtual quanta is

$$\frac{dI(w)}{dw} dw = N(\hbar w) \ d \ (\hbar w) \ (\hbar w) = E \ N(E)dE \qquad (D.14)$$

so that

$$N(E) = \frac{2}{\pi} \frac{q^2}{(\hbar e)} \left\{\frac{c}{v}\right\}^2 \frac{1}{(\hbar w)} \left[x \ K_0(x)K_1(x) - \frac{1}{2} \beta^2 x^2 \ (K_1^2(x) - K_0^2(x))\right] \qquad (D.15)$$

$$= \frac{2}{\pi E} z^2 \cdot \alpha \cdot \frac{1}{\beta^2} \left[x \ K_0(x)K_1(x) - \frac{1}{2} \beta^2 x^2 \ (K_1^2(x) - K_0^2(x))\right] \qquad (D.16)$$

For q = Z e, $\alpha = \frac{e^2}{(\hbar c)}$, $x = \frac{wb_{min}}{\gamma V}$ $\qquad (D.17)$

From (D.9), the equivalent frequency spectrum for pulse P_2 is shown to contain a factor $\frac{1}{\gamma^2}$. At relativistic speeds, this pulse P_2 is, therefore, of negligible importance. This was the justification for adding a magnetic field $B_1(t) = \beta E_1(t)$. The time integral of the

field $E_1(t)$ was shown to yield zero by symmetry, so that this did not contribute to momentum transfer. The frequency spectrum confirms the above and justifies our retaining the transverse component in (5.21).

AUTOBIOGRAPHICAL STATEMENT

Ferdous Khan was born on the 20th of June, 1957 in Chittagong, Bangladesh, the son of Yunus Khan and Khaleda Khan.

He was graduated from Faujdarhat Cadet College in Chittagong, Bangladesh in 1975. He then attended Yale College in New Haven, Connecticut from 1977-1981 and earned a Bachelor of Arts degree in Physics. He earned his Master of Science degree in Physics from the University of Rhode Island at Kingston, R.I. He started his graduate studies at Old Dominion University in the Fall of 1984 under NASA research grant NCCI-42. Ferdous has coauthored ~10 publications in heavy-ion physics, radiation physics as well as atomic theory. He will work as a postdoctoral research associate at Old Dominion University and the High Energy Science Branch at NASA Langley Research Center from the Fall of 1989.